Distribution Agreement

In presenting this thesis or dissertation as a partial fulfillment of the requirements for an advanced degree from Emory University, I hereby grant to Emory University and its agents the non-exclusive license to archive, make accessible, and display my thesis or dissertation in whole or in part in all forms of media, now or hereafter known, including display on the world wide web. I understand that I may select some access restrictions as part of the online submission of this thesis or dissertation. I retain all ownership rights to the copyright of the thesis or dissertation. I also retain the right to use in future works (such as articles or books) all or part of this thesis or dissertation.

Signature:

_____ _____

Annika Kriisa

Date

Influence of Electric Fields on the Miscibility of Polystyrene / Poly (vinyl methyl ether) Blends

By

Annika Kriisa
Doctor of Philosophy
Physics

_____
Connie B. Roth
Advisor

_____
George Hentschel
Committee Member

_____
Zhiqun Lin
Committee Member

_____
Kurt Warncke
Committee Member

_____
Eric Weeks
Committee Member

Accepted:

_____
Lisa A. Tedesco, Ph.D.
Dean of the James T. Laney School of Graduate Studies

_____
Date

Influence of Electric Fields on the Miscibility of Polystyrene / Poly (vinyl methyl ether) Blends

By

Annika Kriisa
M.Sc., Tallinn University of Technology, 2006

Advisor: Connie B. Roth, PhD

An abstract of
A dissertation submitted to the Faculty of the
James T. Laney School of Graduate Studies of Emory University
in partial fulfillment of the requirements for the degree of
Doctor of Philosophy
in Physics
2015

Abstract

Influence of Electric Fields on the Miscibility of Polystyrene / Poly (vinyl methyl ether) Blends

By Annika Kriisa

Techniques which externally control and manipulate the phase behavior of miscible polymer blend systems, without altering chemistry on a molecular level, have great practical benefits. One possible mechanism is the use of electric fields, which can cause shifts in the phase separation temperature T_s for various mixtures. However, at present, there is extensive debate and limited understanding of how uniform electric fields influence the miscibility of polymeric mixtures, or even small molecules. One of the main limitations stems from the lack of experimental data with unambiguously large shifts in T_s outside of experimental error.

In this dissertation, we have characterized the fluorescence emission spectra of pyrene and anthracene dyes covalently bonded to polystyrene (PS) upon phase separation from poly(vinyl methyl ether) (PVME). It is demonstrate that slight differences in the phase separation temperature, T_S, are related to proximity of the fluorophore to the PS backbone in its covalent attachment. The sharp increase in fluorescence intensity upon phase separation that occurs for all fluorophores, with little change in spectral shape, is consistent with a mechanism of static fluorescence quenching resulting from the specific interaction with a nearby quenching molecular unit.

This fluorescence technique is used to investigate the change in T_s due to the presence of electric fields. Results are presented that demonstrate that the presence of uniform electric fields strongly enhance the miscibility of PS/ PVME blends. Reliable shifts in T_s of up to 13.5 ± 1.4 K were measured for electric field strengths of $E = 1.7 \times 10^7$ V/m in a 50/50 PS/PVME mixture. The finding that electric fields enhance miscibility agrees with the vast majority of existing experimental data on various mixtures.

Experimental results also show that electric fields do not have an effect on the temperature dependence of the remixing time scale in the one-phase region.

Influence of Electric Fields on the Miscibility of Polystyrene / Poly (vinyl methyl ether) Blends

By

Annika Kriisa
M.Sc., Tallinn University of Technology, 2006

Advisor: Connie B. Roth, PhD

A dissertation submitted to the Faculty of the
James T. Laney School of Graduate Studies of Emory University
in partial fulfillment of the requirements for the degree of
Doctor of Philosophy
in Physics
2015

Acknowledgements

Most of all, I want to thank my advisor Prof. Connie Roth for all her support and guidance. This dissertation would not exist without her.

I am also very grateful to my committee members for their insightful advice. I want to thank all the lab members I have had an honor to work with over the years, especially undergraduate students Sung Park and Sandra Boyce-Smith.

To my mother who has always believed in me. Thank you mom for taking leave of absence from your work (and life), traveling across the Atlantic Ocean and helping me through chemo. I know it was very hard for you. Thank you Ramesh for everything. Special thank you to my little daughter Uma who keeps me going even when I think I can’t anymore.

Table of Contents

Table of Figures

field increases the phase separation temperature higher. (e) Red and blue circles indicate the remixing time scales found at different temperatures T_{remix} in the presence of zero and non-zero electrical fields, respectively. Before conducting the experiment it is not known whether the blue circle fall on the same curve with the red circles. Dashed vertical blue and black lines indicate the positions of the phase separation temperatures of the sample, with and without the presence of electric fields, $T_s(E)$ and $T_s(0)$, respectively, relative to the temperature T_{remix}.. 142

Table of Tables

Chapter 1
Introduction

Polymers are molecules consisting of large numbers of repeating units (monomers) that form long molecular chains, called macromolecules. Polymers are either naturally occurring (e.g. proteins, cellulose) or artificially synthesized.[1] Mixing different types of polymers together into blends can yield completely new material properties which the individual components cannot provide separately. Typically, it is easier to combine existing polymers into a polymer blend than to develop a completely new polymer. Unfortunately, most polymers do not mix and the miscibility of polymers is an exception rather than a rule. Due to the large macromolecules limiting the entropic gain on mixing, the miscibility is controlled by specific interactions between the blend components.[2] Overall, understanding and controlling the miscibility and phase separation of polymeric blends is one of the major research areas in polymer science and engineering.

Techniques which can externally control and manipulate the phase behavior of miscible systems, without changing the chemistry on a molecular level, have great practical benefits. One such possible mechanism is the use of electric fields. Uniform electric fields have been shown to be responsible for electrohydrodynamic interface

instabilities,[3–6] as well as for orienting and aligning the morphology of polymer solutions,[7] blends[8–12] and block copolymers.[13–30] These alterations to the morphology of polymeric materials by electric fields have been explained by the presence of dielectric contrast $\Delta\varepsilon$ at the interfaces, which then orient in such a way as to minimize the electrostatic energy in the presence of fields.[31–33]

Although it may seem that the application of electric fields should be experimentally simple, as they can be switched on and off instantly and effortlessly, the influence of electric fields on the miscibility, seen as a change in the phase separation temperature T_s, in small molecules and polymeric mixtures is not yet well understood. Available theoretical calculations[15,31,34–39] use thermodynamic arguments for adding an electrostatic free energy term to the total free energy of mixing and predict changes in T_s due to external electric fields that are much smaller than what most experimental results[34,36,40–42] report. Additionally, these theoretical predictions have no clear answer whether uniform electric fields should enhance mixing or demixing. A very recent theoretical study by Orzechowski et al.[43] suggests modifying these thermodynamic arguments by including the next higher order term in the free energy expansion that may become dominant at high electric field strengths and lead to enhanced miscibility of the system. They argued that this extra term accounts for the dielectric contrast between the components, suppressing concentration fluctuations parallel to the field direction and the formation of dielectric interfaces between domains during phase separation.

One of the main limitations for developing a sound theoretical model arises from the lack of experimental data, as there are not that many experimental results[34,36–38,40–

[42,44,45] published over the past several decades. More experiments with unambiguously large shifts in T_s are needed to better understand the electric field effect on miscibility.

The main goal of this Ph.D. research was to determine whether electric fields change the miscibility of polymer blends. In this thesis I have focused on studying polystyrene (PS)/ poly(vinyl methyl ether) PVME polymer blends. PS/PVME blends are one of the most studied polymer blends, due to the fact that they are one of the few polymer blends that show miscibility and exhibit an experimentally easily accessible lower critical solution temperature (LCST) phase diagram. The relevant background on PS/PVME blends in addition to the thermodynamics and kinetics of polymer blend miscibility is given in Chapters 2.1 and 2.2. An overview of the experimental studies as well as the theoretical expectations from the current understanding of how electric fields affect miscibility published in research literature, is given in Chapter 2.3.

In this dissertation research, the phase separation of PS/PVME blends is detected using a fluorescence technique specifically developed for this purpose. In order to obtain information about changes in the molecular environment within PS/PVME blends using fluorescent spectroscopy, the system needs to contain a fluorescent probe. In this research a series of external fluorophores (anthracene and pyrene) covalently attached to the PS backbone in different ways were used. I synthesized three out of four fluorescently-labeled polystyrenes (PS*) as well as unlabeled PS used in this thesis in our lab (details given in Chapters 3.1 and 3.2) because they were not commercially available for purchase. Chapter 3.3 describes the method of using ultraviolet-visible (UV-vis) spectroscopy to determine the amount of fluorescent dye content in polymerized PS chains.

Chapter 4 presents the results of the investigation of the fluorescence emission spectra of pyrene and anthracene dyes covalently bonded to PS upon phase separation from PVME. The specific chemical structure of the fluorescence labels was found to affect the measured phase separation temperature T_s, with fluorophores covalently attached in closer proximity to the PS backbone identifying phase separation a few degrees earlier. The sharp increase in fluorescence intensity upon phase separation that occurs for all fluorophores with little change in spectral shape was consistent with the mechanism of static fluorescent quenching resulting from the specific interaction with a nearby quenching molecular unit. A study by Green et al.[46] has previously identified the presence of a weak hydrogen bond in PS/PVME blends between the aromatic hydrogens of PS and the ether oxygen of PVME. The results presented in Chapter 4 suggest that a similar weak hydrogen bond likely also occurs between PVME and the aromatic dyes explaining the fluorescence quenching in the mixed state and why fluorescence is sensitive to the early stage of phase separation. A version of Chapter 4 was published as:

> A. Kriisa, S. S. Park, and C. B. Roth, "Characterization of Phase Separation of Polystyrene / Poly(vinyl methyl ether) Blends Using Fluorescence," *J. Polym. Sci., Part B: Polym. Phys.* **2012**, *50,* 250-256.

Chapter 5.1 addresses all the necessary adjustments to the experimental protocol described in Chapter 4, to enable measurements of the phase separation temperature T_s in PS/PVME blend, both with and without electric fields, $T_s(E)$ and $T_s(E=0)$, respectively. The main goal of this research was to be able to accurately measure the shift in T_s with electric fields, $\Delta T_s(E) = T_s(E) - T_s(E=0)$. In order to minimize the standard error in $\Delta T_s(E)$, it was most accurate to measure both $T_s(E)$ and $T_s(E=0)$ within the same sample. An annealing protocol was developed so to cycle up and down through the phase diagram

from the mixed state to the unmixed state, repeatedly unmixing and remixing the same sample. As shown in Chapter 5.1, using this method the T_s could be measured repeatedly in the same sample of PS/PVME blend to within ±0.7 ^oC. Chapter 5.2 gives a detailed description of all the changes to the sample preparation protocol that proved to be necessary to able to measure T_s in PS/PVME blends in the presence of electric fields.

In Chapter 6, data showing that uniform electric fields strongly enhance the miscibility of PS/PVME is presented. Reliable shifts in T_s of up to 13.5 ± 1.4 K were measured for electric field strengths of $E = 1.7 \times 10^7$ V/m in a 50/50 PS/PVME mixture. These results agree with the vast majority of experimental data on various mixtures finding that electric fields enhance miscibility, but are opposite to the one single previous study on PS/PVME blends by Reich and Gordon,[44] who report that electric fields induce phase separation. Possible reasons for this discrepancy are discussed in detail in Chapter 6.2.3. A version of Chapter 6 was published as:

> A. Kriisa and C. B. Roth, "Electric Fields Enhance Miscibility of Polystyrene / Poly(vinyl methyl ether) blends," *The Journal of Chemical Physics* **2014**, *141*, 134908.

Due to their large size, compared to small molecules, polymers have a high viscosity and are sluggish to move. Polymeric mixtures do not reach their equilibrium state instantly but take their time. Thus, in order to explain and predict the behavior of polymeric mixtures, and to understanding the thermodynamics, it is equally important to understand the kinetics of polymers. Hence, in this thesis, it was a natural step, after discovering the electric field effect on the phase separation temperature in PS/PVME blends, to try to learn about the electric field effect on the kinetics of this blend. In Chapter 7, experiments conducted to study the electric field effect on the time scale of

remixing dynamics are discussed. The results presented in Chapter 7 indicate that not only can fluorescence spectroscopy be used to find the temperature dependence of the remixing time scale in PS/PVME blends; the electric field does not appear to have any effect on these kinetics.

The thesis ends with Chapter 8, where the main conclusions of this Ph.D. research have been summarized. The implications these results contribute to the science, along with possible future directions for this research, are also addressed.

Chapter 2
Background

The goal of this thesis is to understand how electric fields alter the phase behavior of polystyrene (PS)/ poly(vinyl methyl ether) (PVME) polymer blends. This chapter focuses on explaining the most relevant background necessary for understanding the research described in this thesis. The chapter starts by giving an overview of the research literature of PS/PVME polymer blends. Then the theoretical background of thermodynamics and kinetics of polymer blend miscibility is discussed. And lastly, the literature of experimental studies and the theoretical expectations of our current understanding of the electric field effect on the miscibility of blends is described.

2.1 Polystyrene / Poly (vinyl methyl ether) Blends

Polystyrene (PS)/ poly(vinyl methyl ether) PVME polymer blends are one of the most heavily studied polymer blends. PS/PVME blends are one of the few polymer mixtures among the handful of polymer blends found to be miscible. Additionally, PS/PVME blends have been found to have an experimentally accessible lower critical

solution temperature (LCST) phase behavior.[a] This means that at ordinary temperatures (around room temperature) PS and PVME molecules are in a homogenous mixed blend, but at higher temperatures (around 100 ^{o}C or higher, depending on the molecular weight of the components) the molecules phase separate into domains rich in one component or the other.[47–52] The chemical structures of PS and PVME are shown in Figure 2.1a.

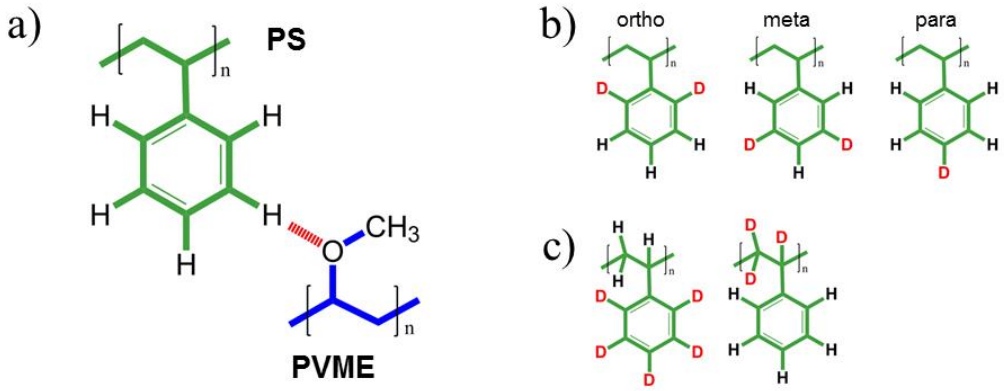

Figure 2.1 (a) Chemical structure of polystyrene (PS) is shown in green and poly(vinyl methyl ether) (PVME) in blue. Red dashed line shows the weak hydrogen bond believed to be responsible for the miscibility if PS/PVME blends, between aromatic hydrogens.

Although PS/PVME blends have been studied for decades, only recently the cause behind the miscibility between its components was learned. In 2006, Green et al.[46] found that weak C – H to O hydrogen bonds between the hydrogens of the aromatic ring of PS and the ether oxygen of PVME account for the miscibility of the blend. The hydrogen bond between PS and PVME is illustrated as a red dashed line in Figure 2.1a. Green et al.[46] studied PS/PVME blends in which the ortho, para and meta positions of the PS phenyl rings were selectively deuterated. Chemical structures of these mono-deuterated

[a] More detailed description of phase diagrams and thermodynamics of phase separation are given in chapter 2.2.

polystyrenes are shown in Figure 2.1b. Using nuclear magnetic resonance to study the intermolecular exchange interaction of the nuclear Overhauser effect, Green et al.[46] found that the participation of the meta and para hydrogens of PS in the interaction with PVME is more likely than the participation of the ortho hydrogens. This was believed to be due to the steric limitations, as approaching the ortho deuteron that is adjacent to the backbone of the PS would be difficult.[46,53]

Green et al.[46] did not provide an exact value for the strength of the weak hydrogen bonds between PS and PVME. However, using values from literature it is possible to estimate that the bond strength is ~1 kcal/mol and the bond length is ~0.2 - 0.3 nm.[54,55] That is about 4 times weaker than the strength of strong hydrogen bonds between the oxygen and hydrogen molecules in water. Such weak interactions are likely too weak to play a role in small molecules, but many such weak bonds can add up and act collectively together in large macromolecules. The presence of these hydrogen bonds also explains the LCST type phase diagram, characteristic to PS/PVME blends. As temperature increases the thermal fluctuations grow, until they are strong enough to break the hydrogen bonds between blend components, leading to phase decomposition.

Earlier literature (that is before the study by Green et al.[46]) showed indications that attractive interactions must be present in PS/PVME blends; however, it was not understood what these interactions were. In the early 1970's, Bank et al.[47,56] demonstrated that the miscibility of PS and PVME is solvent dependent. They found that PS and PVME blends cast from benzene, toluene and tetrachloroethylene were miscible, while films cast from chloroform, dichloromethane and trichloroethylene were not. It is known that chloroform, dichloromethane and trichloroethylene, but not benzene, toluene

and tetrachloroethylene can form C – H to O hydrogen bonds.[46,54] Thus, solvents that form similar hydrogen bonds necessary for the miscibility of PS and PVME could be expected to interfere with similar hydrogen bonding interactions between the blending polymers during the solvent casting process.

Support for the C – H to O hydrogen bonds was also found by infrared spectroscopy experiments showing vibrational changes in the PS C – H out-of-plane vibration and PVME's ether oxygen stretching and vibration modes upon blending.[57–59] In addition, when Yang et al.[60,61] found that deuteration of PS leads to enhanced miscibility of the blend, they suggested a favorable interaction between hydrogens in the phenyl ring of PS and PVME. They saw an increase in the LCST by ~40 ^{0}C.[60,61] However, later it was found that the effect on the LCST was attained only when deuterating the aromatic hydrogens of PS (see Figure 2.1c, left), but not when only the backbone hydrogens were deuterated (see Figure 2.1c, right).[62,63]

In the 1980's, Halary and coworkers[61,62,64] developed a technique of fluorescence emission using fluorescently labeled polystyrene to detect the phase separation temperature, T_s, in PS/PVME. They were able to identify the onset of thermally induced unmixing of PS/PVME blend components by measuring the fluorescent emission of anthracene probes covalently attached to the middle of only small number of PS chains in the blend. The chemical structure of the anthracene-labeled polystyrene (PS*) they used is shown in Figure 2.2a. Halary et al.[61] found that when the ternary blend of (PS/PS*)/PVME was heated from the one phase region to the two phase region, then at expected phase separation temperature, T_s, a sharp increase in the fluorescence intensity, as shown in Figure 2.2b, was observed. This change in florescence intensity at T_s can be

understood by recognizing that the nature of the molecules next to PS* depend on the state of the blend. In the one-phase state the PS* molecules are surrounded by both PVME and PS molecules. Once the blend is heated into the two-phase region, the blend components start moving away from each other and as a result, PS* molecules will be mainly surrounded by PS molecules. Thus, it could be argued that the fluorescence emission is greater in the unmixed two-phase state within a PS rich environment than in the mixed state within a PS/PVME environment, because PVME quenches the fluorescence emission of PS*. Although the exact origin of this fluorescence quenching was not known, it was reasoned to be highly probable that this quenching is cause by a non-fluorescent complex formed between the oxygen in the polar ether group of PVME and the anthracene attached to PS.[65] The fluorescence lifetime measurements conducted by Halary et al.[61] showed that this fluorescence quenching is static rather than dynamic. This means that the oxygen in PVME forms a complex with the anthracene in the ground state, before the excitation occurs.[65]

Halary et al.[61] also found that the phase separation temperatures obtained from the fluorescence emission experiments in PS/PVME blends were strongly heating rate dependent, shown in Figure 2.2c. At high heating rates the plateau, seen in Figure 2.2c, was associated with spinodal decomposition, while at low heating rates, the temperature plateau was associated with binodal decomposition[b]. Halary et al.[61] found a temperature plateau at high heating rates for all the different molecular weight polystyrenes used in their study (from M_w = 9 kg/mol to M_w = 233 kg/mol); however, at low heating rate

[b] Spinodal and binodal decomposition and corresponding phase diagrams in polymer blends are discussed in more detail in Section 2.2.

range, PS with sufficiently high molecular weight (M_w = 62 kg/mol in their experiments) was required to get a temperature plateau. In an LCST type phase diagram, the boundary line for spinodal decomposition is positioned higher than for the binodal. Halary et al. argued that when the PS/PVME blend was heated at a fast pace, the beginning of the binodal decomposition will not be detected and the first indication of phase separation corresponds to spinodal decomposition. On the other hand, if the samples are heated very slowly, binodal decomposition will be detected first and as the sample is slowly heated further spinodal decomposition can also be seen. Thus, depending on the heating rate, the fluorescence emission technique could provide boundaries for both the spinodal and binodal lines. An example of a PS/PVME blend LCST type phase diagram measured by Halary et al. using the fluorescence emission technique is shown in Figure 2.2d. The phase boundaries in Figure 2.2d were obtained by plotting the phase separation temperatures measured with the florescence emission technique at different compositions and two different heating rates 10 ^{o}C/min (○) and 16 ^{o}C/min (Δ). As seen in Figure 2.2d the phase separation temperatures collected by a fast heating rate of 16 ^{o}C/min (Δ) match well with the phase separation temperatures collected by light scattering (●).

The fluorescence emission technique was shown to detect phase separation temperatures on a scale smaller than light scattering and on scales comparable to small-angle neutron scattering.[64] This is not surprising as fluorescence quenching is a very local phenomenon, with the local sphere of effective quenching extending out a few nanometers at most.[65] Additionally, unlike in small-angle neutron scattering, both hydrogenated and deuterated systems can be measured with fluorescence.

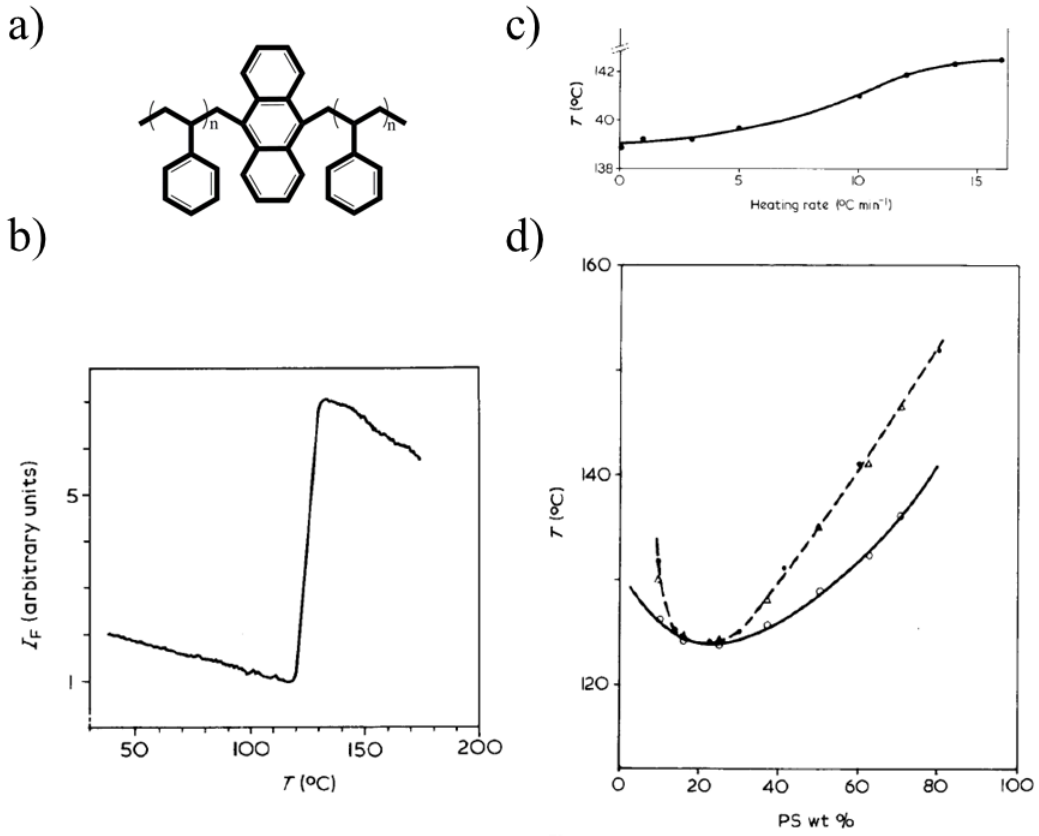

Figure 2.2(a) Chemical structure of the anthracene-labeled PS (PS*) used by Halary et al.[61] (b) Fluorescence intensity versus temperature collected while simultaneously heating sample of (PS/PS*)/PVME (32.9/0.1)/67 blends at a rate of 10 ^{o}C/min. Sharp increase in the fluorescence intensity indicates the onset of phase separation. (c) Phase separation temperature dependence of the heating rates in (PS/PS*)/PVME (11.9/0.1)/88 blends. (d) The phase diagram of PS/PVME: Phase separation temperatures, T_s, collected by light scattering (●) and by florescence emission techniques with heating rates of 0.2 ^{o}C/min (○) and 16 ^{o}C/min (Δ).In Figures (c) and (d), the circles correspond to data measured, while black curves drawn through the data act as guide to eye. (Figures (b), (c) and (d) taken from Halary, J. L., Ubrich, J. M., Nunzi, J. M., Monnerie, L. & Stein, R. S. Phase separation in polystyrene-poly(vinylmethylether) blends: a fluorescence emission analysis. *Polymer* **25,** 956–962 (1984), with permission from Elsevier.)

2.2 Thermodynamics and Kinetics of Polymer-Polymer Miscibility

The most important characteristic of polymer-polymer blends is their phase behavior. Polymer blends can exhibit miscibility or phase separation and various levels of mixing in between. In general, a polymer blend is considered miscible if its components upon mixing give a material with properties expected for a single phase material.[66] However, it is believed that perfectly mixed polymer blends do not exist. Even the most highly miscible polymers show evidence of domains of one or the other component on the order of 1 - 2 nm.[66]

The thermodynamic basis for solubility is determined by the change in Gibbs free energy of mixing ΔG (at constant pressure and temperature):

$$\Delta G = \Delta H - T\Delta S,$$

where ΔH is the change in enthalpy due to mixing, T is the absolute temperature and ΔS is the change in entropy due to mixing. In the 1940's, using the regular solubility theory, Huggins and Flory independently derived an equation for the free energy of mixing in systems where at least one of the components is polymeric, now commonly referred to as the Flory-Huggins Equation:[67]

$$\frac{\Delta G_m}{k_B T} = \frac{\phi_A ln\phi_A}{v_A N_A} + \frac{\phi_B ln\phi_B}{v_B N_B} + \frac{\phi_A \phi_B \chi}{v_{ref}}, \quad (2.1)$$

where ΔG_m is the system's total free energy of mixing per unit volume, k_B is the Boltzmann constant and T is the absolute temperature. The first two terms on the right side, represent the contribution to the entropy of mixing per unit volume, while the third term is the enthalpy of mixing per unit volume. Here, ϕ_A and ϕ_B are volume fractions (ϕ_A = 1 - ϕ_B) and v_A and v_B are monomer volumes of the two blend components with degree

of polymerization N_A and N_B; while v_{ref} is a reference volume of monomer size and χ is the empirical interaction parameter. $v_A N_A$ and $v_B N_B$ represent the molecular volume of each polymer, with v_{ref} accounting for the fact that v_A and v_B are likely not the same size.[2,66,67]

Although the entropy contribution in Eq. (2.1) to the total free energy of mixing always promotes mixing (as the molecules become more disordered when dissolved in a mixture, or $ln\varphi$ is always negative as $\varphi < 1$), for high molecular weight polymers the entropy of mixing is negligibly small. Qualitative illustration for why in high molecular weight polymers the entropy contribution in mixing is very small is given in Figure 2.3. In a low molecular weight mixture (for example styrene monomer in toluene) the molecules may be distributed randomly throughout the lattice, only restriction being that a lattice slot cannot be occupied simultaneously by two (or more) molecules. This gives rise to a large number of configurational possibilities, that is, high entropy (Figure 2.3a). In a polymer-solvent however (for example polystyrene in toluene) each chain segment is confined to a lattice site adjacent to the next chain segment, greatly reducing the configurational possibilities, leading to a tiny entropy gain on mixing (Figure 2.3b).[68]

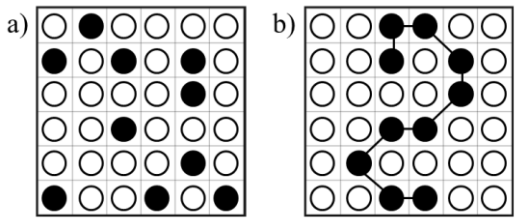

Figure 2.3 Lattice model of solubility: (a) low molecular weight solution with large number of configurational possibilities; (b) polymer solution, where configurational possibilities are reduced due to the fact that each chain segment is confined to a lattice site adjacent to the next chain segment. Filled and empty circles denote chain segments of solute and solvent, respectively.

Due to the fact that typically the entropy term in Eq. (2.1) is always tiny in polymer blends, the miscibility of polymeric mixtures will be dominated by the third term in Eq. (2.1), that is the enthalpy part of mixing. The enthalpy term can be positive, zero or negative depending on the interaction parameter χ. If the enthalpy is negative, the internal interactions are attractive and promote miscibility; on the other hand, if the enthalpy is positive, the internal interactions are repulsive and promote phase separation. The interaction parameter, χ, in its original definition by Flory and Huggins was considered as purely energetic, varying only as $1/T$ and always $\chi > 0$.[2,67,68] This means that in order for the blend to be able to phase separate, the systems total free energy of mixing has to be driven to more negative values, meaning, the temperature must be lowered. This type of behavior, where lowering the temperature leads to phase separation, is typically found in mixtures comprised of small molecules and is called an upper critical solution temperature (UCST) type phase diagram behavior, shown in Figure 2.4d. However, additionally to UCST type phase behaviors, polymeric mixtures have been found to exhibit many different phase diagrams, as shown in Figure 2.4. For example, phase behavior where heating leads to phase separation, called lower critical solution temperature (LCST) phase behavior is typically observed in high molecular weight polymers, as shown in Figure 2.4c.[66,67]

One of the major assumptions of the original Flory Huggins theory was that there is no volume change on mixing and the components are randomly mixed. In real polymeric mixtures this is usually not true. Thus, in order to "improve" Flory-Huggins theory, so it would match better with real systems, and also predict LCST type phase

behaviors, a temperature- independent constant is added in the expression of the interaction parameter:

$$\chi(T) = A + \frac{B}{T},$$

where *A* and *B* are empirical parameters and have been tabulated for many polymers. The temperature independent term *A* is referred to as the "entropic part" of χ, while *B*/*T* is called the "enthalpic part".[67] It is now recognized that there is an interactive as well as configurational contribution to the entropy of mixture. The first two terms on the right of Eq. (2.1) therefore represent the configurational entropy contribution to ΔG_m, while the third term is the interaction contribution and includes both and entropy effects (accounting for packing constrains on the level of polymer segments) and enthalpy effects (accounting for the interactions between blend components).[68]

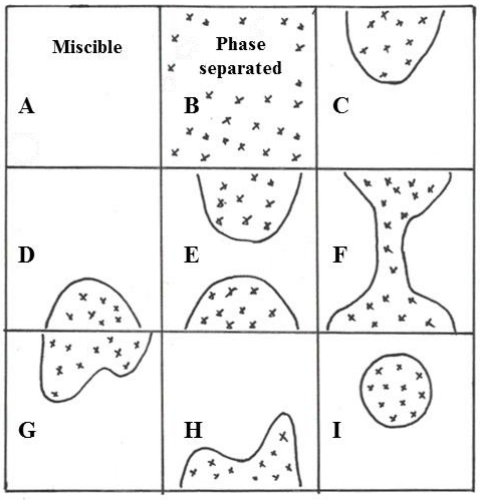

Figure 2.4 Different possible phase diagrams observed for polymer blends. Areas containing x's represent phase separated regions. The y-axis for each diagram represents temperature and the x-axis represents composition.

Nowadays, the interaction parameter, χ in Flory Huggins theory is treated as just an effective fitting parameter. For example, a composition dependent interaction parameter is expressing as

$$\chi(T,\phi) = \left(A + \frac{B}{T}\right)(1 - C\phi),$$

where A, B, and C are the empirical constants.[2] Additionally it has been shown that χ also depends on molecular weight.[69–71]

There has been considerable subsequent work to overcome the deficiencies in lattice-type theories describing polymer blending. For example, Lipson and her coworkers, have developed a simple lattice-based theory, Locally Correlated Lattice (LCL) equation of state model that is considerably more advanced than the classical Flory-Huggins model, accounting for the effects of free volume (the model is compressible) and the effects of nonrandom mixing.[72–75] Their theory has not only been shown to successfully model the thermodynamic behavior of polymer solutions,[76,77] polymer blends,[78,79] and small molecule fluids and mixtures[74,75] but also produce physically meaningful molecular parameters giving insight into what drives the miscibility.[78–80]

Figure 2.5a illustrates the free energy change ΔG (ϕ) due to a temperature jump from T_1, in the homogeneous state to temperature T_2, in the two-phase region. Depending upon the location in the two-phase region, the phase separation occurs either by a mechanism known as nucleation and growth (red) or by spinodal decomposition (blue). In Figure 2.5, the concentrations ϕ'_2 and ϕ''_2 are the equilibrium binodal concentrations, and $\phi'_{2,sp}$ and $\phi''_{2,sp}$ are the equilibrium spinodal concentrations. The phase diagram

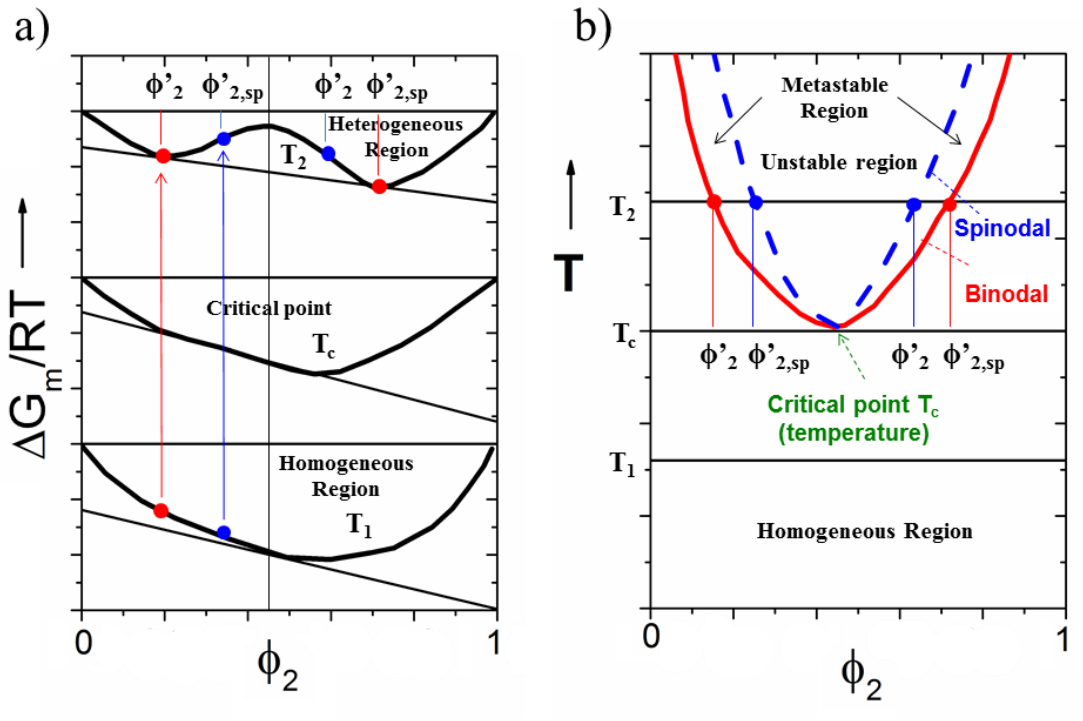

Figure 2.5 (a) Free energy change ΔG versus volume fraction, ϕ upon temperature jump from T_1 (the one-phase region) into T_2 (the two-phase region). The compositions ϕ'_2 and ϕ''_2 are the equilibrium binodal compositions and $\phi'_{2,sp}$ and $\phi''_{2,sp}$ are the spinodal compositions. (b) Phase diagram (temperature versus volume fraction) of an LCST type phase behavior. The binodal separates the one-phase (homogeneous) region at low temperatures from the two-phase region at high temperatures. The spinodal curve separates the unstable and metastable windows within the two-phase region. The spinodal and binodal meet at the critical point.

describing the phase behavior of a polymer blend can be constructed from the free energy at different temperatures. In Figure 2.5a the corresponding regions of an LCST type phase diagram are shown. If the system, as a result of the temperature jump from T_1 to T_2 crosses the spinodal line, it becomes unstable and spinodal decomposition will occur due to any small change in composition fluctuation as a result of thermal fluctuations. If the system enters the region between the spinodal and binodal curve, it will be considered metastable and can phase separate by nucleation and growth.[66] In principle, a system may

stay in the metastable region indefinitely as a metastable system is stable against small, spontaneous fluctuations,[2] however, in practice the system typically undergoes phase separation via nucleation and growth due to impurities.

The spinodal curve, also known as the limit of metastability, is found from

$$\frac{\partial^2 \Delta G}{\partial \phi^2} = 0.$$

The binodal curve is found from the common tangent to the ΔG curve of the free energy at the compositions ϕ'_2 and ϕ''_2 corresponding to the two equilibrium phases,[67] as shown in Figure 2.5b,

$$\left(\frac{\partial \Delta G}{\partial \phi}\right)_{\phi=\phi'} = \left(\frac{\partial \Delta G}{\partial \phi}\right)_{\phi=\phi''}.$$

The critical point where the binodal and spinodal intersect, is found from[2]

$$\frac{\partial^3 \Delta G}{\partial \phi^3} = 0.$$

It has been shown, using optical microscopy that the patterns of phase separation by nucleation and growth (showing spherical precipitates in a matrix) considerably differ from spinodal decomposition (showing interpenetrating continuously extending domains). [81] The mechanism driving the nucleation and growth is different from the mechanism through which the spinodal decomposition occurs. The cause for the occurrence of the two different modes of phase separation become clear when observing the free energy curve $\Delta G(\phi)$ at T_2 in Figure 2.5a. Immediately after the jump from one the phase region into the two phase region, the structure is still unmixed but no longer stable. What is different in the two cases is the character of the instability. The difference shows up when the consequences of a spontaneous local concentration fluctuation are

considered. Depending on the sign of the curvature $\frac{\partial^2 \Delta G}{\partial \phi^2}$ the local concentration fluctuations, always present due to thermal fluctuations, can lead to either an increase or decrease in the free energy of mixing. If the curvature is negative, as is the case between the compositions $\phi'_{2,sp}$ and $\phi''_{2,sp}$ in Figure 2.5a, the free energy decreases even for infinitesimally small fluctuations. There is no restoring force, on the contrary, any small fluctuation in composition is amplified and the phase separation by spinodal decomposition proceeds continuously.[81] However, between compositions ϕ'_2 and ϕ''_{2sp} in Figure 2.5a, similar small concentration fluctuations lead to an increase in free energy. Only when a relatively large fluctuation takes place, with a corresponding high energy cost, the system can lower its energy and phase separate. [82] This means the system is locally stable with respect to small concentration fluctuations and yet globally unstable with respect to large fluctuations, in other words it is metastable. If a large composition fluctuation takes place, it is called a nucleus, and the work of forming such a nucleus is a measure of the metastability of the phase.[83] The total free energy change to form a nucleus of size *r*, is

$$\Delta G(r) = \frac{4}{3}\pi r^3 \Delta G_V + 4\pi r^2 \gamma,$$

where the energy change ΔG_V results from the fact that the mixture is initially globally unstable. If it does succeed in phase separating this will lower the free energy in proportion to the volume of the droplet.[82] γ is the surface free energy. This term is proportional to the surface area of the droplet with the cost of forming a droplet with an interface.[82]

The total change in free energy ΔG has a maximum value $\Delta G^* = \frac{16\pi\gamma^3}{3\Delta G^2{}_V}$ for a critical droplet size r^*. Until the nucleus reaches this critical size r^*, it is energetically unfavorable for the system to form a nucleus. After the droplet reach size r^*, the growth of the droplet will lower the energy of the system and the droplet continues to grow. The driving force for growth is the reduction in interfacial energy that occurs as the domains get larger. Thus, nucleation is an activated process, it can only occur if a large enough fluctuation occurs increasing the local free energy by an amount ΔG^*.[82]

The progress of spinodal decomposition can be separated into three stages: early, intermediate and late stage. In the early stage, a small-amplitude sinusoidal composition wave develops against a homogeneous background. The amplitude of this wave grows exponentially in time, while the wavelength stays almost constant.[84] Departures from uniform composition are small, and a linear theory by Cahn is applicable. In this theory, the total free energy density per unit volume, is written as

$$\Delta G(\phi, \boldsymbol{x}) = \Delta G(\phi) + \kappa(\nabla\phi)^2. \qquad (2.2)$$

Here $\Delta G(\phi,\boldsymbol{x})$, is the inhomogeneous free energy density, which varies from place to place in the phase-separating sample. It consists of the homogeneous term, $\Delta G(\phi)$, the free energy change upon mixing, discussed earlier, and a term $\kappa(\Delta\phi)^2$ accounting for the gradients in composition (the coefficient κ is a phenomenological constant).[84] Systems with non-uniform compositions are known to evolve according to diffusion equations, and the early stages of spinodal decomposition are no different. It can be shown that combining Eq. (2.2) with diffusion equations gives an equation called the Cahn – Hilliard equation (in one dimension)[82]

$$\frac{\partial \phi}{\partial t} = M \frac{\partial^2 \Delta G}{\partial \phi^2} \frac{\partial^2 \phi}{\partial x^2} - 2M\kappa \frac{\partial^4 \phi}{\partial x^4}. \quad (2.3)$$

Here, M is the Onsager coefficient, a positive transport coefficient. Solutions to the Cahn-Hilliard equation give the time evolution of a phase separating mixture. In the absence of the gradient term, which is proportional to κ, Eq. (2.3) takes a form of a simple diffusion equation (Fick's second law) where an effective diffusion coefficient $D_{eff} = M \frac{\partial^2 \Delta G}{\partial \phi^2}$.[82]

In the intermediate stage of spinodal decomposition, the concentration variations continue to grow producing well defined domains, whose compositions differ distinctly from the surrounding stage. In the late stage, phase separation proceeds by a coarsening process in which the domains get larger while their composition and interfacial width stay constant.[84] The laws describing the intermediate and late stage are complicated and outside the scope of this thesis.

When discussing the kinetics of phase behavior of polymer blends, it is important to remember that due to the high viscosity of polymers, the rate of unmixing (or mixing) is considerably slower than for example in simple liquids.[c] The system, when going through phase transition and adopting a certain minimum free energy structure, will not instantly adopt its new structure. It takes time for molecules to move and rearrange.[82]As a result, the evolution of the two-phase structure subsequent to a temperature jump can often be continuously monitored in real-time (often optical microscopy or scattering experiments are used) and the kinetic theories of phase separation can be tested.[81]

[c] For example, the viscosity of water is 0.1 Ns/m^2, whereas polymeric fluids may have viscosity in the range of $10^1 – 10^5$ Ns/m^2 (depending on how long the chains are and whether there is solvent).[1]

2.3 Understanding How Electric Fields Affect the Phase Separation Temperature T_s of Mixtures

Electric fields have been shown to alter the morphology of polymeric mixtures by elongating and aligning the domains in polymer solutions,[7] polymer blends,[8–12] and block copolymers,[13–30] as well as induce electrohydrodynamic surface instabilities[3–6]. These electric field effects of the morphology of different polymeric mixtures have been well explained by the presence of dielectric contrast in the dielectric constant, $\Delta\varepsilon$, at the interfaces between the mixture components. Under electric fields these interfaces are driven to orient parallel to the external field as it is energetically most favorable.[31–33] This mechanism of domain alignment in the presence of electric fields has been frequently exploited. For example, it has been used to form conducting pathways in polymer photovoltaics and batteries where electrodes are already present.[85–90]

Electric fields have also been shown to shift the phase separation temperature T_s and order disorder transition temperature T_{ODT} in polymeric mixtures.[31,34,36–38,40–45,91–99] However, it is not well understood why electric fields influence the compatibility of polymeric mixtures, or even of small molecules. This chapter lists all the experimental data reported in the research literature for the electric field effect of phase separation temperature T_s and gives an overview of the current theoretical treatment to explain this data.

2.3.1 Experimental Literature

Only a few experimental results have been published over the past several

decades, with no clear consensus on the size of the shift in phase separation temperature T_s, or even whether electric fields consistently enhance mixing or induce phase separation. The first experimental results on the subject were published by Debye and Kleboth,[34] who studied a small molecule mixture of nitrobenzene/isooctane. They reported that electric fields of $E = 0.45 \times 10^7$ V/m enhance mixing, causing T_s to shift up by 0.015 K for this upper critical solution temperature (UCST) type mixture. Later, Debye and Kleboth's results were verified with greater accuracy by Orzechowski[42] for the same mixture. Beaglehole[40] reported shifts of $\Delta T_s = 0.08$ K towards enhanced mixing under fields of $E = 0.03 \times 10^7$ V/m in solutions of cyclohexane/aniline. However, Early,[41] who later worked on the same mixture with similar magnitude of electric fields as Beaglehole, reported not seeing shifts in T_s at all. Early suggested Beaglehole's results could be explained by Joule heating from current conduction through the sample. Similar concerns have also been expressed about the Debye and Kleboth results.[39,41]

Wirtz and Fuller[36] studied three different solutions: small molecule mixtures of nitrobenzene/*n*-hexane, and polymeric solutions of PS/cyclohexane and poly(*p*-chlorostyrene)/ ethylcarbitol. They saw enhanced mixing in all three systems, reporting shifts of $\Delta T_s = 0.02$ K for $E = 0.1 \times 10^7$ V/m in nitrobenzene/*n*-hexane, $\Delta T_s = 0.04$ K for $E = 0.05 \times 10^7$ V/m in PS/ cyclohexane, and $\Delta T_s = 0.03$ K for $E = 0.05 \times 10^7$ V/m in poly(*p*-chlorostyrene)/ethylcarbitol. Much bigger shifts, up to $\Delta T_s = 1.5$ K for $E = 0.85 \times 10^7$ V/m, have also been recently reported in poly(styrene-*block*-isoprene) (SI) solutions by Schoberth et al.[45] towards enhanced mixing.

All the above mentioned experimental data show enhanced compatibility, lower UCST or higher lower critical solution temperature (LCST) behavior, in the

presence of uniform electric fields. However, there are two research groups who have reported the opposite. According to Reich and Gordon,[44] who reported the largest shifts with $\Delta T_s = 54$ K for $E = 2.72 \times 10^7$ V/m in PS/PVME polymer blends, and Lee et al.,[37,38] who also showed large shifts of $\Delta T_s = 18$ K for $E = 0.9 \times 10^7$ V/m in poly(vinylidene fluoride) (PVDF) / poly(butyl acrylate) (PBA) and $\Delta T_s = 2.5$ K for $E = 0.7 \times 10^7$ V/m in PVDF / poly(methyl methacrylate) (PMMA), electric fields strongly reduce compatibility. Note, however, these last two blend systems by Lee et al.[37,38] involving PVDF are unique in that PVDF is strongly piezoelectric. PVDF, having a negative piezoelectric coefficient, undergoes volume contraction when in the presence of electric fields.[100,101] As blend miscibility and T_s are very sensitive to many perturbations like shear, pressure, temperature etc.,[66] it would be difficult to distinguish between the effects of mechanical stress in PVDF due to the presence of electric fields and other possible electric field effects leading to shifts in T_s. Volume changes on blending have historically been particularly challenging to account for theoretically.[102] For example, White and Lipson recently showed that individual component volume changes associated with thermal expansion is a strong factor affecting blend miscibility.[80] Thus, for the present discussion I exclude consideration of these piezoelectric PVDF systems. This leaves only one outlying study, by Reich and Gordon on PS/PVME blends,[44] not reporting that the presence of electric fields enhance miscibility.

Comparing solely the absolute maximum magnitude of the T_s shifts observed in the experiments listed above, there appears, at first glance, to be a trend of electric fields causing smaller T_s shifts in small molecule systems and larger shifts in polymeric systems. However, when the *relative* change of $\Delta T_s/E^2$ between published results is

compared, this trend disappears. The one agreement between all experimental results, and theoretical approaches, is that the shift in T_s is proportional to the square of electric field, E^2. Comparing relative $\Delta T_s/E^2$ changes among the available experimental literature makes it clear that no correlation exists between the relative size of the shift in T_s as a function of electric field and the system molecule size. The Debye and Kleboth[34] and Orzechowski[42] studies, both in solutions of nitrobenzene/isooctane, showed $\Delta T_s/E^2 = 0.08 \times 10^{-14}$ Km^2/V^2, which is almost 1000 times smaller than $\Delta T_s/E^2 = 87 \times 10^{-14}$ Km^2/V^2 reported by Beaglehole[40] in cyclohexane/aniline. For Wirtz and Fuller's data,[36] $\Delta T_s/E^2 = 2 \times 10^{-14}$ Km^2/V^2 in nitrobenzene/*n*-hexane, $\Delta T_s/E^2 = 16 \times 10^{-14}$ Km^2/V^2 in PS/cyclohexane, and $\Delta T_s/E^2 = 12 \times 10^{-14}$ Km^2/V^2 in poly(*p*-chlorostyrene)/ethylcarbitol. For the Schoberth et al.[45] data in SI solutions, $\Delta T_s/E^2 = 2.1 \times 10^{-14}$ Km^2/V^2, while the Reich and Gordon[44] data in PS/PVME give $\Delta T_s/E^2 = 7.3 \times 10^{-14}$ Km^2/V^2. And included simply for completeness, the Lee et al.[37,38] studies give $\Delta T_s/E^2 = 22 \times 10^{-14}$ Km^2/V^2 in PVDF/PBA and $\Delta T_s/E^2 = 4.6 \times 10^{-14}$ Km^2/V^2 in PVDF/PMMA. Hence, there appears to be little if any discernable trend among the different systems with the $\Delta T_s/E^2$ shifts varying from 0.08–87 ($\times 10^{-14}$ Km^2/V^2).

2.3.2 Theoretical Expectations

The few theoretical studies published on the subject of how electric fields affect the miscibility in polymeric mixtures use a thermodynamic argument of adding an electrostatic free energy term to the free energy of mixing.[15,31,34–40] For polymers this is typically written as an extension of the classic Flory-Huggins equation:[31,36–38]

$$\Delta G_m = k_B T \left(\frac{\phi_A ln\phi_A}{v_A N_A} + \frac{\phi_B ln\phi_B}{v_B N_B} + \frac{\phi_A \phi_B \chi}{v_{ref}} \right) - \frac{1}{2} \varepsilon_0 E^2 [\varepsilon(\phi) - \phi_A \varepsilon_A - \phi_B \varepsilon_B \,] \quad (2.4)$$

where ΔG_m is the system's total free energy of mixing per unit volume. The term within brackets on the right side, is the sum of the entropy and enthalpy of mixing per unit volume, where ϕ_A and ϕ_B are volume fractions and v_A and v_B are monomer volumes of the two blend components with degree of polymerization N_A and N_B; while v_{ref} is a reference volume of monomer size and χ is the empirical interaction parameter.[67,103] The last term in Eq. (2.4), $\Delta G_{E-field} = \frac{1}{2} \varepsilon_0 E^2 [\varepsilon(\phi) - \phi_A \varepsilon_A - \phi_B \varepsilon_B \,]$ accounts for the additional contribution to ΔG_m due to the presence of a uniform electric fields E in dielectric medium; it is the free electrostatic energy density equal to the difference between the electrostatic energy of the blend and the ϕ-weighted average of the pure components A and B. Here, ε_0 is the absolute permittivity of vacuum, $\varepsilon(\phi)$ is the composition dependent dielectric constant of the binary mixture, and ε_A and ε_B are the dielectric constants of the pure components A and B.[33,36,104] This equation for the free electrostatic energy density in dielectric medium was first introduced by Landau and Lifsitz[33] and can now be found in any classic textbook on electromagnetism.

In Eq. (2.4), a negative sign has been included in front of the electrostatic energy term, as this is the most accepted treatment,[31,35,37–40] however there exists discussion among theoretical studies, whether a plus sign should be used instead.[31,34–36,39] The negative sign is applicable to dielectrics for the case of a constant applied potential, where the work done by an external power supply to maintain a constant voltage is included in the total free energy of the system.[31,33,104] When a positive sign is used, the sample (a capacitor setup with dielectric medium) is considered to have a constant charge

on its plates, such that the external voltage supply is not included in the total free energy.

Considering the standard conditions for stability $\frac{\partial^2 \Delta G_m}{\partial \phi^2} = 0$ and criticality $\frac{\partial^3 \Delta G_m}{\partial \phi^3} = 0$, and the empirical form for the interaction parameter $\chi = A + \frac{B}{T}$ (where empirical parameters $A > 0$ and $B < 0$ for LCST and $A < 0$ and B > 0 for UCST type phase diagrams), it follows from Eq. (2.4) that

$$\frac{T_s(E) - T_s(0)}{T_s(0)} = \frac{\varepsilon_0 v_{ref} E^2}{4Bk} \frac{\partial^2 \varepsilon(\phi)}{\partial^2 \phi}. \quad (2.5)$$

Here, $T_s(E)$ and $T_s(0)$ are the phase separation temperatures measured with and without electric field defining $\Delta T_s(E) = T_s(E) - T_s(0)$ as the shift in phase separation temperature due to the electric field. The derivation of Eq. (2.5) is shown in Appendix 1. We notice that Eq. (2.5) does not include dielectric constants for pure components, ε_A and ε_B. This is because they cancel out during derivation of Eq. (2.5), as shown in Appendix 1. For that reason, the last two terms in Eq. (2.4) containing parameters ε_A and ε_B are often omitted from the electrostatic energy contribution to total free energy.

Assuming that $\frac{\partial^2 \varepsilon(\phi)}{\partial^2 \phi} > 0$, as is typically seen for mixtures of polar and non-polar components,[34,35,40,42] and using the negative sign for the electrostatic energy term in Eq. (2.4), it follows from Eq. (2.5) that a shift towards a reduction of compatibility on the order of only a few mK is predicted for the presence of moderate to strong fields.[15,31,35,39,40] Thus overall, these theoretical predictions are in conflict with the vast majority of experimental results.[31,34,36–38,40–42,44,45,105] As discussed above, all experimental results, except the single study by Reich and Gordon[44] (and excluding the piezoelectric PVDF data by Lee et al.[37,38]), find that electric fields enhance mixing with significantly larger

shifts in T_s than theory predicts.

This controversy between the theory and experimental data of the electric field on the phase separation temperature was examined in detail in a very recent study by Orzechowski et al.[43] They argue that the inconclusiveness of the theoretical predictions could be improved by amending the Landau and Lifshitz's formula for the free electrostatic energy density $\Delta G_{E-field} = -\frac{1}{2}\varepsilon_0\varepsilon(\phi)E^2$ added to the total energy of mixing in Eq. (2.4) to account for the energy change due to the presence of electric fields. Orzechowski et al.[31,43] discuss that the change in concentration fluctuations induce variations in the concentration dependent dielectric constant $\varepsilon(\phi)$ and since the dielectric constant and electric fields are coupled via Laplace's equation the electric field and electrostatic energy are also altered.[31,43] In other words, they argue that the original Landau and Lifshitz's formula for the free electrostatic energy needs to be modified to incorporate the aspect that in the presence of electric fields, local changes in the mixture's composition lead to long-range changes in the field.[43]

Orzechowski et al. define $\phi(\boldsymbol{r})$ as an order parameter, a spatially dependent dimensionless quantity denoting the relative composition of one mixture component, $0 < \phi < 1$. And they define φ as the variation in ϕ from the average value ϕ_o, where $\phi(\boldsymbol{r}) = \phi_o + \varphi(\boldsymbol{r})$ and $\langle\varphi(\boldsymbol{r})\rangle = 0$. If concentration fluctuations are assumed to be small, then the dielectric constant $\varepsilon(\phi)$ can be written as a Taylor series expansion[31,43]

$$\varepsilon\big(\phi(\boldsymbol{r})\big) \approx \varepsilon(\phi_0) + \frac{\partial\varepsilon}{\partial\phi}\varphi + \frac{1}{2}\frac{\partial^2\varepsilon}{\partial\phi^2}\varphi^2 , \tag{2.6}$$

$\varepsilon(\phi_o)$ is the average dielectric constant if $\frac{\partial^2\varepsilon}{\partial\phi^2}$ is absent from Eq. (2.6).

When considering that variations in composition φ lead to variations in dielectric constant ε and knowing the electric field and dielectric constant are coupled via Laplace's equation, it can be assume that variations in compositions lead to variations in the electric field in the system. Thus, the electric field can be written as[43]

$$\boldsymbol{E} \cong \boldsymbol{E}_0 + \boldsymbol{E_1} + \boldsymbol{E_2} ,$$

where $\boldsymbol{E}_0$ is the electric field which is present in the system when ε is constant everywhere, ($\varphi = 0$). $\boldsymbol{E}_1$ and $\boldsymbol{E}_2$ correspond to linear and quadratic corrections in φ. The electrostatic energy density can now be written in orders of φ as[31,43]

$$\Delta G_{E-field} = -\frac{1}{2}\varepsilon_0\varepsilon(\phi_0)\boldsymbol{E}_0^2 - \frac{1}{2}\varepsilon_0\left(2\varepsilon(\phi_0)\boldsymbol{E}_0\boldsymbol{E}_1 + \frac{1}{2}\frac{\partial\varepsilon}{\partial\phi}E_0^2\varphi\right)$$

$$-\frac{1}{2}\varepsilon(\phi_0)\left(\frac{\partial\varepsilon}{\partial\phi}(E_1^2 + 2\boldsymbol{E}_0\boldsymbol{E}_2) + \boldsymbol{2}\frac{\partial\varepsilon}{\partial\phi}\varphi\boldsymbol{E}_0\boldsymbol{E}_1 + \frac{1}{2}\frac{\partial^2\varepsilon}{\partial\phi^2}E_0^2\varphi^2\right) + O(\varphi^3) \quad (2.7)$$

The first line contains the contribution of the uniform medium and the term linear in φ. In the quadratic terms (second line), the term proportional to $\boldsymbol{E}_o\boldsymbol{E}_2$ integrates to zero because $\boldsymbol{E}_2$ is a gradient that vanishes at the boundaries. The last term on right side $O(\varphi^3)$ can be considered an unimportant constant.[43]

When the assumption is made that the composition fluctuations are specially asymmetric, it can be shown from Eq. (2.7) that at high field strengths the contribution from the quadratic order term in the free energy expansion may be dominating the influence behind the change in T_s due to the presence of electric fields.[43] Their expanded expression for the shift in phase separation temperature with electric field, replacing Eq. (2.5), is:

$$\frac{\Delta T_s(E)}{E^2} = \frac{\varepsilon_0 v_{ref} T_s(0)}{4k\,B}\left[\frac{\partial^2\varepsilon(\phi)}{\partial^2\phi} - \frac{2}{\varepsilon(\phi)}\left(\frac{\partial\varepsilon(\phi)}{\partial\phi}\right)^2\right] \quad (2.8)$$

The second term in the brackets accounts for the dielectric contrast of dielectric constant **Δε** between the components, suppressing concentration fluctuations parallel to the field direction.[99,106]

The effect of this second term in Eq. (2.8) on the phase separation behavior can be understood by considering the kinetic mechanism through which phase separation occurs. At the phase separation temperature, concentration fluctuations increase quickly and lead to the formation of interfaces between the domains of demixing components. However, if a force suppressing the concentration fluctuations is present, then the formation of dielectric interfaces between domains during phase separation would be delayed and so would be the phase separation of the mixture components. In other words, the second term in Eq. (2.8) takes into account the energy penalty for the formation of dielectric interfaces oriented perpendicular to the field direction. Thus, this term always favors increased miscibility with increasing electric field strength, consistent with the majority of experimental results described above.

The theoretical design behind the extra term in Eq. (2.8) is exactly the same as the model that is considered to be responsible for the electrohydrodynamic surface instabilities[3–6] and elongation and alignment of the domains in polymer solutions,[7] polymer blends,[8–12] and block copolymers.[13–30] The explanation of the orientation of morphologies in the presence of electric fields in these mixtures is based on the dielectric contrast between mixture components leading to a minimum electrostatic free energy whenever the dielectric interfaces are oriented parallel to the field.[32,33] The gain in free energy is proportional to $E^2 \frac{(\Delta\varepsilon)^2}{\langle\varepsilon\rangle}$, where Δε is the dielectric contrast, that is the difference

between the dielectric constants of the components and ε is the average dielectric constant of the system.[32]

Orzechowski et al.[43] demonstrated quantitative agreement between their theoretical predictions and experiment for electric field shifts in the nitrobenzene/n-octane system. It should also be noted here that the mixture of nitrobenzene/n-octane is somewhat unusual, and does not necessarily represent a typical mixture. This is because the dielectric constant ε = 34.2 of nitrobenzene[34] differs considerably from the ε = 2.0 of n-octane. More typical mixtures are comprised of components where Δε is an order of magnitude smaller than in nitrobenzene/n-octane. Also, Orzechowski et al.[43] did not directly measure the shift in T_s under electric field, but calculated this shift $\Delta T_s(E)$ from the results of the nonlinear dielectric effect (NDE) measurements. In NDE the change in electric permittivity, Δε, in high- and low-intensity electric fields is found from measuring the difference in the resonance frequency in the presence and in the absence of electric fields.

Chapter 3
Synthesis and Characterization of Fluorescently Labeled Polystyrene

---

In this thesis the phase separation of polystyrene (PS) / poly (vinyl methyl ether) PVME polymer blends was investigated using steady state fluorescence spectroscopy. In order to obtain information about the PS/PVME blend using a fluorescence technique, the blend has to contain a fluorescent probe. Although the phenyl ring of PS is an intrinsic fluorophore,[107] I found that the quantum yield is not sufficiently high for convenient experimental exploration of the blend, and thus it was necessary to use extrinsically labeled PS. Also, the indium tin oxide (ITO) layer, used on the sample substrates when investigating the electric field effect on the phase separation temperature of the PS/PVME blends, has low transparency at the fluorescence excitation and emission wavelengths characteristic to the phenyl ring of PS.

Despite the fact that a wide variety of polymers can be purchased commercially, several of the differently labeled PS's (and unlabeled PS) used for this study had to be polymerized in our lab, as they were either not offered at the desired molecular weight or not available at all. Using free radical polymerization, 1- pyrenylmethyl methacrylate

labeled PS, 1-pyrenylbutyl methacrylate labeled PS, 9-anthracenylmethyl methacrylate labeled PS, and 2-naphtyl methacrylate labeled PS were synthesized (chemical structure of fluorescent methyl methacrylate monomers are shown in Figure 3.1). 1-pyrenylbutyl methacrylate monomer was synthesized by esterification of 1-pyrenebutanol and methacryloyl chloride because it is not sold commercially. The chemical structure of the synthesized 1-pyrenylbutyl methacrylate monomer was confirmed using 300 MHz Proton Nuclear Magnetic Resonance (^{1}H NMR) spectrometry.

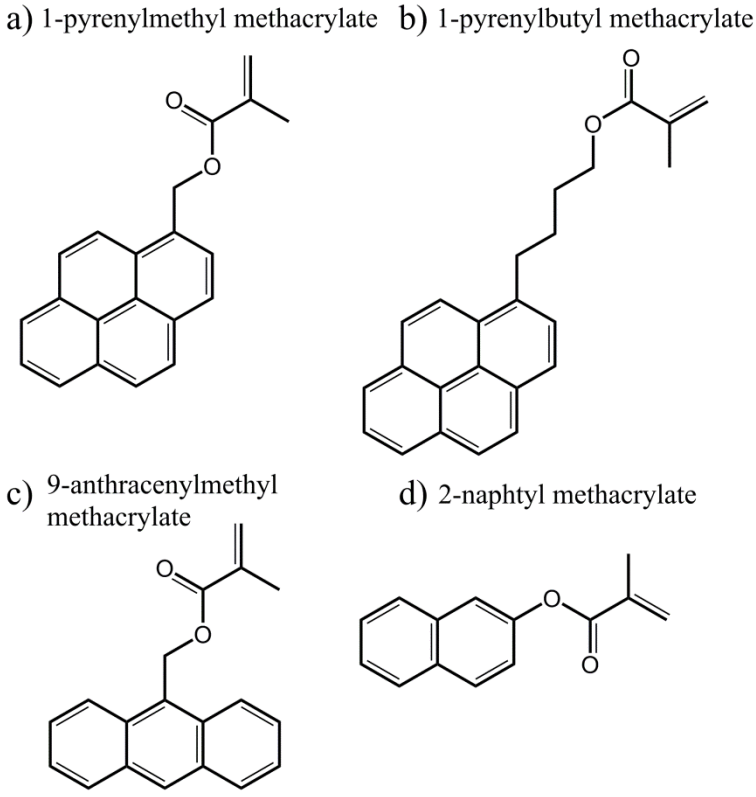

Figure 3.1 Chemical structure of fluorescent monomers used during free radical polymerization of fluorescently labelled PS: (a) 1- pyrenylmethyl methacrylate, (b) 1-pyrenylbutyl methacrylate, (c) 9-anthracenylmethyl methacrylate, (d) and 2-naphtyl methacrylate.

This chapter describes the free radical polymerization of unlabeled and labeled PS (Section 3.1), and esterification of 1-pyrenylbutyl methacrylate monomer (Section 3.2). Additionally the determination of the amount of fluorescent dye content in polymerized PS chains using ultraviolet-visible (UV-vis) spectroscopy is described (Section 3.3).

3.1 Free Radical Polymerization of Unlabeled and Labeled Polystyrene

One of the most common polymerization mechanisms is chain-growth polymerization. The main chain-growth polymerization method is called free radical polymerization. For this study I used free radical polymerization to synthesize unlabeled PS and fluorescently labeled PS.

Free radical polymerization is a relatively simple chemical procedure, as it mainly only requires mixing monomer molecules (M) with initiator molecules (I) and raising the temperature of the mixture. Free radical polymerization happens via three kinetic steps: initiation, propagation and termination.[68] In the initiation step, the initiator molecule (I) is activated by elevated temperature. The raised temperature thermally decomposes the initiator molecule (I) into two free radicals (R·):

$$I \xrightarrow{k_d} 2\,R\cdot,$$

where k_d is rate constant for initiator decomposition.[68] Decomposition of the initiator used in these studies, azobisisobutyronitrile (AIBN) into two 2-cyanoprop-2-yl radicals and a nitrogen gas molecule is shown in Figure 3.2a. Due to the unpaired valence electron, free radicals (R·) are chemically very reactive with surrounding molecules. As a result, addition of monomer starts immediately, where free radicals attack (R·) the

monomer (M) by taking an electron from monomer's carbon-carbon double bond and forming a single bond with the monomer. Polymerizing radical ($P_1\cdot$), that is a monomer with an unshared electron at the other end, is created:

$$R\cdot + M \overset{k_a}{\rightarrow} P_1\cdot,$$

where this addition step is characterized via rate constant k_a. As an example, the addition of a styrene monomer to an initiator 2-cyanoprop-2-yl radical is shown in Figure 3.2b.[68]

The polymerizing radical ($P_1\cdot$) then adds another monomer unit regenerating another polymerizing radical ($P_2\cdot$) by transferring the unshared electron to the chain end. This polymerizing radical ($P_2\cdot$) then adds another monomer, which adds another monomer and so on:

$$P_1\cdot + M \overset{k_p}{\rightarrow} P_2\cdot$$

$$P_2\cdot + M \overset{k_p}{\rightarrow} P_3\cdot$$

As a result the growth of polymer occurs. This step of free radical polymerization, called the propagation step, can be abbreviated as

$$P_x\cdot + M \overset{k_p}{\rightarrow} P_{(x+1)}\cdot,$$

where k_p is the propagation rate constant. As an example, styrene chain propagation is illustrated in Figure 3.2c.[68]

Growing chains are terminated either by combination or disproportionation. In the combination reaction, two polymerizing radicals combine and form a single terminated chain:

$$P_x\cdot + P_y\cdot \overset{k_{tc}}{\rightarrow} P_{(x+y)},$$

In the disproportionation reaction, two polymerizing radicals combine and form two terminated chains:

$$P_x \cdot + P_y \cdot \xrightarrow{k_{td}} P_x + P_y,$$

where k_{tc} and k_{td} are rate constants for termination by combination and disproportionation, respectively. Because of the random nature of the termination reaction with regard to chain length, a distribution of chain lengths is always obtained in a free radical polymerization. As an example, termination by combination (a) and disproportionation (b) of growing polystyrene chains are shown in Figure 3.3.[2,68,108]

Generally, the rate of addition of monomers into chains is much greater than that of the rate of initiator decomposition. This means that the initiator decomposition is rate controlling. As soon as the initiator radical is formed, it grabs the monomer and chain growth begins. The addition of monomers into chains happens almost immediately. The growing chains may react with other growing chains and terminate or they may add another monomer unit and continue its growth. The more there are monomer molecules in the vicinity of the chain radical, the higher the probability of another monomer addition. On the other hand, the more initiator radicals that are present competing for the available monomer, the shorter the chains will be, as there are more reactive ends available and thus the termination is more likely. Although the random nature of termination reaction always leads to a distribution of chain lengths, the overall molecular weight of the polymer is relatively unaffected by the reaction time. High molecular weight polymer can be produced almost immediately and the only thing that is

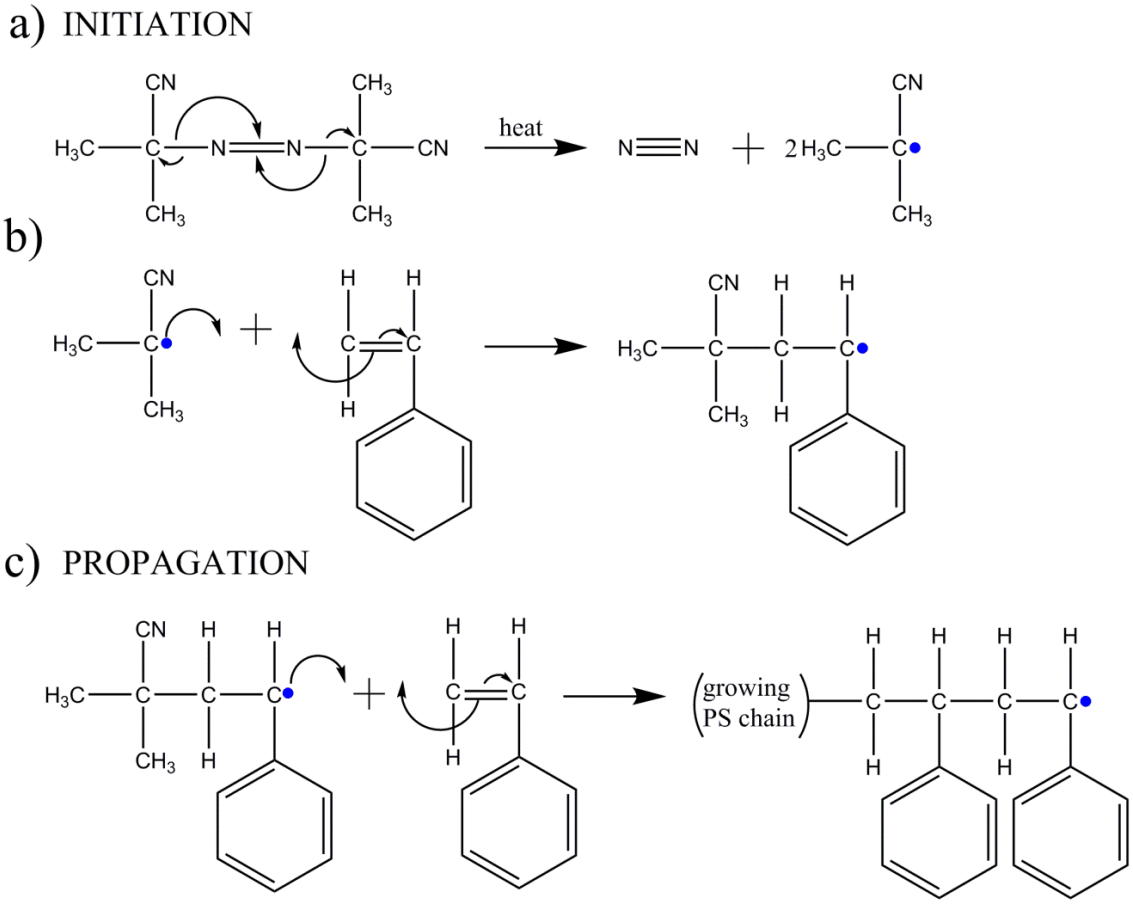

Figure 3.2 Initiation (a and b), and propagation (c) steps of free radical polymerization of polystyrene. Initiation step starts with (a) thermal decomposition of initiator azobisisobutyronitrile (AIBN) molecule into two free radicals and a nitrogen gas molecule, and continues with (b) addition of initiator radical to styrene monomer. (c) Additional styrene monomers add to the initiated monomer. Propagation of the polystyrene chain continues until termination occurs. Blue dot denotes the radical.

accomplished by allowing the reaction to proceed further is to increase the yield of polymer.[68]

It is difficult to quantitatively determine the chain radical concentration in the reaction mixture, as it is usually very low. However, a standard kinetic assumption of steady-state concentration of chain radicals can be made. It is reasonable to presume that

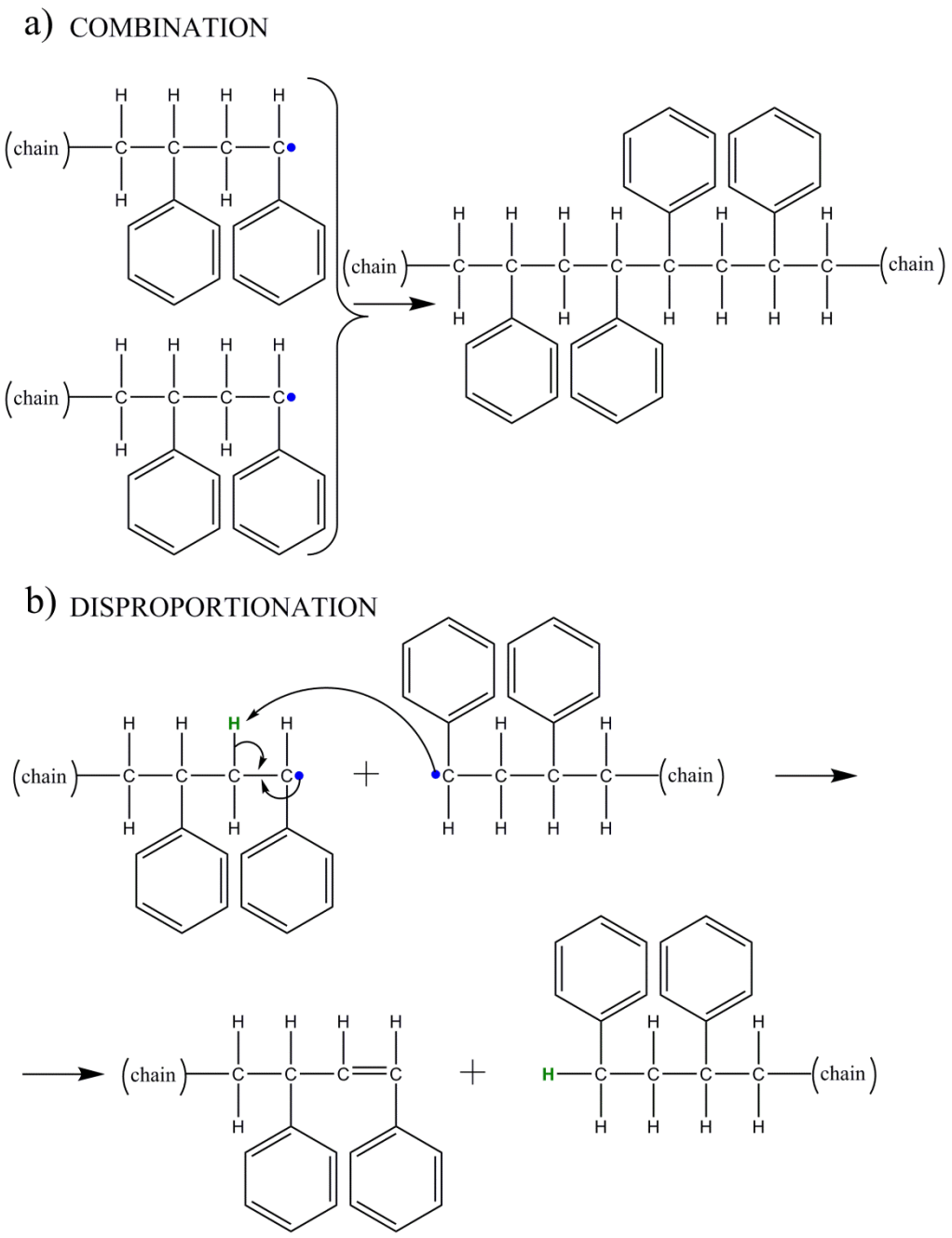

Figure 3.3 Termination by combination (a) and disproportionation (b) reaction in free radical polymerization of polystyrene. In both reactions two growing chains combine and form terminated chain(s). In disproportionation reaction, the free radical strips a hydrogen atom (green) from an active chain and a carbon-carbon double bond takes the place of the missing hydrogen, thus forming two terminated chains.

even though in the very beginning of the polymerization reaction the radical concentration increases, it reaches a constant value almost instantly and the growth of polymer happens at the same rate as the termination of polymer. When this steady state concentration of chain radicals is assumed, it can be shown that the overall rate of homogeneous free radical polymerization r_p, the rate at which monomer is converted to polymer, is

$$r_p = k_p \left(\frac{f k_d}{k_t}\right)^{1/2} [I]^{1/2}[M], \tag{3.1}$$

where f is the fraction of radicals generated that actually do initiate chain growth (~ 0.6 for AIBN over a wide range of monomer concentration), $k_t = k_{tc} + k_{td}$ is the termination rate, [I] is the initial initiator concentration (moles/volume) and [M] is the monomer concentration (moles/volume). Thus, from Eq. (3.1), the polarization rate scales with initiator concentration to the half power and monomer concentration to the first power.[68]

The degree of polymerization (DP) equals the rate of polymerization divided by the rate of initiation, resulting in

$$DP = \frac{k_p[M]}{(f k_d k_t)^{1/2}[I]^{1/2}}, \tag{3.2}$$

The initial concentration of initiator molecules determines the rate at which the polymer forms and the eventual molecular weight of the polymer, since each free radical is a growth site. Thus, when higher molecular weight polymer is desired, less initiator is needed.[2,68,108]

Reaction temperature has a strong effect on the degree and rate of free radical polymerization. The temperature dependence of the individual rate constants are given by the Arrhenius expression:

$$k_i = A_i e^{\frac{-E_i}{RT}},$$

where k_i is the rate constant for a particular elementary reaction, A_i is a frequency factor, and E_i the activation energy. The specifics of the effect of temperature to the polymerization are rather complicated and above the scope of this thesis. However, it can be said that in general, when temperature is increased, the rate of polymerization increases, but the rate of initiation also increases which ultimately decreases the degree of polymerization. The rule of thumb applies that for every 10 ^{o}C increase in reaction temperature, the rate approximately doubles.[68] Therefore, if high molecular weight polymers are desired, lower reaction temperatures with longer reaction times should be used. Or the opposite, if low molecular weight polymers are desired, higher temperatures with shorter reaction times should be used.

For this study the following protocol was used for free radical polymerization of neat PS and fluorescently labeled PS. The initiation and propagation stages of free radical polymerization of PS are shown in Figure 3.2. Prior to synthesizing PS, the styrene monomer needed to be deinhibited. Commercial styrene contains inhibitor, most commonly tertiary-butyl catechol (TBC) is used, to maintain the monomer quality as well as safety reasons, as styrene monomer is naturally reactive and polymerization occurs slowly even at ambient temperatures.[109] To deinhibit commercial styrene monomer, 1g of inhibitor remover with 1 g of calcium hydride per 100 mL of monomer were mixed in a beaker and left to stir overnight (minimum of 18 h). The beaker was covered all-around with aluminum foil to prevent photochemical initiation from light exposure. The next day, the deinhibited monomer was filtered through a funnel with filter paper, and then

stored in a non-transparent container inside the refrigerator until used (no longer than one month).

For polymerization of neat PS, deinhibited styrene was mixed with the initiator azobisisobutyronitrile (AIBN) into a test tube and capped. The exact quantity of deinhibited styrene and AIBN depended on the desired molecular weight and total amount of final polymer. For polymerization of fluorescently labeled PS, a small amount of labelled monomer was also included. A total of four different types of methyl methacrylate fluorophores were used: 1- pyrenylmethyl methacrylate, 1-pyrenylbutyl methacrylate, 9-anthracenylmethyl methacrylate, and 2-naphtyl methacrylate. The chemical structure of these different methyl methacrylate fluorophores used are shown in Figure 3.1 and the chemical structure of the synthesized labeled PS's are shown in Figure 3.4.

Table 3.1 lists all the unlabeled and labeled PS's I synthesized during this thesis. It includes the concentrations of initiator AIBN [I], styrene [S], and fluorescent monomer [label] used in the reaction mixture. Table 3.1 also shows the reaction temperatures (T) and reaction time (t), as well as the resulting number-average molecular weights, M_n, and weight-average molecular weights, M_w, and polydispersity index (PDI $= M_w/M_n$) as measured by gel permeation chromatography (GPC) at the Georgia Institute of Technology.

Prior to initiation, the reaction solution was purged with nitrogen gas for 15 – 30 min to remove oxygen, because oxygen can be an effective inhibitor for free radical polymerization.[68] The reaction was then initiated by submerging the test tube into an oil bath with oil pre-heated and equilibrated at the desired reaction temperature. As

discussed, the reaction temperature and reaction time depended on the desired molecular weight and total amount of final polymer (see Table 3.1). The reaction was terminated by precipitation into a large beaker of methanol at room temperature (typical ratio of reaction mixture : methanol was 1 : 10) for purification. Polymer was then filtered using a Bucher funnel and vacuum filtration, and subsequently re-dissolved into as little tetrahydrofuran (THF) as possible. Once dissolved, polymer and THF solution was precipitated again into methanol and filtered. In order to remove all unreacted monomer this dissolution and precipitation wash was repeated 4 times for unlabeled PS and 7 times for labeled PS, because it is extremely important to ensure that no labeled monomer remain. After final precipitation into methanol followed by filtration, the polymer was first dried in the fume hood at room temperature for ~ 24 h and then under vacuum at 50 ^{o}C for ~ 24 h.

Data in Table 3.1 confirms what was already discussed above, that decreasing the concentration of initiator in the reaction mixture increases the degree of polymerization (DP) (see Eq. (3.2)), but lowers the rate of polymerization, r_p (see Eq. (3.1)). In other words less initiator is needed to synthesize higher molecular weight polymers, however reaction has to run longer to yield sufficient amount of product. However, using less initiator also lowers the rate of polymerization, r_p (see Eq. (3.1)) and thus reaction has to run longer to yield sufficient amount of product. Additionally, lowering reaction temperature decreases the rate of polymerization and increases the degree of polymerization. For example, when we compare polymer "neat PS #17" of M_w = 19.3 kg/mol to polymer "long-Py-PS* #21" of M_w = 582.2 kg/mol in Table 3.1, we see that the lower molecular weight polymer "neat PS #17" was synthesized at 70 ^{o}C for only 40 min

with 1.00 g of AIBN, while the very high molecular weight polymer "long-Py-PS* #21" was synthesized only at 50 ^{o}C for 24 h with only 0.0045 g of AIBN present in reaction mixture.

The label content of different fluorescently labeled PS's is given in Table 3.1. We see that for this synthesis the label content varied from one dye unit per every 50 to 345 unlabeled styrene units. The details of determining the label content using ultraviolet-visible (UV-Vis) spectroscopy are given in Section 3.3.

Table 3.1 Specifics of all unlabeled and labeled PS's synthesized during this thesis.

Name given to polymer synthesized	Date made	S (ml)	Label (g)	AIBN (g)	Reaction temperature *T*	Reaction time *t*	M_n (kg/mol)	M_w (kg/mol)	PDI	Label content	
										mol %	Label per polymer chain
neat PS #1	10/23/09	25	N/A	0.25	60 °C	6 h	46.2	79.6	1.72	N/A	
long-Py-PS* #2	11/02/09	25	0.15	0.25	60 °C	6 h	46.3	77.5	1.67	0.30	1/333
short-Py-PS* #3	12/07/09	25	0.15	0.25	60 °C	6 h	45.0	76.7	1.70	0.33	1/300
neat PS #4	10/14/10	25	N/A	0.25	60 °C	6 h	42.0	75.0	1.79	N/A	
naphthalene-PS* #5	2/16/10	25	0.15	0.25	60 °C	6 h	46.3	79.1	1.71	Not measured	
ant-sgr-PS* #6	3/30/10	25	0.15	0.25	60 °C	6 h	35.9	64.2	1.79	0.29	1/345
short-Py-PS* #10	4/07/11	25	0.78	0.25	60 °C	6 h	52.4	86.8	1.65	1.93	1/52
ant-sgr-PS* #11	4/04/11	25	0.15	0.046	60 °C	6 h	69.6	111.0	1.59	0.55	1/180
neat PS #17	8/15/11	25	N/A	1.00	70 °C	40 min	12.0	19.3	1.61	N/A	
long-Py-PS*#21	7/01/11	25	0.15	0.0045	50 °C	24 h	367.8	582.2	1.58	0.34	1/293
short-Py-PS* #23	9/23/11	25	0.78	0.79	70 °C	40 min	14.7	24.1	1.63	2.4	1/42
short-Py-PS* #25	7/29/12	25	0.30	0.0045	50 °C	24 h	Not measured				

In Table 3.1, "Name" in the first column indicates which fluorescent label was used during polymerization of labelled PS. Here neat PS is used for unlabeled PS. Abbreviations: long-Py, short-Py, naphthalene and ant-sgr in the names indicate using 1-pyrenylbutyl methacrylate, 1- pyrenylmethyl methacrylate, 2-naphtyl methacrylate, and 9-anthracenylmethyl methacrylate, respectively.

Notations: (S) stands for styrene, (label) for fluorescent monomer, (I) for initiator AIBN, PDI for polydispersity index. Label per polymer chain of 1/300 reads as one fluorescent dye per 300 styrene unit.

3.2 Synthesis of Pyrene Labeled Monomer: 1-Pyrenylbutyl Methacrylate

In order to synthesize 1-pyrenylbutyl labeled PS (designated as long-Py-PS* in Figure 3.4) by free radical polymerization, the pyrene labeled monomer, 1-pyrenylbutyl methacrylate was first synthesized by esterification of methacryloyl chloride with 1-pyrene butanol (both purchased from Sigma Aldrich), as it was not available commercially. The procedure is based on protocol outlined by Jungki Kim, Connie Roth, and Rodney Priestley in June 2007 in Northwesten University and modified with the help of undergraduate student Sandra Boyce-Smith majoring in chemistry at Emory University.

The esterification of 1-pyrenylbutyl methacrylate is shown in Figure 3.5. The reaction is known as a nucleophilic addition/elimination reaction between an acyl chloride (methacryloyl chloride) and an alcohol (1-pyrene butanol). The first stage (addition) of the reaction involves a nucleophilic attack on the fairly positive carbon atom by one of the lone pairs on the oxygen of a 1-pyrene butanol molecule. The second stage (elimination) happens in two steps. In the first, the carbon-oxygen double bond reforms and a chloride ion is pushed off. That is followed by removal of a hydrogen ion by the chloride ion to give 1-pyrenylbutyl methacrylate and hydrogen chloride (HCl).[110]

1-pyrenylbutyl methacrylate is synthesized in 3 steps – reaction, separation and purification. Each step needs a minimum of one day to complete. In the first day, 5.25 g of 1-pyrene butanol, 200 ml of anhydrous tetrahydrofuran (THF) and 10 ml of tri-ethylamine (in that order) were mixed into a 500 ml round bottom flask that was pre

cooled in an ice/water bath at 0 ^{o}C sitting on top of stirring plate. Next, 40 ml of anhydrous THF and 7 ml of methacryloyl chloride was mixed and added drop-wise over the course of ~ 2 hours to the reaction mixture in the round bottom flask. The drip rate was kept at 1 drop every two seconds. Here, the tri-ethylamine is a used as an HCl scavenger, as it encourages the chlorine ion to leave and then helps in deprotonation (removal of a proton H^{+}) of the reaction intermediate (see Figure 3.5). Here, anhydrous THF is used, as opposed to regular THF, because it is important to eliminate all traces of water. Water reacts with methacryloyl chloride faster than 1-pyrene butanol and creates carboxylic acid instead of the desired product. As the esterification reaction between methacryloyl chloride and 1-pyrene butanol is exothermic, the ice/water bath is replenished every 10 minutes.

After all the THF/methacryloyl chloride was added, the reaction mixture was allowed to come to ambient temperature and left to react for total of 65 h under continuous dry N_2 flow. The reaction progress was checked every 24 h using thin layer chromatography (TLC).

The reaction stage was followed by liquid-liquid extraction (separation stage), where the reaction mixture was poured into a separatory funnel pre-filled half full with an aqueous saturated sodium bicarbonate solution (60 mg sodium bicarbonate and 600 ml of deionized water). The reaction product does not only contain the desired product 1-pyrenylbutyl methacrylate, but also residual alcohol and acid. The different polarity of these compounds causes them to prefer different phases, either non-polar organic or polar aqueous phase. All components, with the exception of 1-pyrenylbutyl methacrylate, which favors the non-polar THF solvent, prefers the polar aqueous phase. Thus, after

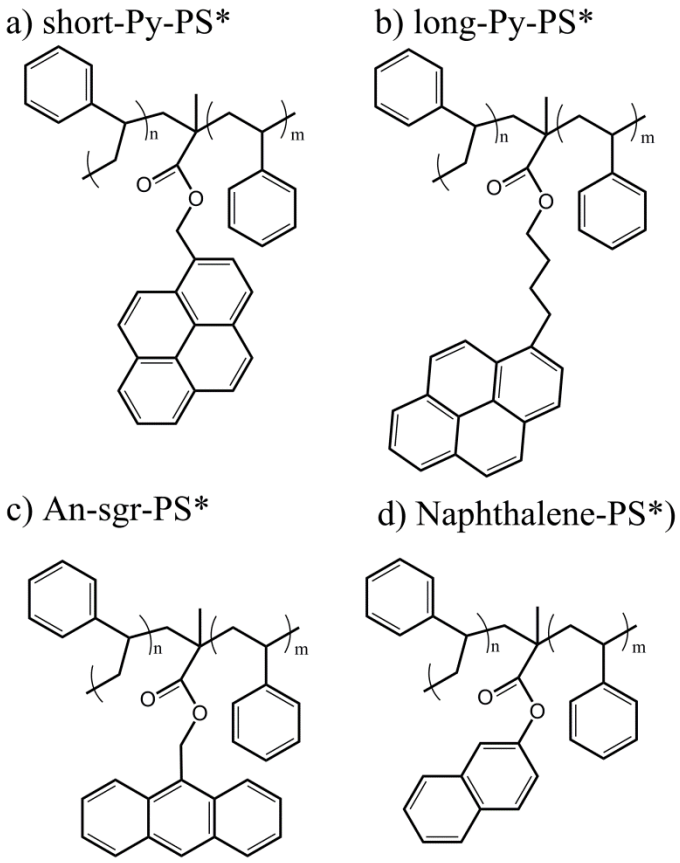

Figure 3.4 Chemical structure of fluorophore labeled polystyrenes synthesized by free radical polymerization: (a) 1- pyrenylmethyl methacrylate labeled PS (short-Py-PS*), (b) 1-pyrenylbutyl methacrylate labeled PS (long-Py-PS*), (c) 9-anthracenylmethyl methacrylate labeled PS (An-sgr-PS*), and (d) 2-naphtyl methacrylate labeled PS (Naphthalene -PS*).

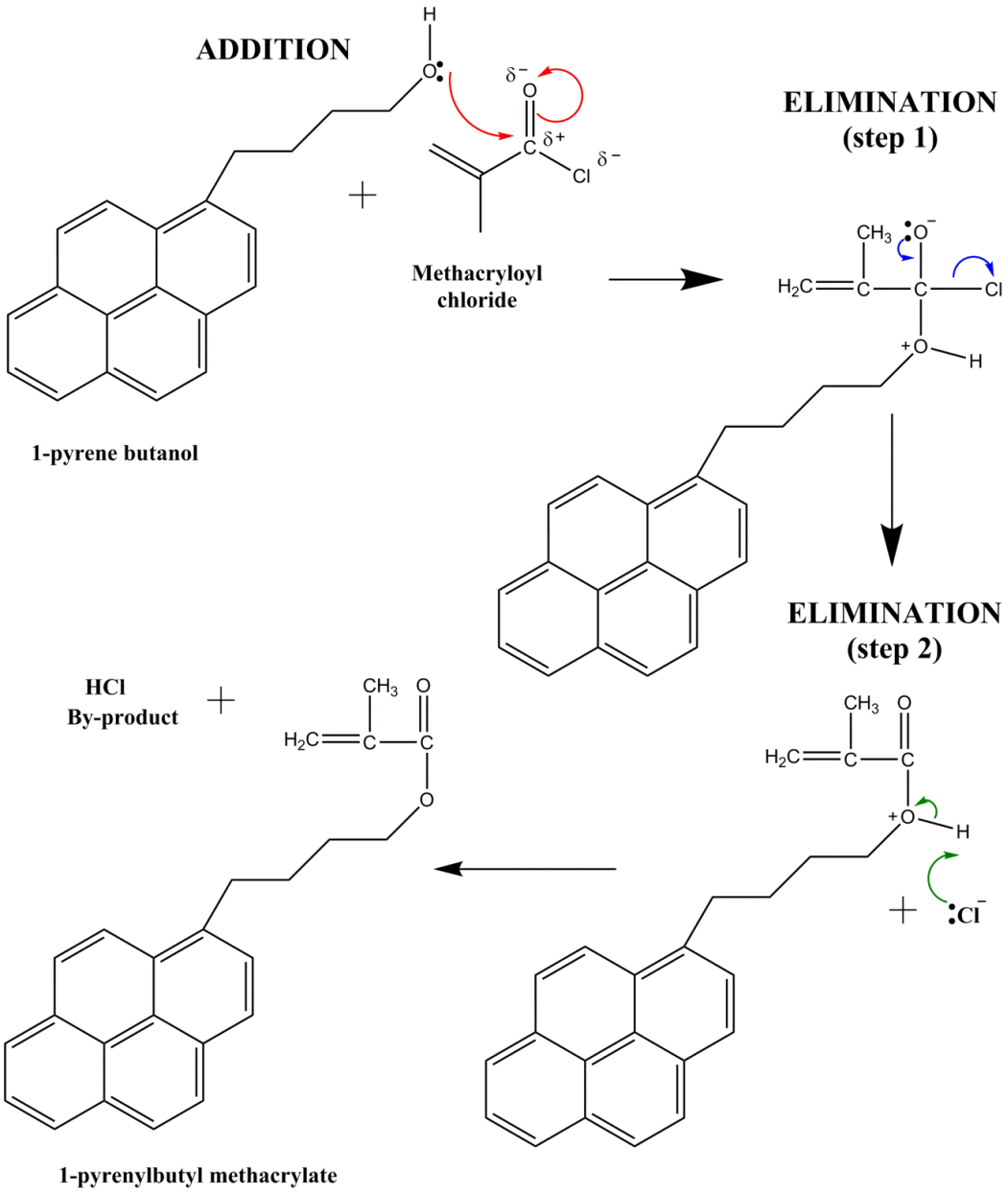

Figure 3.5 The synthesization steps of 1-pyrenylbutyl methacrylate through esterification reaction of methacryloyl chloride and 1-pyrene butanol. In the addition stage, the fairly positive carbon atom is attacked by one of the lone pairs on the oxygen of the alcohol. Next, in the elimination stage, the carbon-oxygen double bond reforms and a chloride ion is removed. The reaction is completed by removal of the hydrogen ion by the chloride ion and forming 1-pyrenylbutyl methacrylate and hydrogen chloride.

contacting the reaction mixture with aqueous sodium bicarbonate solution, three layers are formed in the separatory funnel. The desired product is contained in the uppermost layer of the funnel (a dark brown/yellow layer). The middle aqueous layer and the bottom layer of solids (composed of reaction by-product) are discarded. The solvent, THF is removed from the top organic layer by letting it evaporate at room temperature overnight under reduced pressure. This yields the final product (yellow solid), that is then purified by dissolution in boiling ethanol at 80 ^{o}C followed by recrystallization in an ice/water bath. After recrystallization ~ 3.7 g of 1-pyrenylbutyl methacrylate was obtained.

I confirmed the chemical structure of the synthesized 1-pyrenylbutyl methacrylate using 300 MHz Proton Nuclear Magnetic Resonance (^{1}H - NMR) spectrometer at Emory University Chemistry department NMR Research Center. The location of chemical shifts in the ^{1}H – NMR spectrum of 1-pyrenylbutyl methacrylate, shown in Figure 3.6, corresponds to the different chemical environments of the hydrogens in the molecule. Additionally the integrated area under each signal, that is proportional to the number of such hydrogens in the molecule giving rise to the signal, is shown below the horizontal axis for chemical shift values. As there are 6 different types of hydrogen atoms in 1-pyrenylbutyl methacrylate, the spectrum shows 6 different integrated peaks. The additional peaks at $\delta \sim 7.3$ ppm and at $\delta \sim 0.0$ ppm belong to the chloroform solvent and to the tetramethylsilane used as a reference compound, respectively. The multiplet at $\delta \sim 8$ ppm giving an integration of ~ 9 confirms the presence of a aromatic hydrogens (shown as blue in Figure 3.6). The two peaks at $\delta \sim 6.1$ ppm and $\delta \sim 5.5$ ppm with integration of 1.0 each belong to the vinylic hydrogens in $–C=CH_2$ (shown as red in Figure 3.6). The peaks at $\delta \sim 4.2$ ppm and $\delta \sim 3.4$ ppm with integration of 2.0 each correspond to allylic

hydrogens attached to the carbons on the ends of the tether connecting pyrene with methyl methacrylate (shown as purple and pink in Figure 3.6). The peaks at $\delta \sim 2.0$ ppm and $\delta \sim 1.9$ ppm with summative integration of ~ 7 correspond to the methyl hydrogens in $-CH_3$ and methylene hydrogens in $-CH_2$ (shown as orange and green in Figure 3.6).[111]

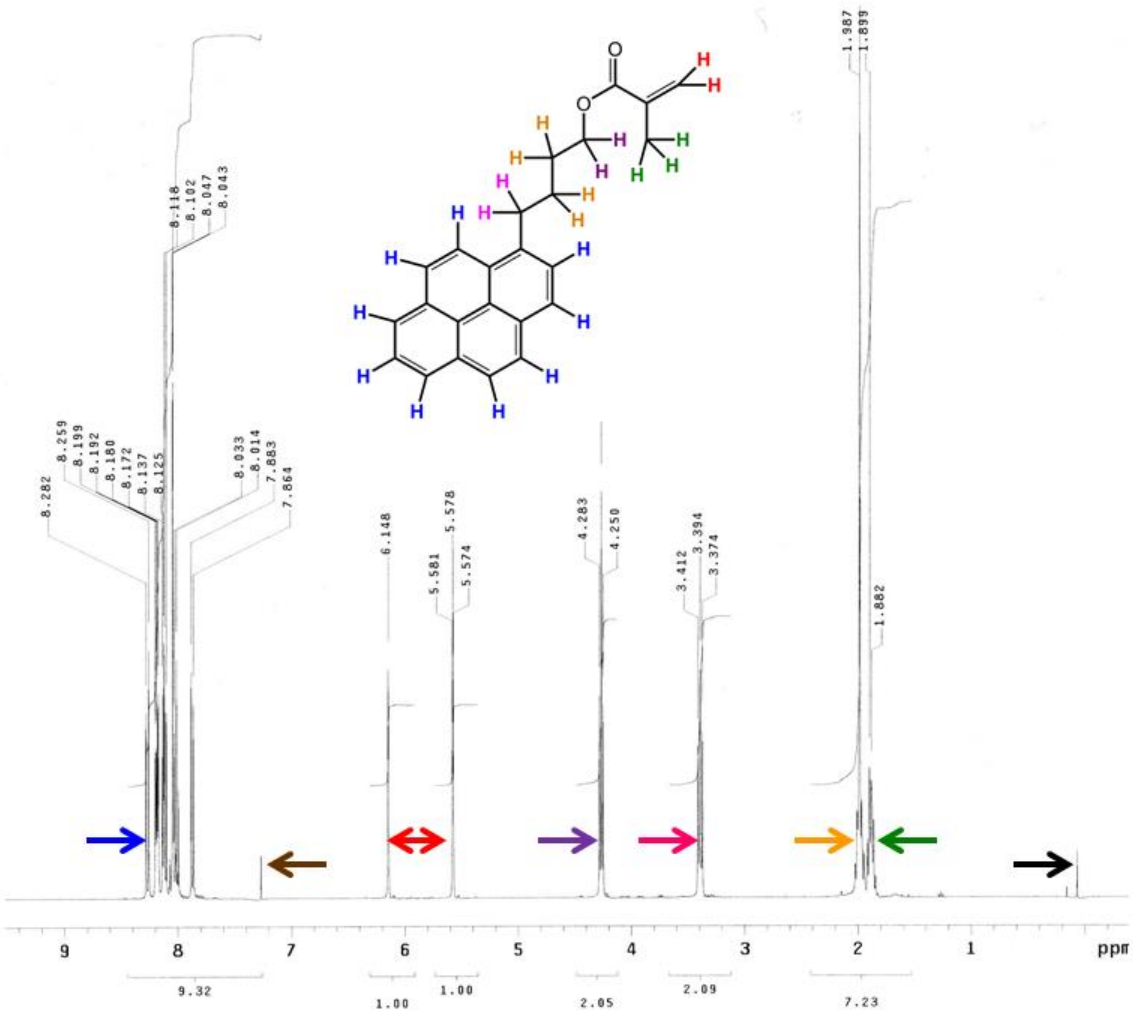

Figure 3.6 Chemical structure of ^{1}H NMR (300 MHz) spectrum of 1-pyrenylbutyl methacrylate dissolved in deuterated chloroform. Chemical structure is verified by the location of the chemical shifts (ppm) along with integral area under each peak (values given underneath the horizontal axis of chemical shifts). The color of the arrows next to the integrated peaks corresponds to the color of hydrogens (blue, red, purple, pink, orange and green) shown in the chemical structure of 1-pyrenylbutyl methacrylate. Peaks at $\Delta \sim 7.3$ ppm (brown) and 0.0 ppm (black) represent the hydrogen atoms in the chloroform solvent and reference compound, respectively.

3.3 Determination of Label Content of Fluorescently Labeled Polystyrene

The label content of all the fluorescently labeled PS (listed in Table 3.1) was determined using Ultraviolet-Visible (UV-Vis) spectroscopy. In UV-Vis spectroscopy, as the name hints, ultraviolet (wavelength from 180 to 400 nm) and visible light (wavelength from 400 to 780 nm) are shined onto molecules in the sample cuvette. As a result the electrons in the compound absorb light energy and transition to higher orbitals. UV-Vis spectrometer detects the energy at which the absorption occurs and displays a graph of the degree of absorption at each wavelength. The transmittance of the solution (ratio of transmitted light intensity to incident light intensity, I_t/I_0) is related to the concentration of the absorbing molecules through the Beer – Lambert Law:

$$\log\frac{I_0}{I_t} = A = \varepsilon L c,$$

where A is the absorbance (unitless), L is the path length through the sample (cm), c is the concentration of absorbing species in solution ($\frac{L}{mol}$) and ε is the molar absorptivity of the solute at the wavelength of interest ($\frac{L}{mol\ cm}$). The molar absorptivity ε (also called extinction coefficient) is constant for specific absorbing species and is used for comparing the relative absorbing strengths of different compounds. The absorbance depends on the total number of absorbing molecules in the light path through the sample cuvette. This means that when the concentration is doubled, so is the absorbance. However, it should be noted here that the Beer-Lambert law is not valid at concentrations where the absorbance $A > 1$.[2,111]

In this study, I determined the label content of 1- pyrenylmethyl methacrylate, 1-pyrenylbutyl methacrylate, and 9-anthracenylmethyl methacrylate labeled PS dissolved in HPLC[d] (spectroscopic) grade tetrahydrofuran (THF), by measuring the absorbance of these differently labeled polymers using UV-Vis spectroscopy (label content values are given in Table 3.1). The absorbance of labeled PS was measured at a wavelength for which the absorbance of the label (A_{label}) is much greater than that of a polymer ($A_{polymer}$). Thus, $A_{label} >> A_{polymer}$ and it can be assumed that

$$A_{solution} = A_{polymer} + A_{label} \approx A_{label} = \varepsilon_{label} L c_{label}$$

Here, the absorbance peak for neat polystyrene at around 260 nm is sufficiently far from the absorbance peaks A_{max} for pyrene monomers (1- pyrenylmethyl methacrylate and 1-pyrenylbutyl methacrylate) at 343.7 nm , and anthracene monomer (9-anthracenylmethyl methacrylate) at 386.6 nm.

The label content x of the labeled polymer was found as a ratio of the number of moles of labeled monomer c_{label} to the number of moles of labeled polymer $c_{polymer}$ and multiplied by 100:

$$x = \frac{c_{label}}{c_{polymer}} \times 100$$

Thus, the unit for dye content is mole percent (mol %). Using the Beer Lambert Law, the number of moles of labeled monomer c_{label} can be found from the absorbance spectra of the labeled polymer if the molar absorptivity ε of that dye label is known. In this study, I also assumed that the fluorophore attached to the polymer chain has the same absorptivity

[d] High Performance Liquid Chromatography

ε at its absorbance maximum A_{max} as the fluorescent monomer. In reality, the absorbance spectrum of the labeled polymer is slightly shifted (about 1 nm) as a result of covalent attachment to the polymer. As an example, the UV-Vis absorbance spectra as a function of wavelength for 1- pyrenylmethyl methacrylate monomer and 1- pyrenylmethyl methacrylate labeled PS ("short-Py-PS* #10" in Table 3.1) is shown in Figure 3.7. We see from Figure 3.7, that the pyrene monomer absorbance maximum at 343.7 nm is 1.1 nm lower than the absorbance maximum at 344.8 nm for pyrene labeled PS.

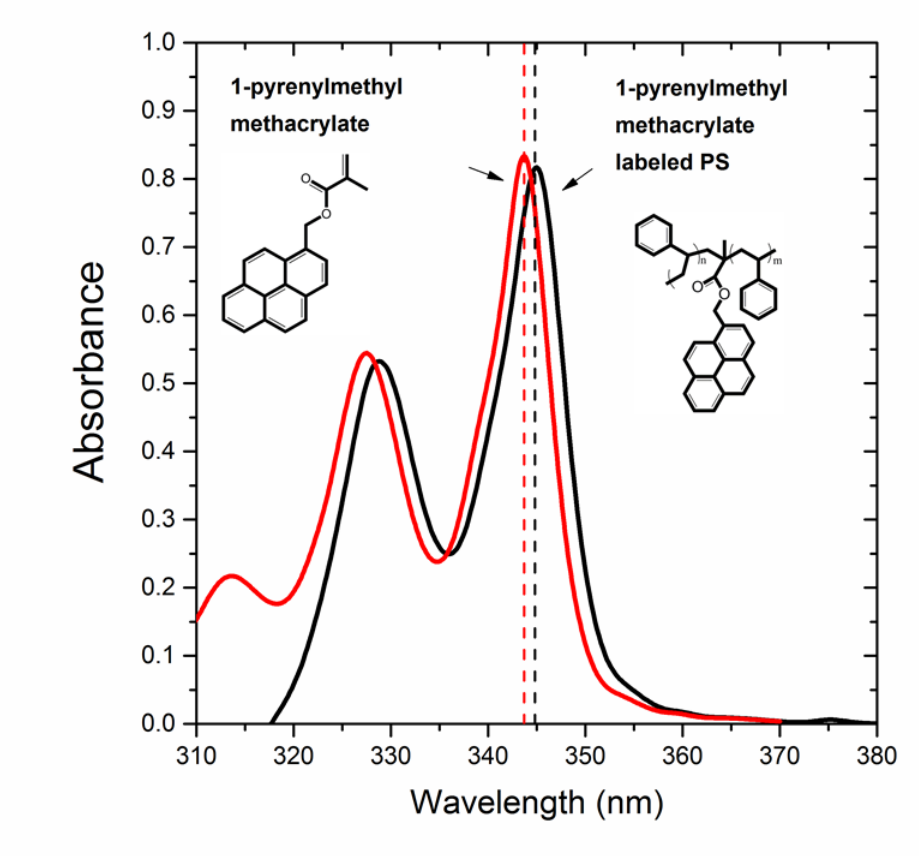

Figure 3.7 Normalized UV-Vis absorbance spectra as a function of wavelength for (red) 1- pyrenylmethyl methacrylate monomer with absorbance maximum A_{max} = 343.7 nm and (black) 1- pyrenylmethyl methacrylate labeled PS (corresponds to polymer "short-Py-PS* #10" in Table 3.1) with absorbance maximum A_{max} = 344.8 nm. Chemical structure shown for fluorescently labeled monomer (left) and labeled PS (right).

In this study I determined the molar absorptivity ε for 1-pyrenylmethyl methacrylate, 1-pyrenylbutyl methacrylate, and 9-anthracenylmethyl methacrylate monomers (the values are given in Table 3.2) by measuring the absorbance spectra of the labeled monomer dissolved in HPLC (spectroscopic) grade THF at different concentrations. We see from the Beer-Lambert Law that absorptivity ε is the slope of the linear plot of absorbance maximum A_{max} as a function of concentration c_{label} times the path length through sample L. Figure 3.8 shows the UV-Vis absorbance spectra for 1-pyrenylmethyl methacrylate monomer dissolved in HPLC (spectroscopic) grade THF at three different concentrations. The absorbance peak at wavelength of 343.7 nm versus concentration times light path length through sample along with a linear fit through data is plotted in the inset.

In this study, for each labeled monomer, at least three different absorbance spectra at different concentrations were measured. For all spectra collected, the concentrations were chosen so that the absorbance maximum $A_{max} < 1$. Table 3.2 lists the molar absorptivity values determined. We see that pyrene as an absorbing species absorbs light more strongly per molar concentration at a given wavelength than the anthracene monomer.

Table 3.2 Molar absorptivity ε for different fluorescently labeled monomers at wavelengths corresponding to the absorbance peak.

Fluorescent monomer	**Molar absorption ε ($\frac{L}{mol\ cm}$)**	**Wavelength at peak (nm)**
1- pyrenylmethyl methacrylate	49000	343.7
1-pyrenylbutyl methacrylate	48000	343.7
9-anthracenylmethyl methacrylate	8000	386.6

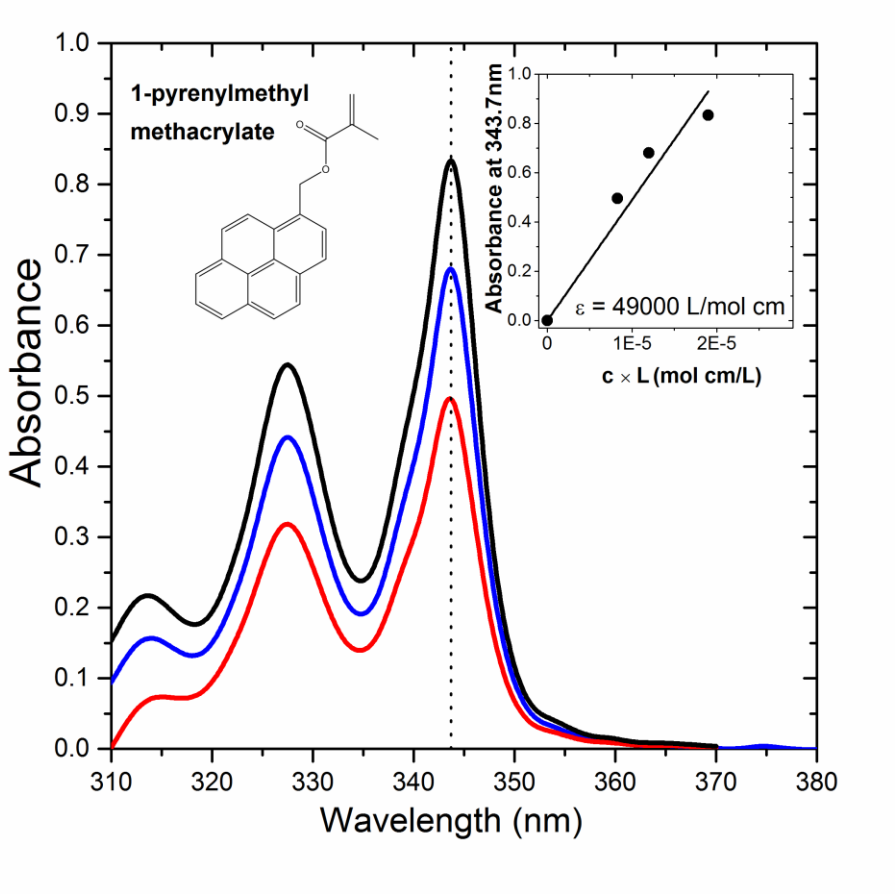

Figure 3.8 Figure 3.9 UV-Vis absorbance spectra for 1-pyrenylmethyl methacrylate monomer dissolved in HPLC (spectroscopic) grade THF at three different concentrations c = 5.6×10^{-5} g/ml (black), 3.7×10^{-5} g/ml (blue), and 2.5×10^{-5} g/ml (red), with absorbance maximums 0.83, 0.68, and 0.50, respectively at 343.7 nm (indicated with dashed vertical line). The inset shows the absorbance of monomer as a function of concentration multiplied by the length of light path through the sample *L*. The linear fit is forced to go through the origin corresponding to zero absorbance at zero concentration. From the Beer Lambert Law, the slope of the linear fit through data gives the molar absorptivity ε = 49000 $\frac{L}{mol\ cm}$ at the absorbance peak at 343.7 nm.

As an example, the calculation for determining the label content in 1-pyrenylmethyl methacrylate labeled PS ("short-Py-PS* #3" in Table 3.1) is shown. From the Beer-Lambert Law, the label concentration $c_{label} = \frac{A}{L\varepsilon_{label}}$ = 1.25 × 10^{-8} mol/ml. Here the absorbance maximum A_{max} = 0.61 at wavelength of 344.8 nm for labeled polystyrene dissolved into HPLC (spectroscopic) grade THF with concentration $c_{polymer}$ = 3.9 × 10^{-4} g/ml, the absorptivity ε = 49000 $\frac{L}{mol\ cm}$ from Table 3.2 and the length of light path through the sample L = 1 cm. Thus, the label content can be found:

$$x = \frac{c_{label}}{c_{polymer}} \times 100 = \frac{1.25 \times 10^{-8}\ \frac{mol}{ml}}{3.9 \times 10^{-4}\ \frac{g}{ml} \times \frac{1}{104\ \frac{g}{mol}}} \times 100 = 0.33\ mol\ \%$$

Here units of polymer concentration $c_{polymer}$ (g/ml) are converted to match the units of label concentration (mol/ml) by dividing the concentration with the molecular weight M_o = 104 g/mol of PS repeat unit. The label content x = 0.33 mol % means the labeled polystyrene has about one pyrene dye monomer per 300 styrene monomer units. The approximate chain length of this 1- pyrenylmethyl methacrylate labeled PS ("short-Py-PS* #3" in Table 3.1) with molecular weight of M_n = 45 kg/mol is 432 styrene units. Hence, it can be said that there is about one, maybe two, fluorescent dye monomers per polystyrene chain.

Chapter 4
Developing a Fluorescence Method for Detection of Phase Separation in Polystyrene / Poly (vinyl methyl ether) Blends

---

A version of this chapter was published as A. Kriisa, S. S. Park, and C. B. Roth, "Characterization of Phase Separation of Polystyrene / Poly(vinyl methyl ether) Blends Using Fluorescence," *J. Polym. Sci., Part B: Polym. Phys.* **2012**, *50*, 250-256.

Miscibility and phase separation of polymer blends has long been studied with the goal of understanding the specific interactions that affect blending.[112–116] This is especially important for polymers because large macromolecules limit the entropic contribution to the free energy of mixing allowing even weak interactions to play a significant role in miscibility. Specific information about these interactions, associated with the chemical structure of the polymers, has long been sought because it would facilitate the objective of being able to predict blend properties from those of their individual components, enabling the development of new polymer blends.[112]

Polystyrene (PS) / poly(vinyl methyl ether) (PVME) is one of the most prototypical miscible blends because of its easily accessible lower critical solution temperature (LCST).[47–52] Recent work by Green et al.[46] has brought new insight into the miscibility of PS/PVME blends providing specific information about the weak hydrogen bonding that is believed to make this blend miscible at room temperature. Previous work in the literature has long suggested that a specific interaction was present between PS and PVME leading to its LCST-type phase diagram. For example, this blends is miscible when cast from benzene, toluene, or tetrachloroethylene, yet the miscibility of this blend is disrupted when cast from chloroform, dichloromethane, or trichloroethylene[47,56] solvents which can form C-H to O hydrogen bonds.[46,54] In addition, infrared spectroscopy experiments have shown changes in PS's C-H out-of-plane vibration and PVME's ether oxygen stretching and vibration modes upon blending.[57–59] However, perhaps the most well-known peculiarity of this blend is the large ~40 ^{o}C increase in LCST when PS is deuterated.[60,61] Interestingly, the increase in LCST is only observed when the phenyl rings are deuterated, but not when only the backbone hydrogens are deuterated.[62,63] Green et al.'s measurements took this idea of selective deuteration further by investigating PS/PVME blends in which the ortho, para, or meta positions of the PS phenyl rings were selectively deuterated.[46] Using nuclear magnetic resonance to study the intermolecular exchange interaction of the nuclear Overhauser effect, Green et al. demonstrated the presence of a weak C-H to O hydrogen bond between the aromatic hydrogens of PS and the ether oxygen of PVME.[46,53] This hydrogen bonding interaction was found to be strongest for the meta and para positions, but slightly weaker for the ortho position due to steric limitations. The presence of such weak C-H to O hydrogen bonds have been well-

documented in small molecules[57,117] and tend to be more pronounced for sp^2, as opposed to sp^3, hybridized carbons such as in aromatic compounds. They are considerably weaker than the traditional (strong) hydrogen bonds more commonly studied in miscible polymer blends,[113,118] with bond lengths of 2-3 Å and bond strengths of only 0.5-1.0 kcal/mol,[54,55] comparable in strength to van der Waals forces, but still directional in nature.

Fluorescence is an ideal technique for identifying the early stages of phase separation because of its high sensitivity to local changes in composition. For their LCST comparison between backbone and side-group deuterated PS, Halary and coworkers[62,64] used the fluorescence intensity of an anthracene dye covalently labeled into the backbone of PS (anthracene-center-labeled PS) to measure the phase separation temperature T_s. The increase in fluorescence intensity observed at T_s was attributed to removal of static quenching of the anthracene dye when the PVME component phase separates from PS and moves away from the dye.[61] Beyond the added benefit of being able to measure both hydrogenated and deuterated systems, Halary et al.[64] demonstrated that fluorescence was as sensitive as small-angle neutron scattering, and considerably more sensitive than light scattering, in identifying the early stages of phase separation. This is not surprising given that fluorescence quenching is a very local phenomenon, with the local sphere of effective quenching extending out a few nanometers at most.[65] In addition, very low dye content is needed such that the fluorescently labeled PS chains (PS*) act as a tracer to measure the phase separation of the unlabeled PS chains, even if the molecular weight (MW) of the labeled-PS* does not match exactly with the unlabeled PS.[61]

Intrinsic fluorescence from the phenyl ring of PS has also been used to identify phase separation in PS/PVME blends with low PS concentration from changes in the

intensity ratio of excimer to monomer fluorescence. Monomer fluorescence originates from individual excited-state phenyl rings, whereas excimer fluorescence occurs when two neighboring phenyl rings can form an excited-state complex with the two rings in a parallel, sandwich-like orientation.[119,120] The excimer-to-monomer intensity ratio is roughly proportional to the local concentration of phenyl rings, thus as PS/PVME phase separates forming domains rich in PS, the excimer to monomer intensity ratio increases. Using intrinsic fluorescence, Gelles and Frank[121,122] investigated the dynamics of phase separation of 10/90 PS/PVME blends and demonstrated that fluorescence is sensitive enough to observe the early stages of phase separation with time scales in reasonable agreement with Cahn-Hilliard theory.[121] For PS concentrations greater than ~45% PS, the amount of excimer fluorescence is already sufficiently high in the one phase region making it difficult to observe changes upon phase separation.[123] However, overall fluorescence intensity does appear to increase upon phase separation for all blend compositions providing some measure of the phase separation temperature.

Here, I have investigated the effect of varying the chemical structure of an extrinsic fluorescent label on the measured phase separation of PS/PVME blends. This is the first study to investigate the changes in fluorescence emission spectra of various aromatic dyes covalently bonded to PS upon phase separation. I have observed that the proximity of the dye to the PS backbone in its covalent attachment influences the measure of the early stages of phase separation, with fluorophores covalently attached in closer proximity to the PS backbone identifying phase separation a few degrees earlier. Aromatic dyes such as pyrene and anthracene behave similarly, exhibiting a uniform increase in intensity at all wavelengths consistent with static fluorescence quenching

occurring in the one phase region. Based on work by Green et al., who identified a weak hydrogen bond between PS and PVME,[46] it seems likely that the fluorescence quenching in the presence of PVME is a result of a weak hydrogen bond between the PVME ether oxygen and the aromatic hydrogens on the pyrene and anthracene dyes. Pyrene has the advantage of having a higher quantum yield,[65] and that its fluorescence spectra is known to be sensitive to local polarity[124,125]and the glass transition temperature.[126,127]

4.1 Experimental

PS was synthesized via free radical polymerization resulting in a neat (no fluorescent label) PS with weight-average molecular weight, M_w = 75.0 kg/mol, and polydispersity index (ratio of weight-average molecular weight over number-average molecular weight), M_w/M_n = 1.79, which was used as the matrix PS for the majority of our studies. A higher MW, neat PS purchased from Pressure Chemical with M_w = 400 kg/mol, M_w/M_n = 1.06, was also used. Fluorescently labeled PS was synthesized by free radical polymerization in the presence of trace levels of methyl methacrylate fluorophores: 1- pyrenylmethyl methacrylate labeled PS (designated short-Py-PS* in Figure 4.1a) with M_w = 76.7 kg/mol, M_w/M_n = 1.70, at 0.33 mol % label content; 1-pyrenylbutyl methacrylate labeled PS (long-Py-PS* in Figure 4.1b) with M_w = 77.5 kg/mol, M_w/M_n = 1.67, at 0.30 mol %; and 9-anthracenylmethyl methacrylate labeled PS (An-sgr-PS* in Figure 4.1d) with M_w = 64.2 kg/mol, M_w/M_n = 1.79, at 0.29 mol %, and a second higher MW An-sgr-PS* with M_w = 111 kg/mol, M_w/M_n = 1.59, at 0.55 mol %. The specifics of the free radical polymerization of unlabeled PS and fluorescently labeled PS (short-Py-PS*, long-Py-PS*, and An-sgr-PS*) are discussed in detail in Chapter 3.1.

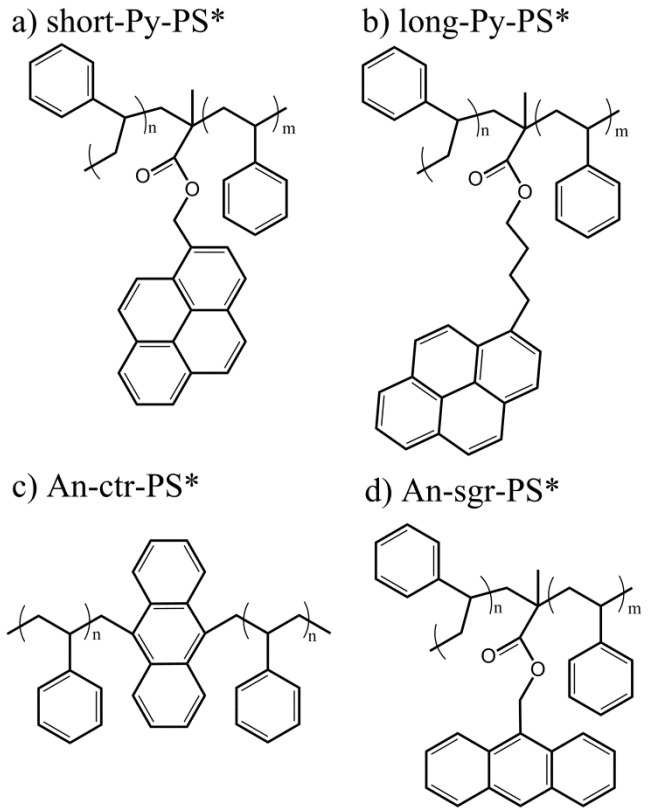

Figure 4.1 Chemical structure of fluorophore labeled polystyrenes: (a) 1-pyrenylmethyl methacrylate labeled PS (short-Py-PS*), (b) 1-pyrenylbutyl methacrylate labeled PS (long-Py-PS*), (c) anthracene center-labeled PS (An-ctr-PS*), and (d) 9-anthracenylmethyl methacrylate labeled PS (An-sgr-PS*).

The fluorescent monomers 1-pyrenylmethyl methacrylate and 9-anthracenylmethyl methacrylate were purchased from Polysciences, whereas 1-pyrenylbutyl methacrylate was synthesized by esterification of 1-pyrenebutanol and methacryloyl chloride.[127] The specifics of the synthesis of pyrene-labeled monomer 1-pyrenylbutyl methacrylate are given in Chapter 3.2. In addition, an anthracene center-labeled PS (An-ctr-PS*) with M_w = 108 kg/mol, M_w/M_n = 1.10 was purchased from Polymer Source, which has one anthracene fluorophore per chain located in the center of the backbone (see Figure 4.1c). PVME was purchased from Scientific Polymer Products

and measured to have M_w = 65.5 kg/mol, M_w/M_n = 3.95. Gel permeation chromatography (GPC) was done with tetrahydrofuran (THF) as eluent relative to PS standards, with PVME values determined using universal calibration with Mark-Houwink parameters a = 0.739 and $k = 1.35 \times 10^{-4}$ mL/g by Bauer et al.[128,e] Fluorophore label content was measured using UV-visible absorbance spectroscopy in high-performance liquid chromatography (HPLC) grade THF. The label content is less than 1:300 styrene monomers for the labeled-PS* polymers used in this study; thus, on average there is only one, maybe two, fluorophores per chain. The details on determining the label content using UV-vis absorbance spectroscopy are given in Chapter 3.3.

Blends were prepared by dissolving PS and PVME in toluene to produce solutions with 20 wt % total polymer content. 50/50 PS/PVME blends containing 5 wt % fluorescently labeled-PS were made by combining 45 wt % neat PS, 5 wt % labeled-PS*, and 50 wt % PVME, that is, (45/5)/50 (PS/PS*)/PVME, producing samples with <0.02 mol % total fluorescent dye content. Samples were spin coated onto quartz slides at 1500 rpm producing films of 2-2.5 μm in thickness. This thickness is larger than the < 1 μm thicknesses at which changes in phase separation temperature can be observed due to boundary effects.[129] Film thickness was confirmed by spin coating a second film at the same time from the same solution onto a silicon wafer with a native oxide layer and measuring the blend thickness with spectroscopic ellipsometry (J. A. Woollam M-2000).

---

[e] In our publications,[131,151] we made a numerical mistake by stating an incorrect value for parameter $k = 13.5 \times 10^{-3}$ mL/g. The correct value, stated here in the thesis, is $k = 1.35 \times 10^{-4}$ mL. This mistake does not affect the molecular weight values measured with gel permeation chromatography (GPC), as accurate values for parameter k were used during those measurements. Recently we have become aware of more accurate Mark-Houwink parameters a = 0.70 and $k = 2.33 \times 10^{-4}$ mL/g by Hess and Muller,[152] estimating the molecular weight for PVME as M_w = 55.7 kg/mol.

Before measurement, films were dried under vacuum at 80 ^{o}C for 24 h to remove residual solvent, and then stored under vacuum at room temperature until needed.

Steady-state fluorescence measurements were carried out using a Photon Technology International QuantaMaster fluorimeter. The polymer blends on quartz slides were covered by a second, clean quartz slide to minimize airflow to the sample during measurement, and placed in a home-built heater. Film temperature was controlled to within ±0.1 ^{o}C using a microprocessor controlled Kapton ribbon heater with resistance temperature detector (RTD) temperature sensor. The fluorescence measurements used a front-face geometry with an angle of incidence of 24^{o} for samples containing fluorophores, or 30^{o} for measurements using the intrinsic fluorescence of the PS phenyl ring. Excitation and emission slits were set to 5.0 nm (ex) and 4.5 nm (em) bandpass for pyrene and 6.0 (ex) and 5.0 (em) bandpass for anthracene. All fluorescence measurements (both emission scans and time-based) started by letting the polymer blend reach 80 ^{o}C and waiting at least 10 min for the sample to equilibrate. In the case of the fluorescence emission scans, an emission spectrum was recorded at constant temperature, then the temperature was successively increased by 2.5 ^{o}C, waiting 5 min to ensure thermal equilibrium before taking another emission scan, until at least 150 ^{o}C was reached. For the time-based measurements, the samples were heated from 80 to 160 ^{o}C at a ramp rate of 1, 10, or 16 ^{o}C/min, while simultaneously measuring the fluorescence intensity during a 3 s time window every 15 or 30 s, at a wavelength of 382 nm for pyrene or 449 nm for anthracene.

4.2 Results and Discussion

Figure 4.2 shows select emission spectra of short-Py-PS* in a (45/5)/50 (PS/PS*)/PVME blend collected at constant temperature, every 2.5 ^{o}C on heating. Before phase separation (Figure 4.2a), the fluorescence intensity of the spectra is found to decrease slowly with increasing temperature with little change in shape of the spectrum. After phase separation (Figure 4.2b), a sharp increase in fluorescence intensity is observed, which has been attributed to the removal of fluorescence quenching of the dye by the local presence of the more polar PVME component in the miscible state.[61] Based on the work by Green et al.,[46] we believe weak hydrogen bonds are also forming between the aromatic hydrogens of the dye and the ether oxygen of PVME, thus providing a very local (few nanometer) sensitivity to the phase separation process. Figure 4.2a also gives a direct comparison of the fluorescence emission spectra before, at 80 ^{o}C (solid black curve), and after, at 135 ^{o}C (dashed black curve), phase separation. A small horizontal red shift of ~2 nm is evident from 80 to 135 ^{o}C. However, this small red shift appears to be primarily due to the temperature difference between the two spectra because it is not present when spectra before and after phase separation are compared at the same temperature. In addition, such small red shift with increasing temperature has been previously observed for pyrene in 100 % PS films.[130]

Figure 4.3 plots the temperature dependence of the intensity of short-Py-PS* in a (45/5)/50 (PS/PS*)/PVME blend where the sharp increase in intensity upon phase separation of the blend is evident. The reproducibility of the measurement across multiple samples is demonstrated in Figure 4.3a with several time-based measurements of the

intensity at 382 nm (vertical dashed line in Figure 4.2) and the integrated intensity from 376 to 416 nm of the emission spectra in Figure 4.2. A time-based scan for a (90/10) (PS/PS*) sample is also shown illustrating that the small decrease in intensity before phase separation is not due to the presence of PVME, but the large increase in intensity indicating phase separation from the PVME is clearly absent. This small reduction in overall fluorescence intensity with increasing temperature is commonly observed for fluorophores and is explained by the increased ability of excited-state fluorophores to return to their ground state via internal conversion or nonradiative recombination with higher thermal energy.[65,127,130] There is good agreement in the onset temperature of the sharp increase in fluorescence intensity between the time-based and integrated intensity data sets. The sharp increase in intensity upon phase separation is less intense for the integrated intensity measurements collected every 2.5 ^{o}C, which wait 5 min between heating steps, because the effective heating rate is slower (<1 ^{o}C/min) and the phase separation process is continuing. In general, the sharp increase in fluorescence intensity upon phase separation is larger for faster heating rates as demonstrated in Figure 4.3b for a series of time-based measurements ramping at 1, 10, and 16 ^{o}C/min. To quantify the phase separation temperature T_s, we have made linear fits to the data in the region before and after the sharp increase in fluorescence intensity and have chosen to identify T_s as the intersection of these linear fits. As expected for a dynamical process such as phase separation, the measured phase separation temperature increases with increasing ramp rate: 124.2 ^{o}C at 1 ^{o}C/min, 130.8 ^{o}C at 10 ^{o}C/min, and 134.8 ^{o}C at 16 ^{o}C/min. A similar trend was observed and discussed by Halary et al.[61]

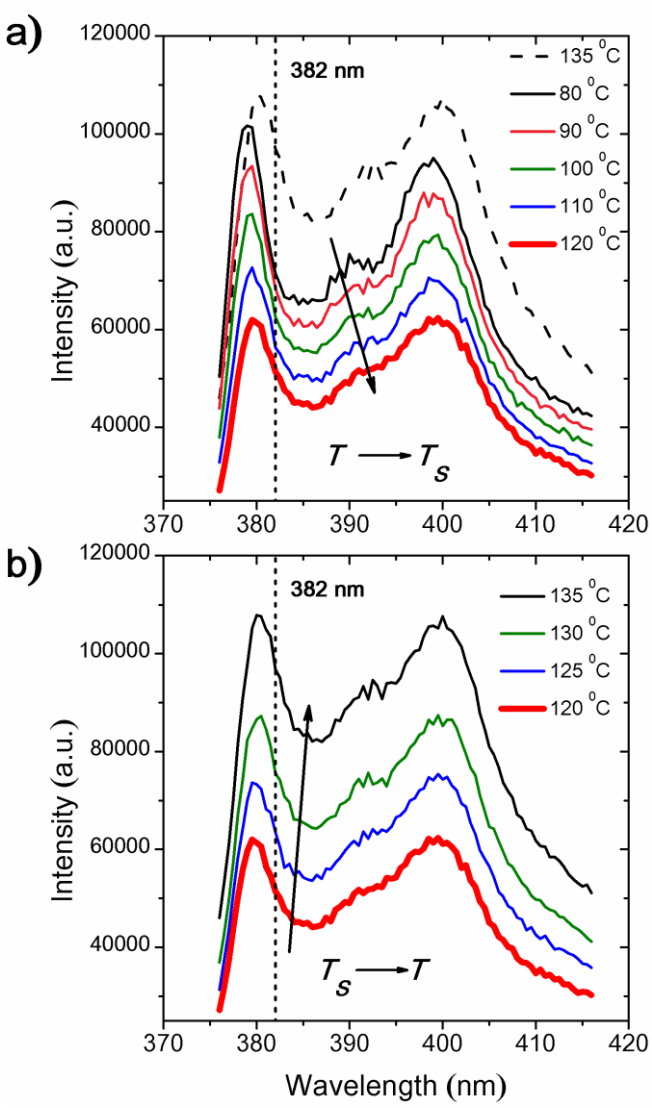

Figure 4.2 Fluorescence emission spectra for short-Py-PS* in a (45/5)/50 (PS/PS*)/PVME blend collected at different temperatures: (a) before phase separation ($T \rightarrow T_s$), the fluorescence intensity decreases slowly with increasing temperature; (b) after phase separation ($T_s \rightarrow T$), a sharp increase in intensity is observed resulting from the reduction in fluorescence quenching of the pyrene dye when in the presence of PVME. Phase separation occurred at T_s = 124.2 ^{o}C for this sample. The dashed curve in (a) corresponding to 135 ^{o}C is the same as the solid black line in (b), facilitating direct comparison of the emission spectra before and after phase separation and indicating a slight red shift of ~2 nm.

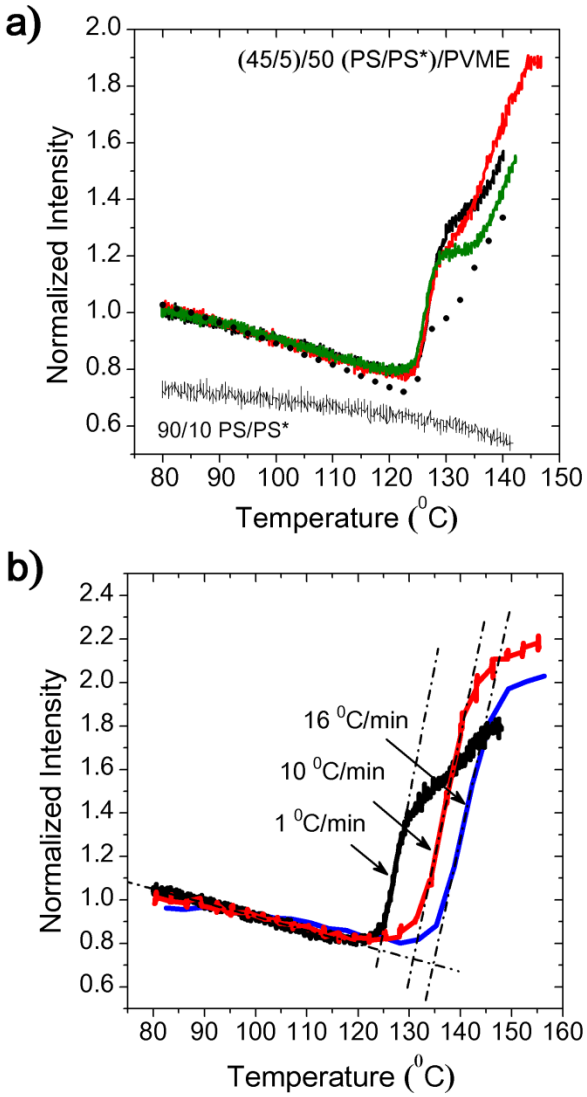

Figure 4.3 Fluorescence intensity of short-Py-PS* in a (45/5)/50 (PS/PS*)/PVME blend as a function of temperature: (a) intensity at 382 nm (vertical dashed line in Figure 4.2) for time-based scans at 1 °C/min (green, red and black curves) demonstrating reproducibility across multiple nominally identical samples; and the integrated intensity from 376 to 416 nm of emission spectra in Figure 4.2 (circles). For comparison, a time-based scan at 1 °C/min for a (90/10) (PS/PS*) sample (thin black line) is also shown. (b) Intensity at 382 nm collected at different ramping rates, 1 °C/min (black), 10 °C/min (red), and 16 °C/min (blue). Dash-dot lines are linear fits to the data above and below phase separation, with the phase separation temperature T_s identified as the intersection of these linear fits: 124.2 °C at 1 °C/min, 130.8 °C at 10 °C/min, and 134.8 °C at 16 °C/min.

Given the very local interactions that affect the sensitivity of fluorescence to phase separation in PS/PVME blends, we investigate here whether the proximity of the fluorescent dye to the PS backbone in its covalent attachment affects its measure of the phase separation temperature. Figure 4.4 graphs emission spectra at select temperatures for (45/5)/50 (PS/PS*)/PVME blends collected every 2.5 ^{o}C on heating before (Figure 4.4a, c, and e) and after (Figure 4.4b, d, and f) phase separation for the three additional fluorophores shown in Figure 4.1: long-Py-PS* (a,b), An-ctr-PS* (c,d), and An-sgr-PS* (e,f). All these aromatic dyes exhibit similar behavior to short-Py-PS* (shown in Figure 4.2), in that there is a slow decrease in intensity with increasing temperature before phase separation, followed by a sharp increase in intensity upon phase separation resulting from the reduced fluorescence quenching by the local removal of the more polar PVME component in the blend. The shape of all the fluorescence emission spectra remain primarily unchanged after phase separation. (The increase in intensity of the second peak in An-ctr-PS* relative to the first peak, seen in Figure 4.4c, occurs upon heating prior to phase separation.) Because the increase in fluorescence intensity at T_s has been attributed to removal of static fluorescence quenching,[61] which results from specific interactions between the dye and a nearby quenching molecular unit,[65] we would not anticipate a change in the fluorescence spectra upon phase separation. Simply an increase in overall intensity is expected as a larger fraction of dyes are able to fluoresce once the source of the quenching has phase separated from the PS component. Thus, our observations, in Figure 4.4, further support the notion that a weak local interaction is occurring between the PVME and the aromatic dyes. This interaction is likely a weak hydrogen bond

between the ether oxygen in PVME and the aromatic hydrogens of the fluorophores, similar to that observed between PVME and PS by Green et al.[46]

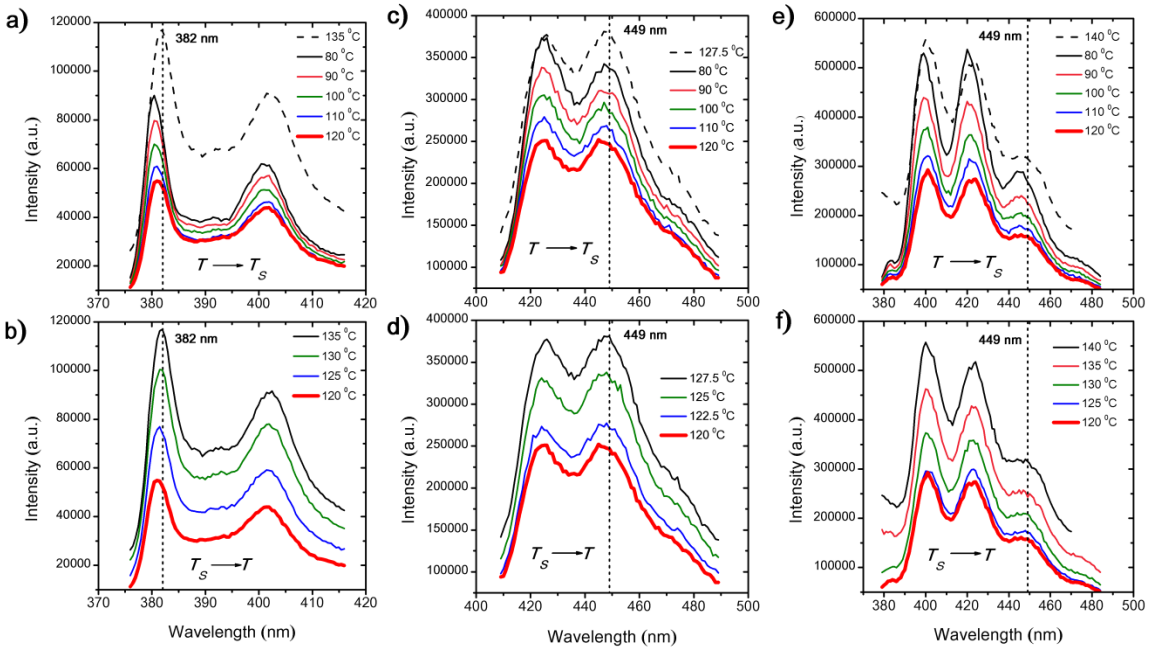

Figure 4.4 Fluorescence emission spectra for (45/5)/50 (PS/PS*)/PVME blends collected at different temperatures for long-Py-PS* (a) before phase separation ($T_s \rightarrow T$) and (b) after phase separation ($T_s \rightarrow T$); and similarly for An-ctr-PS* (c) and (d) and An-sgr-PS* (e) and (f). As in Figure 3.2, the dashed curve in upper graph corresponds to the highest temperature in the lower graph, facilitating comparison of the emission spectra before and after phase separation.

The temperature dependence of the intensity from time-based scans collected on heating at 1 ^{o}C/min are shown in Figure 4.5 comparing the four different fluorophores investigated in this study (Figure 4.1). Although only a single measurement for each dye is plotted in Figure 4.5, an average of 3-7 measurements for each fluorophore was done to determine the phase separation temperatures T_s. Figure 4.5a compares the pyrene dyes for which the intensity was measured at 382 nm. We find that the short-Py-PS* fluorophore (T_s = 124.6 ± 1.3 ^{o}C), located closer to the PS backbone, consistently

indicates phase separation a few degrees earlier than the long-Py-PS* fluorophore (T_s = 127.5 ± 1.5 ^oC) with longer tether. Similarly for the anthracene dyes shown in Figure 4.5b, measured at an intensity of 449 nm. The An-ctr-PS* fluorophore (T_s = 125.4 ± 1.5 ^oC), located within the PS backbone, consistently indicates phase separation a few degrees earlier than the An-sgr-PS* fluorophore (T_s = 128.3 ± 1.5 ^oC), located to the side of the PS backbone. Interestingly, the pyrene dyes exhibit the sharp increase in fluorescence intensity, indicating that phase separation begun, earlier than the anthracene dyes. This is especially apparent comparing short-Py-PS* fluorophore (T_s = 124.6 ± 1.3 ^oC) with the An-sgr-PS* fluorophore (T_s = 128.3 ± 1.5 ^oC), which have the dyes located at the same distance from the PS backbone (see Figure 4.1). This effect may result from the higher quantum yield of the pyrene fluorophores.[65] A standard t-test analysis was used to verify that the measured T_s values are statistically different. These differences in the measured phase separation temperature do not result from the slight differences in MW of the labeled-PS chains. To verify this, a second An-sgr-PS* with higher MW was polymerized (M_w = 111 vs 64.2 kg/mol, roughly a factor of two larger, see Table 3.1 in Chapter 3) and the same phase separation temperature T_s was measured, to within experimental error, as the lower MW An-sgr-PS*.

To demonstrate that the 5 % fluorophore labeled-PS* chains are measuring the phase separation temperature of the 45 % unlabeled PS matrix, Figure 4.6 compares the temperature dependence of the fluorescence intensity for An-ctr-PS* (M_w = 108 kg/mol) in (45/5)/50 (PS/PS*)/PVME blends, from time-based scans at 449 nm measured on heating at 1 ^oC/min, for two different matrix PS MWs. The 45 % unlabeled PS matrix was changed from M_w = 75.0 kg/mol to M_w = 400 kg/mol, which decreased the phase

separation temperature T_s from 126.7 ^oC to 111.1 ^oC, as would be expected. These values are in good agreement with literature values,[50,61,62] although direct comparisons are difficult to make given the different MWs used in the literature. For instance, Larbi et al.[62] measure $T_s \approx 131$ ^oC for a 50/50 mixture of PS (M_w = 65k, M_w/M_n = 1.73) and PVME (M_w = 99k, M_w/M_n = 2.13) and $T_s \approx 113$ ^oC for a 50/50 mixture of PS (M_w = 514k, M_w/M_n = 1.80) and the same PVME. We note that Nishi and Kwei found that phase separation scales with the weight average molecular weight M_w.[49]

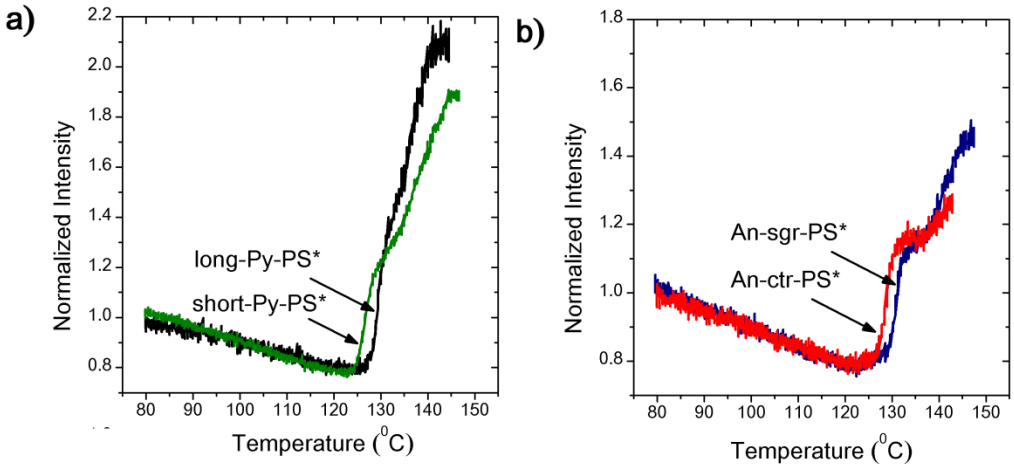

Figure 4.5 Temperature dependence of the fluorescence intensity for (45/5)/50 (PS/PS*)/PVME blends measured on heating at 1 ^oC/min. Pyrene intensity at 382 nm (a): the short-Py-PS* fluorophore (green, T_s = 124.6 ± 1.3 ^oC) consistently indicates phase separation a few degrees earlier than the long-Py-PS* fluorophore (black, T_s = 127.5 ± 1.5 ^oC). Anthracene intensity at 449 nm (b): The An-ctr-PS* fluorophore (red, T_s = 125.4 ± 1.5 ^oC) consistently indicates phase separation a few degrees earlier than the An-sgr-PS* fluorophore (blue, T_s = 128.3 ± 1.5 ^oC). T_s values are based on an average of 3-7 measurements for each fluorophore.

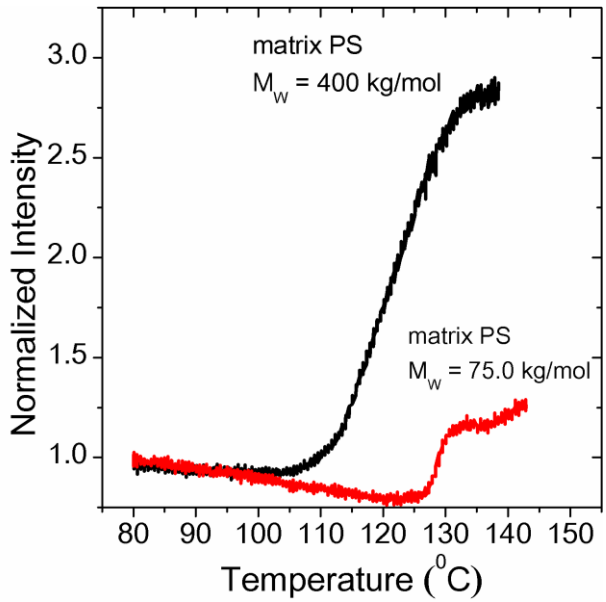

Figure 4.6 Fluorescence intensity at 449 nm for An-ctr-PS* in (45/5)/50 (PS/PS*)/PVME blends as a function of temperature where the 45 % unlabeled PS matrix MW has been increased from M_w = 75.0 kg/mol (red) to M_w = 400 kg/mol (black) shifting the phase separation temperature down from T_s = 126.7 ^oC for the 75k PS matrix to T_s = 111.1 ^oC for the 400k PS matrix. The 5 % An-ctr-PS* label M_w = 108 kg/mol was left unchanged.

The effect of different short-Py label content and different short-Py labeled polystyrene (short-Py-PS*) content on the reproducibility of phase separation temperature T_s was also studied. The reproducibility of fluorescence emission scans of 50/50 PS/PVME blends with 1%, 2%, 3%, 5%, and 10% of short-Py-PS* label content in the blend are shown in Figure 4.7 a- e, respectively.[f] As is clear from Figure 4.7 a- e, the reproducibility of the T_s measurements improves with the increasing amount of short-Py-PS* content in the (PS/PS*)/PVME blend with best reproducibility found for the

[f] The data presented in Figure 4.7 is taken from Sung Park's undergraduate honors thesis. Sung Park worked as an undergraduate student in Connie Roth's lab; during the time the data shown in Figure 4.7 was collected, I was responsible for helping him with the data collection and analyses.

(40/10)/50 (PS/short-Py-PS*)/PVME blend. Next, short-Py-PS* in PS/PVME blend was replaced with another differently labeled PS, 5x-short-Py-PS*, one containing the same fluorescent short-Py dye but with considerably higher amount of fluorescent dyes per polystyrene chain. 5x-short-Py- 5x-short-Py-PS* contains about 1 short-Py monomer per 50 styrene units, while short-Py-PS* contains about 1 label per 300 styrene units. Thus, a composition of (48/2)/50 (PS/5x-short-Py-PS*)/PVME blend would roughly contain about the same amount of fluorescent dyes as the (40/10)/50 (PS/5x-short-Py-PS*)/PVME blend. Comparison of Figures 4.7 e and f demonstrates that the reproducibility of T_s is very good for both (40/10)/50 (PS/5x-short-Py-PS*)/PVME and (40/10)/50 (PS/short-Py-PS*)/PVME blends.

4.3 Conclusions

The results discussed in this chapter, the changes in the fluorescence emission spectra of aromatic dyes covalently bonded to PS upon phase separation from PVME, were never before characterized in the research literature. I investigated if the proximity of the pyrene or anthracene fluorophore to the PS backbone in how it is covalently attached influences the measure of the phase separation temperature T_s. I found that the fluorescence intensity increases primarily uniformly upon phase separation for all fluorophores with little change if any in the spectral shape. This is consistent with a mechanism of static fluorescence quenching of the dyes occurring in the presence of PVME, as originally proposed by Halary et al.[61] for anthracene (An-ctr-PS*). Static quenching is associated with the presence of a specific interaction between the dye and a nearby quenching molecular unit. Recent work by Green et al.[46] has identified the

presence of a weak hydrogen bond in this blend between the aromatic hydrogens of PS and the ether oxygen of PVME. The results discussed in this chapter suggest that a similar weak hydrogen bonding interaction is likely occurring between the hydrogens of the aromatic dyes and the ether oxygen of PVME resulting in the observed fluorescence quenching when the blend is in the single-phase regime. It was demonstrated that aromatic dyes such as pyrene and anthracene are equally sensitive to phase separation in PS/PVME blends, as seen by a sharp increase in fluorescence intensity upon phase separation. I found that pyrene fluorophores signal the initiation of phase separation earlier than the anthracene fluorophores. In comparing similar dyes, fluorophores in which the dye is covalently bonded closer to the PS backbone denote phase separation a few degrees earlier than those fluorophores in which the dye is located further away on a covalent tether. As the PVME component moves further away from the PS component upon phase separation, local breaking of these weak hydrogen bonds connecting the PVME oxygen with the aromatic rings of PS and the aromatic dyes, leads to the observed increase in fluorescence intensity. These observations indicate that fluorescence is sensitive to the early initiation of phase separation.

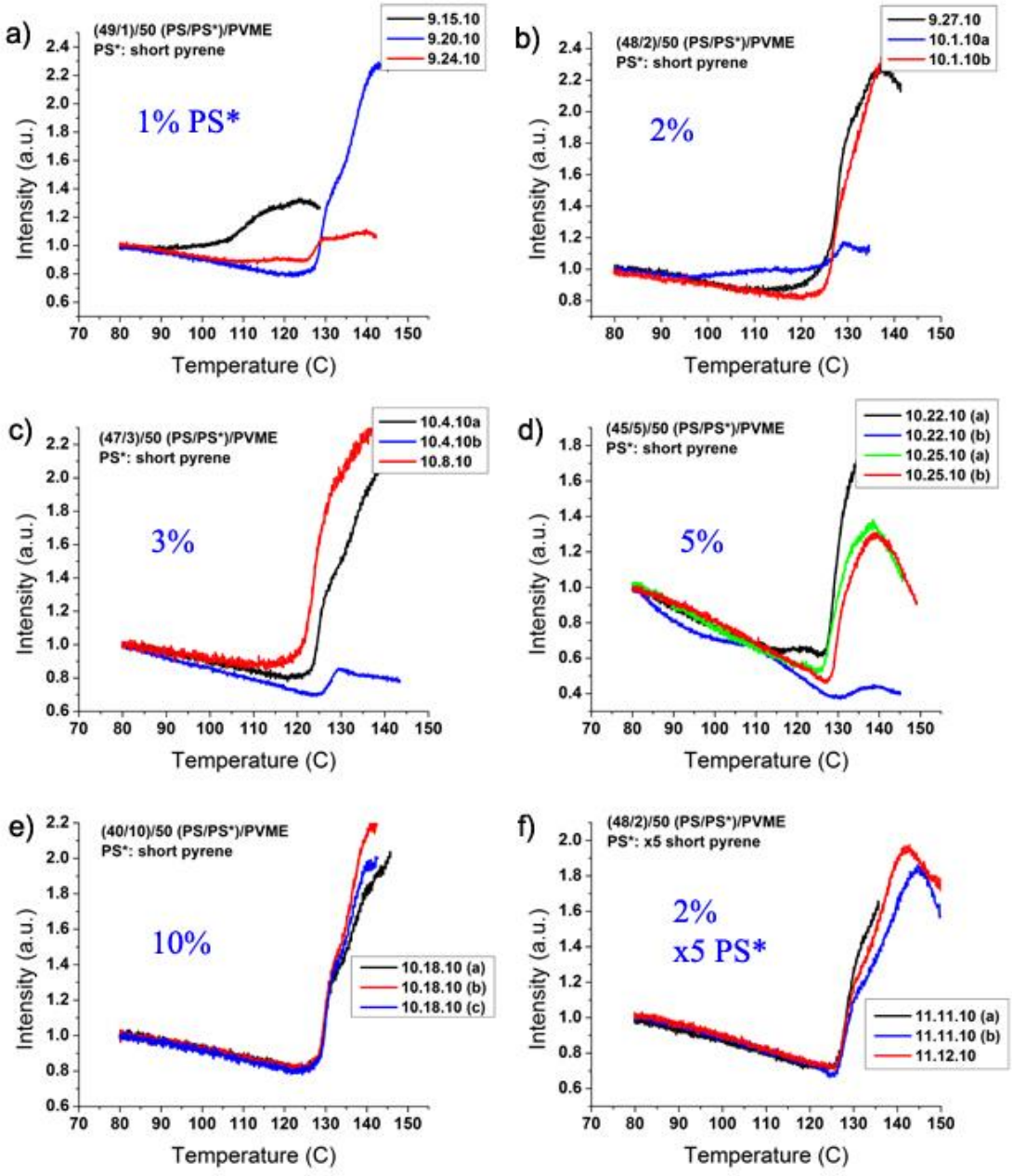

Figure 4.7 The effect of different short-Py label content ((a) 1%, (b) 2%, (c) 3%, (d) 5% and (e) 10%) and different short-Py labeled polystyrene ((e) short-Py-PS* vs (f) 5x- short-Py-PS*) content on the reproducibility of phase separation temperature T_s in PS/PVME blends. Figures taken from Sung Park's undergraduate honors thesis.

Chapter 5
Developing Experimental Protocols for Reliably Measuring Shifts in Phase Separation Temperature T_s Under Electric Fields

---

In the previous chapter, the development of a fluorescence technique to measure the phase separation temperature T_s in PS/PVME polymer blends was described. In the next chapter, the results of using this fluorescence technique to investigate the change in T_s due to the presence of electric fields will be discussed. The present chapter, chronicles all the adjustments to the sample preparation and measurement protocol necessary to measure T_s in PS/PVME blends, both with and without electric fields, $T_s(E)$ and $T_s(0)$, respectively.

5.1 Protocol to Repeatedly Measure Phase Separation Temperature T_s on a Single Sample

As discussed in Chapter 2.3, the majority of the existing experimental data of electric field effects on T_s report shifts in T_s that are tiny in magnitude (less than 0.1 K)[34,36,40,42] and as a consequence leave room for questioning whether the shifts reported are truly present or instead caused by spurious events in the measurements.[39,41] In order to be able to report without a doubt that the shifts in T_s seen in my measurements are well outside of experimental error, it is equally essential to minimize the total error in the shift in T_s due to the electric fields, as well as to maximize the magnitude of the shift in T_s measured. The shift in T_s due to electric fields is defined as $\Delta T_s(E) = T_s(E) - T_s(0)$, thus the total error in the shift in T_s is the sum of the standard errors of the individual measurements of $T_s(E)$ and $T_s(0)$. As was shown in Chapter 4 (and our previous study[131]), the standard error for the T_s values, when measured across different samples of PS/PVME blends, was as high as ± 1.5 K. Thus, it would be more accurate to measure T_s with and without electric fields within the same sample.

It was first demonstrated by Bank et al.,[47] that the thermally induced phase separation process of PS/PVME polymer blends is reversible. Using this information as a starting point, I worked out the annealing conditions necessary for PS/PVME blends to phase separate and subsequently remix over and over again within the same sample, while continually measuring the same T_s value. Figure 5.1a illustrates the experimental steps (positions x, y, z) through phase diagram for measuring T_s repeatedly within the same sample of PS/PVME blend. First, the fluorescence intensity is collected during

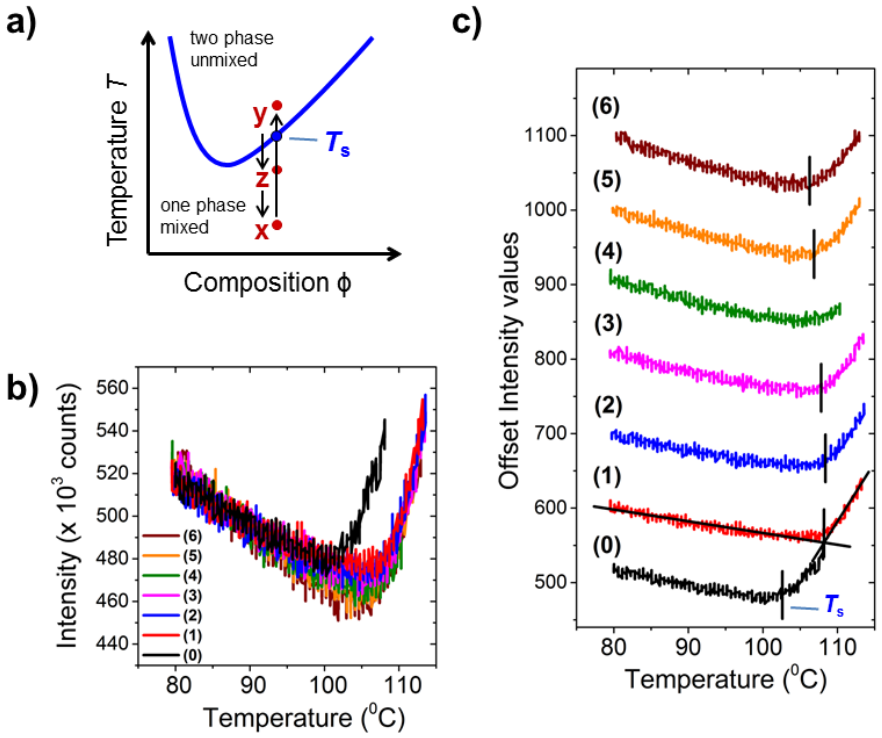

Figure 5.1 (a) Positions x, y, z illustrate the experimental steps of cycling up and down from mixed to unmixed state through phase diagram to repeatedly measure T_s within the same sample of PS/PVME blend. (b) and (c) Fluorescence intensity as a function of temperature for a (40/10)/50 (PS/PS*)/PVME blend measured on heating at 1 K/min. The molecular weight of PS is M_w = 101.3 kg/mol and polydispersity index M_w/M_n = 1.04, the molecular weight of pyrene labeled PS* is M_w = 76.7 kg/mol and M_w/M_n = 1.70, with label content of 0.33 mol %, and the molecular weight of PVME is M_w = 80 kg/mol, M_w/M_n = 2.5. (b) Curves (0)–(6) are collected one after another within the same sample, where between each measurement the blend is quenched back into the one phase region and remixed (see text for details). Panel (c) is the data from panel (b) with the curves (0)–(6) vertically shifted for visual clarity. A short vertical black bar denotes the measured phase separation temperature T_s, identified as the intersection of two linear fits to the data above and below phase separation,[131] as illustrated on curve (1): $T_s^{(0)}$ = 102.4 °C, $T_s^{(1)}$ = 107.7 °C, $T_s^{(2)}$ = 108.1 °C, $T_s^{(3)}$ = 107.7 °C, $T_s^{(5)}$ = 106.9 °C, and $T_s^{(6)}$ =106.5 °C.

heating the sample from mixed to unmixed state (from position x to position y), followed by quenching the sample below T_s (from y to z) and annealed at position z until remixed. This cycling up and down from mixed to unmixed state can be repeated over and over again within the same sample. I found that with the exception of the first ramp, all subsequent T_s values are very reproducible to within ± 0.7 ^oC (as demonstrated in Figure 5.1b). In Chapter 4, it was shown that the standard error for the T_s values, when measured across different samples of PS/PVME blends, was as high as ± 1.5 K. Differences in measured values of T_s from sample to sample can be associated with slight variability in precisely mixing the same composition of the blend each time, environmental conditions affecting moisture uptake in PVME as the polymer is hydroscopic, or from inhomogeneities in composition formed during initial casting of the blend, as has been previously reported.[132–134]

Figure 5.1b plots the fluorescence intensity as a function of temperature for a (40/10)/50 (PS/PS*)/PVME blend measured on heating at 1 K/min. Curves (0)–(6) were collected one after another within the same sample, while cycling up and down through the phase diagram from the mixed stated to the unmixed state. For this sample, the molecular weight of unlabeled PS is M_w = 101.3 kg/mol and polydispersity index of M_w/M_n = 1.04, the molecular weight of pyrene labeled PS* is M_w = 76.7 kg/mol and M_w/M_n = 1.70, with label content of 0.33 mol %, and the molecular weight of PVME is M_w = 80 kg/mol, M_w/M_n = 2.5. A sample geometry, identical to one shown in Figure 5.3 without a Kapton spacer was used (specifics of sample geometry are discussed in detail in Section 5.2). As shown in Chapter 4, the phase separation of the PS/PVME blends is characterized by a sharp increase in fluorescence intensity resulting from the elimination

of fluorescence quenching by the polar PVME component as the non-polar PS component, and covalently attached fluorophore, segregate into domains. Because fluorescence quenching is a very local phenomenon (few nanometer),[65] it is possible to measure the onset of phase separation when the domains are still very small. Previous work by Halary et al.[64] using a similar fluorescence method demonstrated that fluorescence is as sensitive as small angle neutron scattering, and significantly more sensitive than light scattering, at identifying phase separation. Thus, use of fluorescence allows us to identify, measure, and halt phase separation when the domain sizes are still sufficiently small to be easily remixed. Between each fluorescence measurement heating ramp, which starts from a temperature of 80 ^{o}C at a heating rate of 1 K/min and continues till approximately 5–8 ^{o}C after the sharp increase in fluorescence intensity indicative of phase separation is observed, the blend is rapidly quenched at 40 K/min to a temperature 5–10 ^{o}C below the measured T_s and held in the one-phase region for several hours to remix the blend. As described below, I found that this remixing time needed to be at least 18 h after the initial first ramp, but could be reduced to 2–3 h between subsequent ramps.

Figure 5.1c shows the curves (0)–(6) vertically offset for clarity, where for each curve, the measured T_s value is identified by a vertical bar. The T_s values are determined from the intersection of linear fits to the data above and below the sharp increase in intensity signifying phase separation, as illustrated for curve (1). For the data shown in Figure 5.1c, the phase separation temperature values for curves (0)–(6) are: $T_s^{(0)}$ = 102.4 ^{o}C, $T_s^{(1)}$ = 107.7 ^{o}C, $T_s^{(2)}$ = 108.1 ^{o}C, $T_s^{(3)}$ = 107.7 ^{o}C, $T_s^{(5)}$ = 106.9 ^{o}C, and $T_s^{(6)}$ = 106.5 ^{o}C. Note, the value of curve (4) is not identified as there is insufficient data after phase separation for a viable linear fit to be made.

The data shown in Figure 5.1b and c were collected by using the following measurement protocol. After the sample preparation procedure (discussed in detail in Chapter 4.2), the sample was equilibrated at 80 ^{o}C for 30 min, followed by collecting fluorescence intensity while simultaneously heating the blend at a rate of 1 K/min, yielding curve (0). Heating was stopped at 108 ^{o}C (about 6 ^{o}C above $T_s^{(0)}$ = 102.2 ^{o}C) and the sample temperature quenched down to 97 ^{o}C (about 5 ^{o}C below $T_s^{(0)}$), followed by an anneal for 22 h. Next, a second fluorescence heating ramp was made, yielding curve (1) with $T_s^{(1)}$ = 107.7 ^{o}C, notably ~5 ^{o}C higher than $T_s^{(0)}$. In this case, heating was stopped at 113 ^{o}C and the sample quenched, followed by an anneal at 97 ^{o}C for 2 h. Subsequent measurements repeated this protocol for curve (1), yielding curves (2)–(6) with T_s values for the different ramps (excluding the very first) all within a standard error of only ± 0.7 ^{o}C, with an average of $T_s^{(1–6)}$ = 107.4 ^{o}C.

From extensive study of many samples, I found that the phase separation temperature T_s is strongly dependent on the history and thermal treatment of the sample, with the very first phase separation temperature $T_s^{(0)}$ measured after blend casting consistently lower than subsequent measures of T_s after remixing the blend by thermal annealing in the one-phase region. Previous studies have shown that the extent of PS/PVME blend homogeneity after solvent casting can be quite variable depending on casting conditions. The extreme example of this are the reports that PS/PVME blends are only formed in the mixed state when cast from aromatic solvents such as toluene and benzene, but phase separate on casting from chlorinated solvents such as chloroform and trichloroethylene.[46,47,133] This effect has been identified as depending on whether or not the solvent can form C–H to O hydrogen bonds with PVME, displacing the weak

hydrogen bonds formed between the aromatic hydrogens of PS and the ether oxygen of PVME that make this blend miscible.[46] Davis et al.[135] has demonstrated that extended annealing of trichloroethylene cast PS/PVME blends at temperatures between 60–100 ^{o}C can remix these blends. Because of these dependencies on casting conditions, most studies on PS/PVME blends include varying amounts of sample annealing at elevated temperatures within the one-phase region.[47,132–134] In the present study, I similarly wanted to ensure that the T_s measurements were always starting from the same mixed state. I found that the measured T_s value increased with longer annealing time at $T_s^{(0)}$ – 5 ^{o}C (around 95 ^{o}C) up until 18 h of annealing, after which the measured T_s saturated at a value of $T_s^{(1)}$ typically 5–10 ^{o}C above $T_s^{(0)}$. Later remixing of the blend after heating to only 5–8 ^{o}C above T_s required only 2–3 h at $T_s^{(0)}$ – 5 ^{o}C to achieve identical and stable T_s values for the subsequent ramps. Thus, in our study, all the samples were annealed for 18–24 h at $T_s^{(0)}$ – 5 ^{o}C after obtaining the first phase separation temperature $T_s^{(0)}$, with subsequent annealing times of 2–3 h at $T_s^{(0)}$ – 5 ^{o}C between ramps. This procedure resulted in highly reproducible T_s values within a standard error of typically ± 0.7 ^{o}C for $T_s^{(1)}$, $T_s^{(2)}$, $T_s^{(3)}$, etc.

Optical microscopy (with a 63 × objective lens and 0.70 numerical aperture) was used to record the morphologies of the PS/PVME blends. I found the morphologies after phase separation to exhibit uniformly sized domains (~1 μm in size) characteristic of spinodal decomposition, while prior to phase separation and after remixing the blends were featureless.

The time required to remix such PS/PVME blends can be estimated using literature values for the diffusion coefficient D, where the diffusion time $\tau = \frac{x^2}{6D}$,

assuming three-dimensional diffusion for our 24 μm thick samples. For molecular weights M_w = 105 kg/mol, M_w/M_n = 1.06, for PS and M_w = 99 kg/mol, M_w/M_n = 2.10, for PVME (comparable to molecular weights in the present study), Jabbari and Peppas found that $D = 4.2 \times 10^{-14}$ cm^2/s at 85 ^{o}C and $D = 1.1 \times 10^{-12}$ cm^2/s at 105 ^{o}C.[136] Such diffusion coefficients suggest that domains sizes of $x \approx 1$ μm will interdiffuse in ~10 h at 85 ^{o}C or ~30 min at 105 ^{o}C, consistent with the annealing times used in the present study.

I found that the same remixing protocol as described above, where between each measurement the blend is quenched back into the one phase region and annealed until remixed, can also be used for blends of deuterated polystyrene (designated as dPS in Figure 5.2a) and PVME. Figure 5.2b shows the fluorescence intensity as a function of temperature for a (40/10)/50 (dPS/PS*)/PVME blend, measured on heating at 1 K/min. For this data, the molecular weight of unlabeled dPS is M_w = 119.5 kg/mol and M_w/M_n = 1.04, the molecular weight of pyrene labeled PS* is M_w = 86.8 kg/mol and M_w/M_n = 1.65, with label content of 1.93 mol %, and the molecular weight of PVME is M_w = 80 kg/mol, M_w/M_n = 2.5. Sample geometry with a 25 μm thick Kapton spacer, identical to one shown in Figure 5.4 was used (specifics of sample geometry are discussed in detail in Chapter 5.2). Curves (0)–(2) are collected one after another within the same sample. First the sample was equilibrated at 100 ^{o}C for 30 min, followed by collecting fluorescence intensity while simultaneously heating the blend at a rate of 1 K/min, yielding curve (0). Heating was stopped at 128 ^{o}C (about 4 ^{o}C above $T_s^{(0)}$ = 123.5 ^{o}C) and the sample temperature quenched down to 120 ^{o}C (about 4 ^{o}C below $T_s^{(0)}$), followed by an anneal for 21.5 h. Next, a second fluorescence heating ramp was made yielding curve (1) with $T_s^{(1)}$ = 129.3 ^{o}C, notably ~6 ^{o}C higher than $T_s^{(0)}$. In this case, heating was stopped at 134 ^{o}C

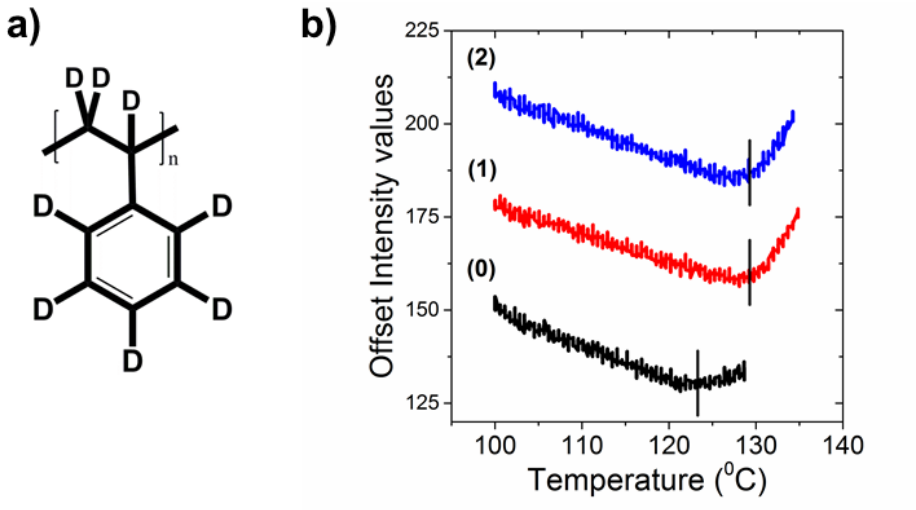

Figure 5.2 (a) Chemical structure of deuterated polystyrene (designated as dPS). (b) Fluorescence intensity as a function of temperature for a (40/10)/50 (dPS/PS*)/PVME blend measured on heating at 1 K/min. The molecular weight of deuterated PS is M_w = 119.5 kg/mol and M_w/M_n = 1.04, the molecular weight of pyrene labeled PS* is M_w =86.8 kg/mol and M_w/M_n = 1.65, with label content of 1.93 mol %, and the molecular weight of PVME is M_w = 80 kg/mol, M_w/M_n = 2.5. Curves (0)–(2) are collected one after another within the same sample, where between each measurement the blend is quenched back into the one phase region and remixed. A short vertical black bar denotes the measured phase separation temperature T_s,: $T_s^{(0)}$ = 123.5 ^{o}C, $T_s^{(1)}$ = 129.3 ^{o}C, $T_s^{(2)}$ = 129.2 ^{o}C.

and the sample quenched, followed by an anneal at 120 ^{o}C for 3 h. Subsequent measurement repeated this protocol for curve (1), yielding curve (2) with $T_s^{(2)}$ = 129.2 ^{o}C. We see that the phase separation temperature values of dPS/PVME blends (T_s = 129 ^{o}C in Figure 5.2b) are substantially higher than the phase separation temperature values for the PS/PVME blends (T_s = 107 ^{0}C in Figure 5.1b). This is to be expected as it is well known that substitution of deuterated polystyrene (dPS) for hydrogenated polystyrene (hPS) considerably raises the phase separation temperature of PS/PVME blends.[60,64]

Less anticipated was the observation of dPS/PVME blends, though remixed at

substantially higher temperatures (at 120 ^{0}C in Figure 5.2) than the PS/PVME blends (at 97 ^{0}C in Figure 5.1), needing more time (at least 3 h) than PS/PVME blends (2 h) to show the same T_s values for the curves (1) and (2). Annealing dPS/PVME blends less than 3 h, produced T_s for curve (2) to be lower than for curve (1). One would expect polymer blends annealed at higher temperatures to remix faster as the mobility of polymer chains increases with measuring increasing temperature. Yang et al.[63] studied the kinetics of dPS/PVME and PS/PVME blends, with PVME of M_w = 99 kg/mol and M_w/M_n = 2.13, hydrogenated PS of M_w = 100 kg/mol and M_w/M_n = 1.05, and deuterated PS of M_w = 119 kg/mol and M_w/M_n = 1.05, using small-angle neutron scattering (SANS) and optical microscopy. They found that the kinetics of phase separation for the dPS/PVME blends was about 10 times faster than for the PS/PVME blends. In other words it took 10 times as long for the domains to grow for PS/PVME as it took for dPS/PVME when the blends had been heated 5 degrees above their respective T_s. They also found that the diffusion coefficient of dPS/PVME blends was about a factor of 6 greater than that of PS/PVME blends. So, if both, dPS/PVME and PS/PVME blends are heated 5 degrees above their corresponding T_s values at rate 1 ^{0}C/min, then the domains in dPS/PVME grow 10 times bigger than the domains in PS/PVME. In my measurements, where the annealing is done at about 5 degrees below T_s, the components in dPS/PVME blends do remix faster than the components in PS/PVME blends, but the interdiffusion of components in dPS/PVME blends is not fast enough to reach a homogenous blend within the same time as do the components in PS/PVME blends.

I additionally tested the remixing protocol for PS/PVME blends with low molecular weight PS component. Figure 5.3 shows the fluorescence intensity as a

function of temperature for a sample of (40/10)/50 (PS/PS*)/PVME blend with low molecular weight PS component, heating at 1 K/min. For this data PS of M_w = 25.0 kg/mol and M_w/M_n = 1.06 (purchased from Pressure Chemical), pyrene labeled PS* of M_w = 24.1 kg/mol and M_w/M_n = 1.63, and with label content of 2.4 mol % (polymerized in lab, see Table 3.1), and PVME of M_w = 80.1 kg/mol, M_w/M_n = 2.1 were used. Samples were prepared by spin coating onto quartz slides and pressed together two at a time (polymer films facing each other), with final sample thickness of ~3.8 μm.

Similarly to the remixing protocol discussed in Figure 5.1, curves (0)–(7) in Figure 5.3 were collected one after another within the same sample. First the sample was equilibrated at 120 ^oC for 30 min, followed by collecting fluorescence intensity while simultaneously heating the blend at a rate of 1 K/min, yielding curve (0) in Figure 5.3. Heating (and collection of fluorescence intensity) was stopped at 151 ^oC (about 10 ^oC above $T_s^{(0)}$ = 139.6 ^oC) and the sample temperature quenched down to 120 ^oC (about 20 ^oC below $T_s^{(0)}$), followed by an anneal for 2 h. Next, a second fluorescence heating ramp was made yielding curve (1) in Figure 5.3 with $T_s^{(1)}$ = 143.1 ^oC, notably ~3.5 ^oC higher than $T_s^{(0)}$. Heating was again stopped at 151 ^oC and the sample quenched, followed by an anneal at 120 ^oC for 2 h. Subsequent measurements repeated this protocol for curve (1) in Figure 5.3, yielding curves (2) and (3) with $T_s^{(2)}$ = 143.5 ^oC and $T_s^{(3)}$ = 143.6 ^oC. After collecting curve (3), the sample was quenched to room temperature and left in the sample holder (heater) overnight. The next day the measurements were continued by heating the sample to 120 ^oC and annealing for 2h followed by a fluorescence heating ramp yielding curve (4) in Figure 5.3 with $T_s^{(4)}$ = 143.0 ^oC. Heating was stopped at 151 ^oC and the sample temperature quenched down to 120 ^oC, followed by an anneal for only 1 h.

Subsequent measurement repeated the protocol for curve (4), yielding curve (5) with $T_s^{(5)}$ = 142.5 ^oC. After collecting curve (5) in Figure 5.3, the sample temperature was quenched down to 120 ^oC and annealed for only 30 min followed by a fluorescence heating ramp yielding curve (6) with $T_s^{(6)}$ = 141.9 ^oC. Subsequent measurement repeated the protocol for curve (6), yielding curve (7) with $T_s^{(7)}$ = 141.9 ^oC.

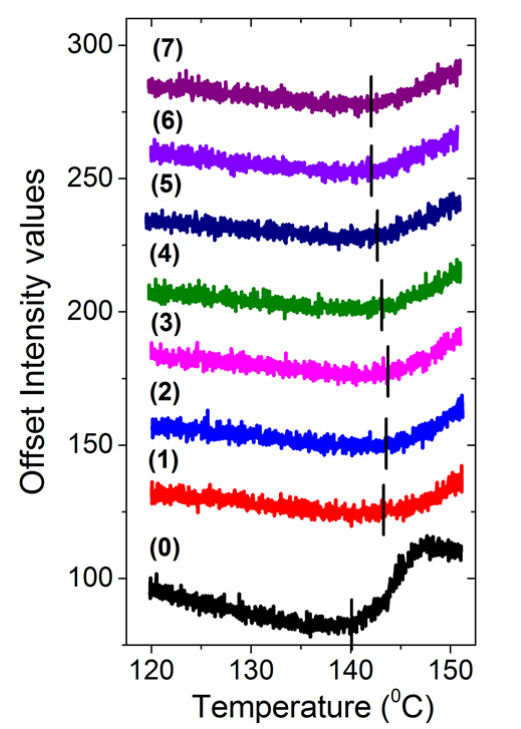

Figure 5.3 The fluorescence intensity as a function of temperature for a sample of (40/10)/50 (PS/PS*)/PVME blend with low molecular weight PS component, heating at 1 K/min. For this data PS of M_w = 25.0 kg/mol and M_w/M_n = 1.06 (purchased from Pressure Chemical), pyrene labeled PS* of M_w = 24.1 kg/mol and M_w/M_n = 1.63, and with label content of 2.4 mol %, and PVME of M_w = 80.1 kg/mol, M_w/M_n = 2.1 were used.

Also, it is clear from the measurement shown in Figure 5.3, that annealing samples between measurements for 2h at 120 ^oC (about 20 ^oC below $T_s^{(0)}$) results in reproducible phase separation temperature values, with average of $|T_s^{(1)-(4)}|$ = 143.3^oC for curves (1)-(4). However, annealing samples less than 2 h at 120 ^oC between

measurements leads to decrease in T_s. For example, annealing only 30 min at 120 ^oC gives a phase separation temperature of $|T_s^{(6)-(7)}| = 141.9^oC$ for curves (6)-(7), that is 1.4 ^oC lower than T_s for curves (1)-(4).

5.2 Sample Preparation Protocol and Experimental Setup for Measuring Phase Separation Temperature T_s in the Presence of Electric Fields

In order to measure the phase separation temperature in the presence of electric fields, $T_s(E)$, the sample preparation protocol used to measure the phase separation temperature without electric fields, $T_s(0)$ (described in Chapter 4), needed to be modified. To generate uniform electric fields across the PS/PVME blend films, the sample geometry took the form of a simple parallel plate capacitor. For measurements with electric fields present, the regular 1 × 1 inch quartz slides, used previously for measurements without electric fields, were switched to special 1 × 1 inch quartz slides covered with a layer of indium tin oxide (ITO). ITO is known for high temperature stability, optical transparency and electrical conduction. The ITO covered quartz slides used for this study, were purchased from SPI Supplies and had an approximately 70 nm thick ITO layer with nominal transmittance of 90 % (for the wavelength range of about 300 nm to 700 nm). The PS/PVME films spin coated onto these ITO covered quarts slides were pressed together, polymer films facing each other, in a bench vice forming a parallel-plate capacitor-like geometry. As seen from the schematic of the sample

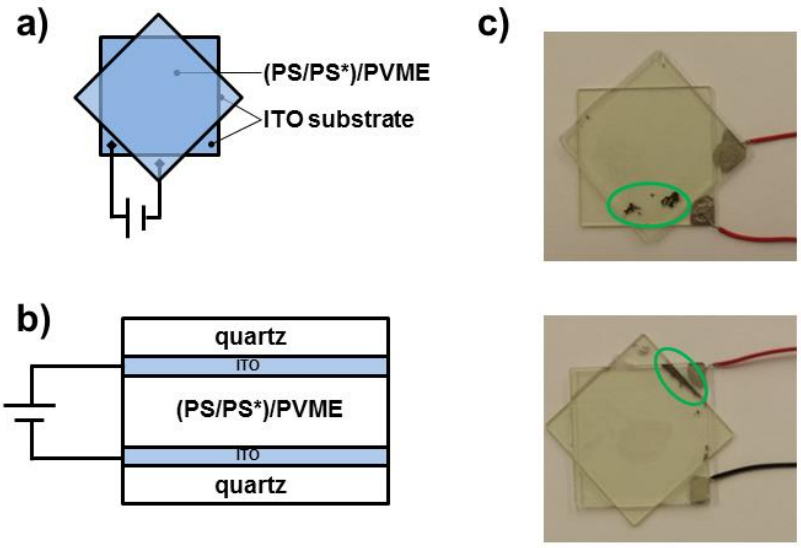

Figure 5.4 Schematic of the sample geometry, (a) top view and (b) side view, placing the PS/PVME blend within a parallel-plate capacitor formed by two ITO-coated quartz slides. (c) Images of samples after the occurrence of dielectric breakdown, indicated inside the green circle, originating from the middle (top) and edge (bottom) of the sample.

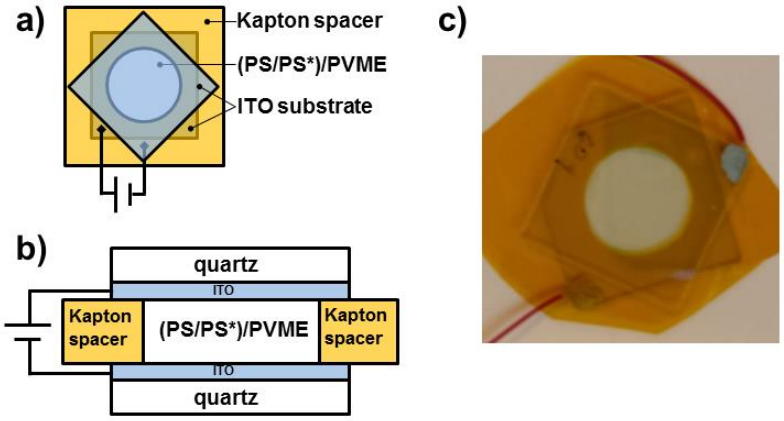

Figure 5.5 Schematic of the sample geometry with a 25 μm thick Kapton spacer, (a) top view and (b) side view. Kapton sheet is used to define the blend thickness and isolate the edges of the samples from dielectric breakdown. (c) Image of a sample with Kapton spacer before measurement.

geometry in Figure 5.4 (a) top view and (b) side view, the ITO layers act as transparent conducting plates of parallel-plate capacitor-like samples. The samples are connected to the power supply via electrical wires glued to the two opposite corners of the ITO layers using silver paste.

As discussed in Chapter 4, four different extrinsic fluorophore labels were tested for suitability for characterizing the phase separation process of PS/PVME blends. The chemical structure of the four fluorophore labeled polystyrenes is shown in Figure 4.1: (a) 1-pyrenylmethyl methacrylate labeled PS (short-Py-PS*), (b) 1-pyrenylbutyl methacrylate labeled PS (long-Py-PS*), (c) anthracene center-labeled PS (An-ctr-PS*), and (d) 9-anthracenylmethyl methacrylate labeled PS (An-sgr-PS*). Although all four fluorophore labels allowed identifying the T_s of PS/PVME, different labels showed slight differences in the T_s values. These small differences (up to 3.7 ^{o}C, between short-Py-PS* with the lowest T_s and An-sgr-PS* with the highest T_s) were associated with how closely the fluorescent dyes are covalently bonded to the PS backbone.[131] For studying the change in T_s in PS/PVME blends due to electric fields, short-Py-PS* was chosen above other labeled polystyrenes. Although both, short-Py-PS* and An-ctr-PS* showed the onset of phase separation slightly earlier than long-Py-PS* or An-sgr-PS*, short-Py-PS* was chosen over An-ctr-PS* because the fluorescence quantum yield for pyrene is about three times higher than that of anthracene.[65] Thus, the amount of dye content necessary to obtain sufficient fluorescence signal can be considerably lower. Also, it is relatively simple to polymerize short-Py-PS* in our lab and fine tune its molecular weights (see Chapter 3.1). The synthesis of An-ctr-PS* on the other hand requires advanced

knowledge in chemistry[137] and is commercially available only in a handful of molecular weights.

For this study short-Py-PS* was synthesized by free radical polymerization from styrene in the presence of trace levels of 1-pyrenylmethyl methacrylate (see Chapter 3). Initially, during the zero-field measurements demonstrating the protocol to remix the PS/PVME blend, short-Py-PS* of M_w = 76.7 kg/mol and M_w/M_n = 1.70, with label content of 0.33 mol % was used. Later, when the initial short-Py-PS* was used up, PS* of M_w = 86.8 kg/mol and M_w/M_n = 1.65, with a label content of 1.93 mol % was used. No significant change in remixing time was observed for this small change in molecular weight or change in label content. Additionally, for PS/PVME blends with low molecular weight PS component, short-Py-PS* with molecular weight of M_w = 24.1 kg/mol, M_w/M_n = 1.63, and label content of 2.4 mol % was synthesized by free radical polymerization from styrene in the presence of trace levels of 1-pyrenylmethyl methacrylate.

Polystyrene (unlabeled), with molecular weight of M_w = 101.3 kg/mol and M_w/M_n = 1.04, was purchased from Scientific Polymer Products, and used as the matrix (neat) PS. For measurements of PS/PVME blends with low molecular weight PS component, unlabeled PS with molecular weight of M_w = 25.0 kg/mol and M_w/M_n = 1.06, was purchased from Pressure Chemical Co., and used as the matrix (neat) PS. For measurements of PS/PVME blends with deuterated polystyrene, dPS of M_w = 119.5 kg/mol and M_w/M_n = 1.04, was purchased from Polymer Source, and used as the matrix (neat) PS.

PVME was purchased from Scientific Polymer Products, and washed prior to use by dissolving in toluene and precipitating into heptane 9 times. The resulting PVME

used, had a molecular weight of M_w = 80 kg/mol, M_w/M_n = 2.5. Molecular weights were determined by gel permeation chromatography, done with tetrahydrofuran (THF) as eluent relative to PS standards, and PVME values determined using universal calibration with Mark-Houwink parameters a = 0.739 and $k = 1.35 \times 10^{-4}$ mL/g.[g, 128] Fluorophore label content was measured using UV-visible absorbance spectroscopy in high-performance liquid chromatography (HPLC) grade THF.

Blends were prepared by dissolving PS and PVME in toluene to produce solutions with 20 wt % total polymer content. Blend compositions of 50/50 PS/PVME were made by combining 40 wt % neat PS, 10 wt % pyrene-labeled PS*, and 50 wt % PVME, that is (40/10)/50 (PS/PS*)/PVME, producing samples with < 0.2 mol % total fluorescent dye content. Samples were spin coated onto ITO covered slides at 5000 rpm producing films of 1.8 – 2.0 μm in thickness. Film thickness was confirmed by spin coating a second film at the same time from the same solution onto a silicon wafer with a native oxide layer and measuring the blend thickness with spectroscopic ellipsometry (J.A. Wollam M-2000). After films were dried under vacuum at 80 ^oC for minimum of 24 h to remove residual solvent, two slides at a time were pressed together with polymer films facing and placed in a bench vice for 1 h under vacuum at 80 ^oC. As a result, the final thickness of samples was 3.6 – 4.0 μm. To avoid moisture uptake, all samples were stored under vacuum at room temperature until measured.

---

[g] In our publications,[131,151] we made a numerical mistake by stating an incorrect value for parameter $k = 13.5 \times 10^{-3}$ mL/g. The correct value, stated here in the thesis, is $k = 1.35 \times 10^{-4}$ mL. This mistake does not affect the molecular weight values measured with gel permeation chromatography (GPC), as accurate values for parameter k were used during those measurements. Recently we have become aware of more accurate Mark-Houwink parameters a = 0.70 and $k = 2.33 \times 10^{-4}$ mL/g by Hess and Muller,[152] estimating the molecular weight for PVME as M_w = 55.7 kg/mol.

As discussed in Chapter 5.1, the potential to measure shifts in T_s due to electric fields well outside experimental error depends not only on the ability to minimize the total error in the shift in T_s but also on the ability to maximize the measured absolute magnitude of the shift in T_s. In order to maximize the shift in T_s due to the electric fields, the highest possible electric field across the polymer blends should be applied. The limit to how high an electric field can be applied across the sample depends on the dielectric strength of the material the sample is made of. Dielectric strength is a characteristic property of insulating materials; it is the strength of an electric field above which the dielectric material breaks down and starts conducting electricity. The expected dielectric strength of PS/PVME blends is roughly about 2×10^7 V/m,[138] however, during the initial measurements the dielectric breakdown of PS/PVME samples happened at electric fields an order of magnitude lower. One explanation to the unusually low dielectric strength of these samples was the presence of impurities in the blend components, a common cause for lowering the dielectric strength of the materials. In order to lower the likelihood of impurities in the sample, the PVME component was purified by dissolving into toluene and followed by precipitation into heptane. Here 300 ml of heptane, 50 g of PVME and 700 ml of toluene was used. In heptane, the higher molecular weight (MW) PVME chains precipitate out, sinking to the bottom of the beaker. The lower MW PVME chains tend to remain dispersed floating in the upper part of the beaker and are thus relatively easy to separate. The heptane along with the lower MW PVME chains is then poured off and the remaining higher MW PVME is dissolved again in toluene. The purification process of dissolution into toluene followed by precipitation into heptane was repeated total of 9 times. As a result, the weight average molecular weight M_w of PVME increased from

65.5 kg/mol to 80 kg/mol and the polydispersity index PDI decreased from 3.95 to 2.5. After the purification of PVME, the occurrence of dielectric breakdown seemed to happen less often, however it did not completely eliminate the problem.

Another reason for the early dielectric breakdown in the PS/PVME samples was the possibility that the breakdown in polymer films was initiated by the dielectric breakdown of the air surrounding the perimeter of the films. The dielectric strength of air is only 0.3×10^7 V/m,[139] which is an order of magnitude lower than that of PS/PVME blends. This would also explain why the dielectric breakdown happened most typically at the edges of the samples and only sometimes in the middle. Figure 5.4c shows images of the samples after the occurrence of dielectric breakdown originating from the middle and edge of polymer film. In order to prevent dielectric breakdown in the air around the edges of the samples, two different solutions were tested. First, I tried putting polydimethylsiloxane (PDMS) around the edges of the samples, however it did not sufficiently help with the early dielectric breakdown of the samples. The second plan for trying to prevent dielectric breakdown in the air around the edges of the samples, that eventually also proved successful, was surrounding the perimeter of the polymer films with a Kapton polyimide sheet. The dielectric strength of Kapton is 24×10^7 V/m,[140] an order of magnitude higher than that of the PS/PVME blend. Additionally Kapton films are experimentally easy to handle, as they are very flexible and have excellent temperature stability (up to 400 ^{o}C).

In order to surround the perimeter of the polymer films with a Kapton sheet, the initial sample preparation protocol described above had to be significantly modified. The biggest obstacle with surrounding the PS/PVME samples with a Kapton sheet was the

difficulty of matching the sample thickness with the Kapton sheet thickness. The thinnest commercially available Kapton sheets are 7 μm (0.0003" nominal) thick. To be able to accurately prepare polymer films with thicknesses of 7 μm, it is necessary to measure the polymer film thicknesses to ensure proper sample preparation protocol. However, in our lab it is not possible to accurately measure polymer films with thicknesses of that range. Ellipsometry only allows measuring film thicknesses up to about 3 μm. For this study the second thinnest commercially available Kapton sheet, 25 μm (0.001" nominal) thick, were chosen. It is possible to measure polymers films with thicknesses of about 25 μm (to within ± 2 μm) using an optical microscope by focusing on the top and bottom of the optically transparent samples and recording the micrometer scale of the microscope.

The following protocol proved to be successful for adding a Kapton sheet around the edges of the PS/PVME samples and was used to make samples for all measurements involving the application of electric fields. Polymer blends, using the same blend components as described above, were prepared by dissolving both PS and PVME in toluene to produce solutions with 18 wt % total polymer content. Blend compositions of 50/50 PS/PVME were made by combining 40 wt % neat PS, 10 wt % pyrene-labeled PS*, and 50 wt % PVME, that is (40/10)/50 (PS/PS*)/PVME, producing samples with < 0.2 mol % total fluorescent dye content. Solutions were poured into the center of a wide glass dish with flat bottom and dried in a fume hood at room temperature for 24 h, followed by annealing in a vacuum oven at 80 ^{o}C for at least 24 h to remove residual solvent. Disks were cut from the dry films having masses of 5.8 ± 0.2 mg and diameters slightly smaller than 5/8 inches. These disks were placed between two 1 × 1 inch quartz slides with the ITO-coating acting as electrodes. A 25 μm (0.001" nominal) thick Kapton

sheet was used as a spacer between the ITO electrodes, which extended laterally beyond the ITO electrodes. A 5/8 inch diameter hole was punched into the Kapton sheet to accommodate the polymer blend sample. Once assembled, the samples were placed under vacuum at 80 ^{o}C and pressed with a 2.2 kg weight for 3–5 days, until the polymer blend filled in the form of the Kapton hole. This process achieved uniform film thicknesses of 24 ± 2 μm on average across the polymer blend dictated by the thickness of the Kapton sheet. The thickness of each sample used for electric field measurements was determined (to within ± 2 μm) by using an optical microscope (Leica DMIRB inverted microscope). Lastly, electrical wires were glued to the corners of the ITO layers using silver paste. All samples were stored under vacuum at room temperature prior to measurement.

The schematic of the sample geometry with Kapton spacer is shown in Figure 5.5 (a) top view and (b) side view. An image of the sample before measurement is shown in Figure 5.5c. Elimination of the air around the polymer films by surrounding them with Kapton, increased the overall dielectric strength of the samples. Using a DC Agilent Technologies N5752A high-voltage power supply, a constant voltage up to 440 V_{DC} could be applied, to achieve electric field strengths of 1.8×10^{7} V/m.

Chapter 6
Electric Field Effect on the Miscibility of Polystyrene / Poly(vinyl methyl ether)

A version of this chapter was published as A. Kriisa and C. B. Roth, "Electric Fields Enhance Miscibility of Polystyrene / Poly(vinyl methyl ether) blends," *The Journal of Chemical Physics* **2014**, *141*, 134908.

Mixtures of different polymers are extensively utilized to achieve blended material properties not available in single component systems. However, the naturally poor miscibility of polymers stemming from their macromolecular character leave the phase behavior of polymer blends extremely sensitive to enthalpic interactions and external perturbations. Techniques which can externally control and manipulate the phase behavior of miscible systems, without altering chemistry on a molecular level, have great practical benefits. One such possible mechanism is the use of electric fields with isolated reports showing that the presence of uniform fields can cause shifts in the phase separation temperature T_s for various mixtures.[31,34–38,40–42,44,45] However, at present, there is extensive debate[31] and limited understanding of how uniform electric fields influence the compatibility of polymeric mixtures, or even small molecules, with one of the main limitations stemming for the lack of experimental data with unambiguously large shifts in

T_s outside of experimental error.

In this chapter, the results demonstrating that the presence of uniform electric fields strongly enhance the miscibility of polystyrene (PS) / poly(vinyl methyl ether) (PVME) blends are presented. This work follows from the previous results discussed in Chapter 4,[131] in which a fluorescence technique for measuring the phase separation temperature T_s of PS/PVME blends was shown. In this method, an aromatic fluorophore is covalently bonded to the non-polar PS component such that upon phase separation a sharp increase in fluorescence intensity is observed as the dye separates from the more polar PVME component. This sensitivity arises from local fluorescence quenching of the dye when in the proximity of PVME,[61] likely the result of a weak hydrogen bond forming between the ether oxygen of PVME and the aromatic hydrogens of the dye.[131] A similar such weak hydrogen bond between PVME and PS is believed to be responsible for making this blend miscible.[46] Using this fluorescence technique to investigate the change in T_s due to the presence of electric fields, I demonstrate that the presence of uniform electric fields strongly enhances the miscibility of PS/PVME polymer blends. Focusing on a 50/50 PS/PVME blend composition, T_s is found to increase by over 13 K for electric field strengths of 1.7×10^7 V/m.

As discussed in Chapter 2.3, only a few experimental results have been published over the past several decades. The first experimental results on the subject were published by Debye and Kleboth,[34] who reported that electric fields of $E = 0.45 \times 10^7$ V/m enhance mixing in a small molecule mixture of nitrobenzene/isooctane, causing T_s to shift up by 0.015 K. Later, Debye and Kleboth's results were verified with greater accuracy by Orzechowski[42] for the same mixture. Beaglehole[40] reported shifts of $\Delta T_s = 0.08$ K

towards enhanced mixing under fields of $E = 0.03 \times 10^7$ V/m in solutions of cyclohexane/aniline. However, Early,[41] who later worked on the same mixture with similar magnitude of electric fields as Beaglehole, reported not seeing shifts in T_s at all. Early suggested Beaglehole's results could be explained by Joule heating from current conduction through the sample. Similar concerns have also been expressed about the Debye and Kleboth results.[39,41]

Wirtz and Fuller[36] reported enhance mixing with shifts of $\Delta T_s = 0.02$ K for $E = 0.1 \times 10^7$ V/m in nitrobenzene/*n*-hexane, $\Delta T_s = 0.04$ K for $E = 0.05 \times 10^7$ V/m in PS/ cyclohexane, and $\Delta T_s = 0.03$ K for $E = 0.05 \times 10^7$ V/m in poly(*p*-chlorostyrene)/ ethylcarbitol. Much bigger shifts, up to $\Delta T_s = 1.5$ K for $E = 0.85 \times 10^7$ V/m, have also been recently reported in poly(styrene-*block*-isoprene) (SI) solutions by Schoberth et al.[45] towards enhanced mixing.

All the above mentioned experimental data show enhanced compatibility, lower UCST or higher lower critical solution temperature (LCST) behavior, in the presence of uniform electric fields. However, a study by Reich and Gordon[44] report very large shifts $T_s = 54$ K for $E = 2.72 \times 10^7$ V/m in PS/PVME polymer blends towards reduced miscibility, opposite to all other published experimental data on the subject. [h] Possible reasons for this discrepancy are discussed below.

Comparing relative $\Delta T_s/E^2$ changes among the available experimental literature makes it clear that no correlation exists between the relative size of the shift in T_s as a

---

[h] Additionally to Reich and Gordon,[44] one other research group by Lee *et al.*[37,38] has also reported reduced miscibility in the presence of electric fields. However, as both of the polymer blends studied by Lee *et al.*[37,38] contained a strong piezoelectric, their data are not included in this chapter for reasons discussed at length in Chapter 2.3.

function of electric field and the system molecule size. The Debye and Kleboth[34] and Orzechowski[42] studies, both in solutions of nitrobenzene/isooctane, showed $\Delta T_s/E^2 = 0.08 \times 10^{-14}$ Km^2/V^2, which is almost 1000 times smaller than $\Delta T_s/E^2 = 87 \times 10^{-14}$ Km^2/V^2 reported by Beaglehole[40] in cyclohexane/aniline. For Wirtz and Fuller's data,[36] $\Delta T_s/E^2 = 2 \times 10^{-14}$ Km^2/V^2 in nitrobenzene/*n*-hexane, $\Delta T_s/E^2 = 16 \times 10^{-14}$ Km^2/V^2 in PS/ cyclohexane, and $\Delta T_s/E^2 = 12 \times 10^{-14}$ Km^2/V^2 in poly(*p*-chlorostyrene)/ethylcarbitol. For the Schoberth et al.[45] data in SI solutions, $\Delta T_s/E^2 = 2.1 \times 10^{-14}$ Km^2/V^2, while the Reich and Gordon[44] data in PS/PVME give $\Delta T_s/E^2 = 7.3 \times 10^{-14}$ Km^2/V^2. Hence, there appears to be little if any discernable trend among the different systems with the $\Delta T_s/E^2$ shifts varying from 0.08–87 ($\times 10^{-14}$ Km^2/V^2).

More confusion arises when considering theoretical expectations of electric field effects on the phase separation temperature T_s. The typical theoretical approach uses a thermodynamic argument of adding an electrostatic free energy term to the free energy of mixing,[15,31,34–40] for polymers this is typically written as an extension of the classic Flory-Huggins equation:[31,36–38]

$$\Delta G_m = k_B T \left(\frac{\phi_A ln \phi_A}{v_A N_A} + \frac{\phi_B ln \phi_B}{v_B N_B} + \frac{\phi_A \phi_B \chi}{v_{ref}} \right) - \frac{1}{2} \varepsilon_0 E^2 [\varepsilon(\phi) - \phi_A \varepsilon_A - \phi_B \varepsilon_B \,] \qquad (6.1)$$

where ΔG_m is the system's total free energy of mixing per unit volume. The term within brackets on the right side, is the sum of the entropy and enthalpy of mixing per unit volume, where ϕ_A and ϕ_B are volume fractions and v_A and v_B are monomer volumes of the two blend components with degree of polymerization N_A and N_B; while v_{ref} is a reference volume of monomer size and χ is the empirical interaction parameter.[67,103] The last term in Eq. (6.1) accounts for the additional contribution to ΔG_m due to the presence of a

uniform electric fields E in dielectric medium; it is the free electrostatic energy density equal to the difference between the electrostatic energy of the blend and the ϕ-weighted average of the pure components A and B. Here, ε_0 is the absolute permittivity of vacuum, $\varepsilon(\phi)$ is the composition dependent dielectric constant of the binary mixture, and ε_A and ε_B are the dielectric constants of the pure components A and B.[33,36,104] In Eq. (6.1), a negative sign in front of the electrostatic energy term is included, as this is the most accepted treatment;[31,34,37–40] however, there exists discussion among theoretical studies, whether a plus sign should be used instead.[31,34–36,39]

Considering the standard conditions for stability $\frac{\partial^2 \Delta G_m}{\partial \phi^2} = 0$ and criticality $\frac{\partial^3 \Delta G_m}{\partial \phi^3} = 0$, and the empirical form for the interaction parameter $\chi = A + \frac{B}{T}$ (where empirical parameters $A > 0$ and $B < 0$ for LCST and $A < 0$ and B > 0 for UCST type phase diagrams), it follows from Eq. (6.1) that

$$\frac{T_s(E) - T_s(0)}{T_s(0)} = \frac{\varepsilon_0 v_{ref} E^2}{4k\,B} \frac{\partial^2 \varepsilon(\phi)}{\partial^2 \phi} \tag{6.2}$$

Here, $T_s(E)$ and $T_s(0)$ are the phase separation temperatures measured with and without electric field defining $\Delta T_s(E) = T_s(E) - T_s(0)$ as the shift in phase separation temperature due to the electric field. As written, this is the most commonly used form, however, formally it is only correct to first order.[31] As we describe in more detail in the discussion, recent work by Orzechowski et at.[43] has argued that the next higher order term may become dominant at high field strengths, demonstrating quantitative agreement between theory and experiment for electric field shifts in the nitrobenzene/*n*-octane system. Assuming that $\frac{\partial^2 \varepsilon(\phi)}{\partial^2 \phi} > 0$, as is typically seen for mixtures of polar and non-polar

components,[34,35,40,42] and using the negative sign for the electrostatic energy term in Eq. (6.1), it follows from Eq. (6.2) that a shift towards a reduction of compatibility on the order of only a few mK is predicted for the presence of moderate to strong fields.[15,31,35,39,40] Thus overall, theoretical predictions are in conflict with the vast majority of experimental results.[29,31,34,36–42,44] As discussed above, all experimental results, except the single study by Reich and Gordon,[44] find that electric fields enhance mixing with significantly larger shifts in T_s than theory predicts.

6.1 Experimental

Polystyrene (unlabeled), with molecular weight of M_w = 101.3 kg/mol and polydispersity index of M_w/M_n = 1.04, was purchased from Scientific Polymer Products, and used as the matrix (neat) PS for all studies. Pyrene-labeled PS (designated as PS* in Figure 6.1a) of M_w = 86.8 kg/mol and M_w/M_n = 1.65, with a label content of 1.93 mol %, was synthesized by free radical polymerization from styrene in the presence of trace levels of 1-pyrenylmethyl methacrylate, as described in Chapter 3.1. PVME (shown in Figure 6.1b) was purchased from Scientific Polymer Products, and washed prior to use by dissolving in toluene and precipitating into heptane 9 times. The resulting PVME used had a molecular weight of M_w = 80 kg/mol, M_w/M_n = 2.5. Molecular weights were determined by gel permeation chromatography done with tetrahydrofuran (THF) as eluent relative to PS standards, and PVME values determined using universal calibration

with Mark-Houwink parameters $a = 0.739$ and $k = 1.35 \times 10^{-4}$ mL/g.[i, 128] Fluorophore label content was measured using UV-visible absorbance spectroscopy in high-performance liquid chromatography (HPLC) grade THF as described in Chapter 3.3.

Polymer blends were prepared by dissolving both PS and PVME in toluene to produce solutions with 18 wt % total polymer content. Blend compositions of 50/50 PS/PVME were made by combining 40 wt % neat PS, 10 wt % pyrene-labeled PS*, and 50 wt % PVME, that is (40/10)/50 (PS/PS*)/PVME, producing samples with < 0.2 mol % total fluorescent dye content. Solutions were poured into the center of a wide glass dish with flat bottom and dried in a fume hood at room temperature for 24 h, followed by annealing in a vacuum oven at 80 ^{o}C for at least 24 h to remove residual solvent. Disks were cut from the dry films having masses of 5.8 ± 0.2 mg and diameters slightly smaller than 5/8 inches. These disks were placed between two 1 × 1 inch quartz slides (SPI Supplies) coated with conducting indium tin oxide (ITO) as electrodes. To prevent dielectric breakdown in the air around the edges of the sample, as the dielectric strength of air is approximately an order of magnitude less than that of the polymer, a 25 μm (0.001" nominal) thick Kapton sheet was used as a spacer between the ITO electrodes, which extended laterally beyond the ITO electrodes. A 5/8 inch diameter hole was punched in the Kapton spacer to accommodate the polymer blend sample. Figure 6.1 (parts c and d) give a schematic of the sample geometry. Once assembled, the samples

[i] In our publications,[131,151] we made a numerical mistake by stating an incorrect value for parameter $k = 13.5 \times 10^{-3}$ mL/g. The correct value, stated here in the thesis, is $k = 1.35 \times 10^{-4}$ mL. This mistake does not affect the molecular weight values measured with gel permeation chromatography (GPC), as accurate values for parameter k were used during those measurements. Recently we have become aware of more accurate Mark-Houwink parameters $a = 0.70$ and $k = 2.33 \times 10^{-4}$ mL/g by Hess and Muller,[152] estimating the molecular weight for PVME as $M_w = 55.7$ kg/mol.

were placed under vacuum at 80 ^{o}C and pressed with a 2.2 kg weight for 3–5 days, until the polymer blend filled in the form of the Kapton hole. This process achieved uniform film thicknesses of 24 ± 2 μm on average across the polymer blend dictated by the thickness of the Kapton sheet. The thickness of each sample used for electric field

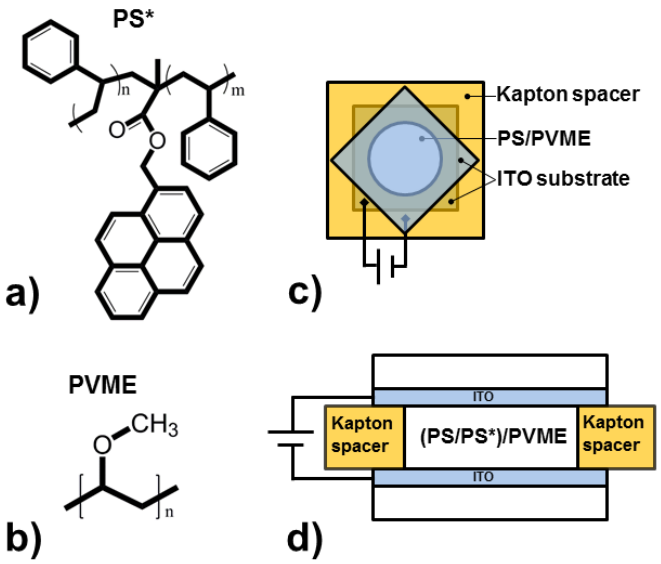

Figure 6.1 Chemical structure of (a) pyrene-labeled polystyrene (designated as PS*) and (b) poly(vinyl methyl ether) (PVME). Schematic of sample geometry, (c) top view and (d) side view, placing the PS/PVME blend within a parallel-plate capacitor formed by two ITO-coated quartz slides. A 25 μm thick Kapton spacer is used to define the blend thickness and isolate the edges of the samples from dielectric breakdown.

measurements was determined (to within ± 2 μm) by using an optical microscope (Leica DMIRB inverted microscope) to focus on the top and bottom of the optically transparent samples and recording the micrometer scale of the microscope. Lastly, electrical wires were glued to the corners of the ITO layers using silver paste in order to apply constant voltage to the sample using a DC Agilent Technologies N5752A high-voltage power supply, up to 440 V_{DC} to achieve electric field strengths of 1.8×10^{7} V/m. All samples

were stored under vacuum at room temperature prior to measurement to avoid moisture uptake.

Steady-state fluorescence measurements were carried out using a Photon Technology International QuantaMaster fluorimeter. Sample temperature was controlled to an accuracy of ± 0.3 K using an Instec HCS402 heater. Fluorescence measurements used a front-face geometry with an angle of incidence of 28^{o}. Excitation and emission slits were set to 4.00 nm (ex) and 4.25 nm (em) bandpass, with an excitation wavelength of 324 nm. During the time-based measurements, the samples were heated at a rate of 1 K/min, while simultaneously measuring the fluorescence intensity during a 3 s time window every 30 s, at a wavelength of 379 nm. This procedure follows the method described in Chapter 4 for measuring the phase separation temperature T_s of PS/PVME blends under zero electric field.[131] After each measurement, samples were quenched to below the phase separation temperature at the rate of 40 K/min using the liquid nitrogen cooling capability of the Instec heater.

6.2 Results and Discussion

6.2.1 Measuring the Shift in T_s with Electric Fields

To accurately determine the shift in phase separation temperature when in the presence of an electric field, $\Delta T_s(E) = T_s(E) - T_s(0)$, first the remixing protocol described in previous chapter (see Figure 5.1 in Chapter 5.1), is used to establish the zero-field T_s value for a given blend. Then, the electric field is applied and the shift in T_s due to the

presence of electric field is measured. Subsequently, the electric field can be removed and the same zero-field T_s value, as measured previously, recovered. In this fashion, clear evidence is provided that the miscibility of PS/PVME blends is substantially and reversibly altered when in the presence of electric fields. Figure 6.2 substantiates this for a single sample by plotting the fluorescence intensity of a (40/10)/50 (PS/PS*)/PVME polymer blend as a function of temperature at zero electric field [traces (1), (2), and (4)] and under an external electric field of $E = 1.4 \times 10^7$ V/m [trace (3)]. Curves (1)–(4) collected on heating at 1 K/min are measured one after another within a single sample following the same protocol as used to collect the data in Figure 5.1b, with the exception of applying an external electric field across the sample during the measurement of curve (3) in Figure 6.2. Note, the very first heating ramp, corresponding to curve (0) in Figure 5.1b, is omitted in Figure 6.2 because it is always anomalous. In Figure 6.2, the phase separation temperature prior to applying the electric field was measured twice, giving $T_s^{(1)}(0) = 94.0\ ^oC$ and $T_s^{(2)}(0) = 93.2\ ^oC$, then an electric field of $E = 1.4 \times 10^7$ V/m was applied shifting the phase separation temperature to $T_s^{(3)}(E) = 102.2\ ^oC$, and finally the electric field was removed shifting the phase separation temperature back to $T_s^{(4)}(0) = 92.8\ ^oC$, very close to its original value. The zero field T_s values for this sample are on average $T_s(0) = 93.3 \pm 0.6\ ^oC$. Thus, Figure 6.2 clearly demonstrates that the presence of the electric field increases the phase separation temperature of the PS/PVME blend by 8.9 K for a field strength of $E = 1.4 \times 10^7$ V/m.

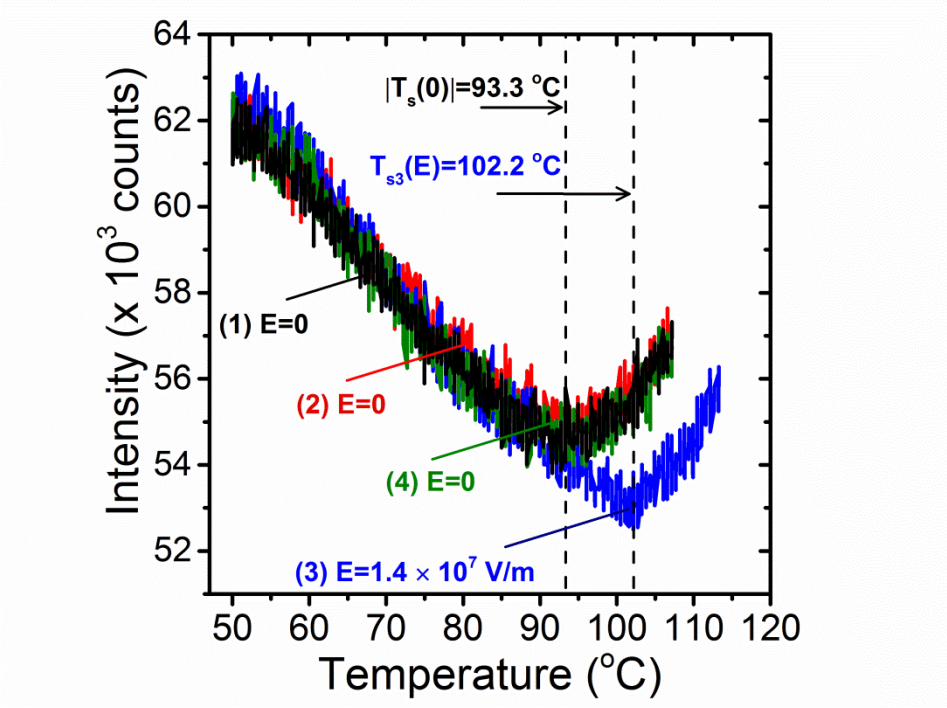

Figure 6.2 Fluorescence intensity as a function of temperature for a (40/10)/50 (PS/PS*)/PVME polymer blend with curves (1) – (4) collected one after another within the same sample following the procedure described for the data in Figure 5.1b where the blend is quenched and remixed between each measurement (note the very first heat, curve (0), is omitted). Curves (1) and (2) establish $T_s(0)$ at zero electric field: $T_s^{(1)}(0) = 94.0\ ^oC$ and $T_s^{(2)}(0) = 93.2\ ^oC$. For curve (3), an external electric field of $E = 1.4 \times 10^7$ V/m is applied, shifting the phase separation temperature up to $T_s^{(3)}(E) = 102.2\ ^oC$. Finally, the electric field is turned off and curve (4) shows that the same zero field value, $T_s^{(4)}(0) = 92.8\ ^oC$, is recovered. For this electric field strength, the shift in the phase separation temperature $\Delta T_s(E) = T_s(E) - T_s(0) = 8.9$ K, relative to the average zero field value $|T_s(0)| = 93.3\ ^oC$ measured for curves (1), (2), and (4).

Note that if Joule heating were present, frequently a concern with such electric field measurements, it would manifest as a decrease in T_s, opposite to the direction in T_s shift observe here, due to changes in miscibility of the blend when in the presence of an electric field. During the T_s measurements, no evidence of current flow through the samples is observed and a current limit is set on the power supply to cut out if dielectric

breakdown occurs at very high field strengths. For example, application of electric field strengths higher than 1.8×10^7 V/m caused electrical shortage in the samples, accompanied by current (200mA or higher) through the samples with fast Joule heating. Also, for a fixed temperature, no change in the pyrene fluorescence emission spectrum is observed, in either shape or overall intensity, when in the presence of electric fields, as compared to the pyrene spectra collected under zero field. From studies of pyrene doped in poly(methyl methacrylate) (PMMA) films,[141] any change in fluorescence intensity with electric field is expected to be less than 0.1% for maximum field strengths used in this study, resulting from a slight change of the molecular polarizability of the excited state of pyrene.

Similar measurements to those described for Figure 6.2 were carried out on a number of different samples to characterize the shift in miscibility at varying electric field strengths. Figure 6.3 plots the fluorescence intensity for (40/10)/50 (PS/PS*)/PVME polymer blends as a function of temperature where traces are given for different electric field values: $E_1 = 0.94 \times 10^7$ V/m, $E_2 = 1.4 \times 10^7$ V/m, and $E_3 = 1.8 \times 10^7$ V/m, with a zero electric field trace also provided for reference. The temperature axis has been referenced to the individual $T_s(0)$ values measured for each sample. This allows explicit comparison of the shift in T_s with electric field, $\Delta T_s(E)$, regardless of any small variability in $T_s(0)$ between different samples. The curves for different E are superimposed atop each other in Figure 6.3a where the intensity of the curves have been specifically matched at $T–T_s = –30$ K, while in Figure 6.3b, the curves have been vertically offset for clarity and a short vertical bar is used to denote the location of $T_s(E)$ for each curve. The data clearly show a progression of larger shifts in T_s with increasing electric field: $T_s(E_1) = 4.1$ K at E_1

= 0.94 × 10^7 V/m, $T_s(E_2)$ = 8.9 K at E_2 = 1.4 × 10^7 V/m, and $T_s(E_3)$ = 11.9 K at E_3 = 1.8 × 10^7 V/m.

Figure 6.4 plots the shift in phase separation temperature $\Delta T_s(E) = T_s(E) - T_s(0)$ as a function of the square of the electric field strength for all the data collected in this study, using electric field strengths up to 1.8 × 10^7 V/m. (The same data as shown in Figure 6.4 is also plotted as the shift in phase separation temperature $\Delta T_s(E)$ vs the electric field strength in figure in Appendix 2) The data consistently show an increase in the phase separation temperature T_s with increasing electric field strength. The magnitude of the T_s shifts are large, up to 13.5 K, and well outside experimental error in $\Delta T_s(E)$ of ± 1.4 K by roughly an order of magnitude. Hence, it can be concluded that electric fields strongly enhance miscibility in PS/PVME blends. To quantify the magnitude of the shift, the data in Figure 6.4 have been fit to a linear trend giving a relative change of $\Delta T_s/E^2$ = (4.8 ± 0.4) × 10^{-14} Km^2/V^2. Such a value is consistent with those previously reported in the literature for different types of blends, although those values vary significantly between 0.08–87 (× 10^{-14} Km^2/V^2).[31,34–36,40–42,45] The results of this study also agree with the vast majority of the experimental data in the literature showing that the presence of electric fields enhances miscibility; however, as will be discussed below, my findings do disagree with the one previous study specifically on PS/PVME blends by Reich and Gordon,[44] which has been considered anomalous in the field.[31]

The magnitude of shift in phase separation temperature $\Delta T_s(E)$ = 13.5 ± 1.4 K demonstrated here represents one of the largest absolute shifts ever reported (excluding the anomalous piezoelectric PVDF blends[37,38] and the Reich and Gordon[44] study to be discussed below). However, the relative magnitude of this shift, $\Delta T_s/E^2$ = (4.8 ± 0.4) ×

10^{-14} Km^2/V^2, is comparable to those previously reported in the literature for blends of small molecules and polymer solutions.[31,34–36,40–42,45] As previously discussed,[15,31,35,39,40] such observed shifts are much larger than those predicted based on Eq. (6.2) incorporating the standard electrostatic energy term for mixtures. Though, a recent study by Orzechowski et al.[43] suggests that the next order term in the free energy expansion may become dominant at high field strengths. Their expanded expression for the shift in phase separation temperature with electric field, replacing Eq. (6.2), is:

$$\frac{\Delta T_S(E)}{E^2} = \frac{\varepsilon_0 v_{ref} T_S(0)}{4k\,B}\left[\frac{\partial^2 \varepsilon(\phi)}{\partial^2 \phi} - \frac{2}{\varepsilon(\phi)}\left(\frac{\partial \varepsilon(\phi)}{\partial \phi}\right)^2\right] \tag{6.3}$$

The second term in the brackets accounts for the dielectric contrast between the components, suppressing concentration fluctuations parallel to the field direction[99,106] and the formation of dielectric interfaces between domains during phase separation. The expression treats composition fluctuations as asymmetric, consistent with previous experimental observations of small-angle light scattering studies on polymer solutions in the presence of uniform electric fields that reported electric-field-induced remixing in the two-phase region.[106] The experimental fluorescence method used for this study is not sensitive to any particular orientation because the local fluorescence quenching is determined by the local composition and polarity of the material. However, the Orzechowski et al.[43] theory predicts a difference in the expected magnitude of the $\Delta T_s/E^2$ shift depending on the orientational dependence of the concentration fluctuations. Efforts to quantitatively evaluate Eq. (6.3) for the present PS/PVME system would require knowing the compositional dependence of the dielectric constant $\varepsilon(\phi)$. Although $\varepsilon(\phi)$ is not known at this time, it should be noted that reasonable estimates for the various

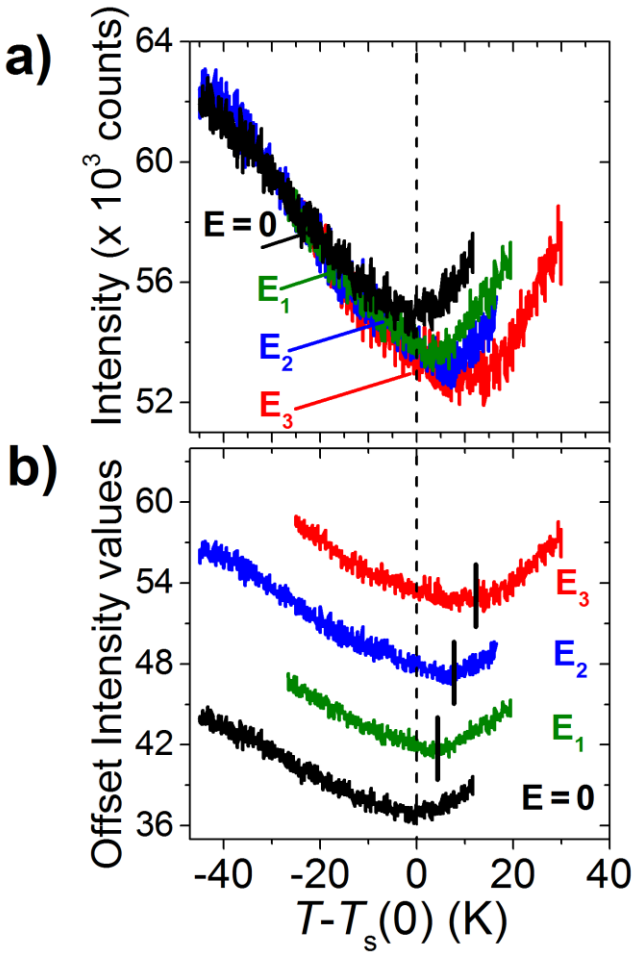

Figure 6.3 Fluorescence intensity as a function of temperature for (40/10)/50 (PS/PS*)/PVME polymer blends, where the temperature axis has been referenced to the individual zero-field $T_s(0)$ values for each sample, enabling explicit comparison of the $\Delta T_s(E)$ shift for different electric field strengths: $\Delta T_s(E)$ = 4.1 K for $E_1 = 0.94 \times 10^7$ V/m, $\Delta T_s(E)$ = 8.9 K for $E_2 = 1.4 \times 10^7$ V/m, and $\Delta T_s(E)$ = 11.9 K for $E_3 = 1.8 \times 10^7$ V/m. Panel (b) shows the same data from (a) vertically shifted for clarity with a vertical black bar designating the $T_s(E)$ value for each curve. A zero electric field curve (black), corresponding to the same sample as E_2, is included for reference.

parameters in Eq. (6.3) do not provide quantitative agreement with the experimental results presented in this study. Specifically, unless $\varepsilon(\phi)$ is particularly different than expected,[j] it is hard to see how the second term in Eq. (6.3) would dominate the first. For the LCST-type phase diagram of PS/PVME, the interaction parameter *B* is negative, meaning that the second term in Eq. (6.3) must dominate for electric fields to enhance mixing. In essence, this term creates an energy penalty for the formation of dielectric interfaces oriented perpendicular to the field direction. Thus, this term always favors increased miscibility with increasing electric field strength, consistent with experimental results demonstrated here.

It is well known that interfaces between two different dielectric media oriented perpendicular to the electric field direction are energetically unfavorable, resulting in alignment of domains along the field direction; an effect frequently exploited in pattern formation and to align block copolymer morphologies.[3,13,15,16,29,142] Such an interface term could be particularly important in understanding polymer phase behavior in the presence of electric fields because chain connectivity may limit complete homogeneity of polymer blends even in the mixed phase. Although PS/PVME blends are regarded as miscible, based on a negative χ value[103,132] and exhibition of a single glass transition temperature,[134,143] several studies[132–134,144–146] have described PS/PVME blends as being

---

[j] Typically the curvature of $\varepsilon(\phi)$ dependence is expected to be positive, that is $\frac{\partial^2 \varepsilon(\phi)}{\partial^2 \phi} > 0$ and the composition dependent dielectric constant, $\varepsilon(\phi)$, is expected to not vary considerably from the dielectric constants of pure components, ε_A and ε_B. However, I want to note here, that PS/PVME blends differ from other mixtures due to the fact that there are hydrogen bonds present between the blend components. It has been shown that in liquids an intermolecular hydrogen bonding is an important variable in raising liquids dielectric constant.[153] Thus, there is a possibility that the $\varepsilon(\phi)$ in PS/PVME blends, being influenced by hydrogen bonding, is considerably different than what is typically expected.

micro- or nano- heterogeneous at the segmental level (~1–5 nm) when in the nominally one-phase mixed state. The experimental data presented here, with strong clear shifts in the phase separation temperature with electric fields, should prove useful for comparison with such theoretical efforts.

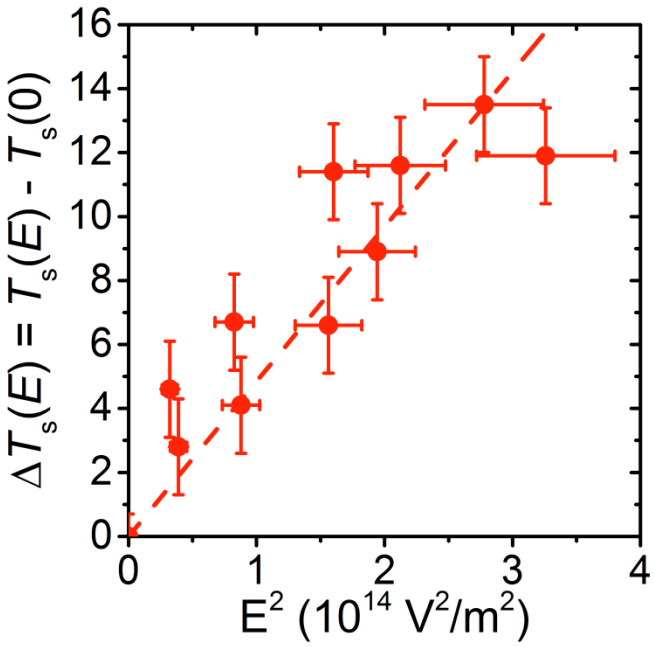

Figure 6.4 Shift in phase separation temperature $\Delta T_s(E) = T_s(E) - T_s(0)$ as a function of square of electric field strength E^2, where $T_s(E)$ is the phase separation temperature in the presence of electric field and $T_s(0)$ is the phase separation temperature under zero field, both measured on the same sample. The dashed line is a linear fit through the experimental data points with slope of $\Delta T_s/E^2 = (4.8 \pm 0.4) \times 10^{-14}$ Km^2/V^2.

6.2.3 Comparison with Reich and Gordon's work

In 1979, Reich and Gordon[44] published a study reporting very large decreases in the phase separation temperature T_s of PS/PVME blends when in the presence of strong electric fields. For $E = 2.72 \times 10^7$ V/m, decreases of up to 54 K were reported for the one 33/67 PS/PVME blend composition investigated. PS/PVME exhibits an LCST-type phase

behavior such that a decrease in T_s with electric field would imply reduced compatibility. This is in strong contrast to the results reported here in which large increases in T_s of up to 13.5 K for $E = 1.7 \times 10^7$ V/m are observed. The findings of my study indicate that electric fields enhance mixing, which is consistent with the larger majority of reports on electric field miscibility effects.[31,34–36,40–42,45] However, as my results show a completely opposite effects relative to the one previous study on PS/PVME, I discuss here possible reasons for this discrepancy. To better understand this contradiction between the Reich and Gordon study and results of this study, it is important to examine the experimental approach used by Reich and Gordon and the context of their study in more detail.

It could be considered surprising that Reich and Gordon did not further continue their studies with electric fields. Before 1979, the year Reich and Gordon published their results, only one experimental study on the electric field effects of phase separation had been published. In 1965, Debye and Kleboth[34] reported seeing minuscule shifts in T_s, up to 0.015 K for $E = 0.45 \times 10^7$ V/m in nitrobenzene/isooctane mixtures towards enhanced compatibility. The relative change of $\Delta T_s/E^2 = 0.08 \times 10^{-14}$ Km^2/V^2 for Debye and Kleboth's results is almost 100 times smaller than that reported by Reich and Gordon, $\Delta T_s/E^2 = 7.3 \times 10^{-14}$ Km^2/V^2. Thus, the large 54 K shifts observed by Reich and Gordon were extremely significant, especially compared to the only other study on a similar subject published at the time.

In 1981, two years after Reich and Gordon published their study on electric field effects on T_s,[44] another study from the same group reporting film thickness effects on T_s in PS/PVME blends was published by Reich and Cohen.[129] Reich and Cohen found shifts in T_s with decreasing film thickness, below approximately 1 μm in thickness, with the

effect found to be substrate dependent. For films on gold substrates, enhanced compatibility with decreasing thickness was observed, while for films on glass substrates, both enhanced and reduced compatibility was observed depending on blend composition.[129] These results by Reich and Cohen[129] may be informative in explaining the observations by Reich and Gordon.[44]

In their electric field study, Reich and Gordon[44] reported that the exact thickness of the polymer layers used in their experiments were not known, but assumed to be approximately 1–2 μm in thickness. In order to accurately determine the electric field strength across the polymer layers without knowing the exact film thickness, a 140 ± 4 μm glass microscope cover-slip was sandwiched in between the two polymer coated, ITO-covered glass slides. In such a sample geometry, the additional 1–2 μm thick polymer layers could be taken to be insignificantly small compared to the total sample thickness, such that the electric field strength due to the applied voltage was primarily determined by the 140 μm thickness of the intervening glass cover slip. The inserted cover slip also had the added benefit of virtually eliminating concerns of dielectric breakdown.

Reich and Gordon prepared their polymer blends by dip-coating ITO-covered glass substrates into PS/PVME solutions of 10 wt% total polymer content, where the molecular weights were reported to be 31.5 kg/mol for PS and 14.4 kg/mol for PVME (neither the polydispersity, nor whether these values were number or weight average were specified).[44] In the later study by Reich and Cohen,[129] an extensive correlation is included plotting the resulting film thickness obtained by dip coating PS/PVME blends from solutions of different concentrations, for weight average molecular weights of M_w =

36 kg/mol for PS and M_w = 10.7 kg/mol for PVME. The data indicates a strong dependence of film thickness on concentration. For 10 wt% PS/PVME total polymer content, the resulting film thickness is expected to be 750 nm thick, with film thicknesses varying between 600–1000 nm for concentrations 9–11 wt%.[129] Reich and Cohen's results suggest that the polymer layers in Reich and Gordon's experiments may be thinner than the presumed 1–2 μm, and be within the regime, below ~1 μm, where the phase separation temperature exhibits some film thickness dependence. There may also be considerable variation in film thickness from sample-to-sample depending on the concentration of the solutions used. Unfortunately, it cannot be estimated how this might or might not have affected Reich and Gordon's reported shifts in T_s with electric field.

Based on the details given in their publication, it is likely that Reich and Gordon[44] determined their shift in the phase separation temperature, $\Delta T_s(E) = T_s(E) - T_s(0)$, by comparing measurements at zero and non-zero field on different samples. They quote errors for T_s to within 3 K, averaging measurements over multiple samples. Phase separation was measured using a light scattering setup with a helium-neon laser, ramping up in temperature at 1 K/min and identifying the cloud point temperature at which the phase separated domains became large enough to scatter the light. There is no mention of remixing samples, as such domain sizes may be too large to feasibly remix in a timely manner. The as-cast samples were given typical annealing treatments of 24 h at 70 ^{o}C under a vacuum of 1 Torr, prior to measurement. Thus, such T_s values would have corresponded to values on first heat, which I have found to be the most variable because some preparation conditions are difficult to standardize precisely.

Despite all these possible factors, it is not possible to ascertain why Reich and

Gordon[44] observed, reproducibly for their samples, a direction of T_s shift opposite to the results presented here. It is should be mentioned here that if their samples, which were immersed in an oil bath, experienced local Joule heating, such an uncontrolled temperature increase would manifest as an apparent decrease in T_s that would be expected to increase with increasing electric field strength. Their sample design containing a glass cover-slip between the electrodes may have effectively eliminated any current flow within the sample, but it is conceivable that some current flow through the surrounding oil may have locally increased the temperature, undetectable in the larger oil bath reservoir.

6.3 Conclusions

An experimental protocol was developed using fluorescence by which the phase separation temperature T_s of PS/PVME blends can be repeatedly re-measured on the same sample by iteratively heating this LCST-type blend to determine T_s, followed by a quench and subsequent anneal of the blend in the one-phase region of the phase diagram. This remixing protocol enables to reproducibly measure T_s to within ± 0.7 ^{o}C on the same sample with and without the presence of strong uniform electric fields. I demonstrate conclusively that the presence of electric fields substantially enhances the miscibility of the blend by measuring large increases in T_s, significantly outside of experimental error by over an order of magnitude, and subsequently recovering the same original T_s at zero field after the electric field has been turned off. Note that any presence of Joule heating would result in a decrease in T_s, opposite in direction to the increase in T_s observed when in the presence of an electric field. The measured shifts $\Delta T_s(E)$ of up to 13.5 K for

electric field strengths of $E = 1.7 \times 10^7$ V/m are some of the largest absolute shifts in T_s ever reported, although the relative magnitude of the shift $\Delta T_s/E^2 = (4.8 \pm 0.4) \times 10^{-14}$ Km^2/V^2 is comparable to values from previous studies on other blends. These results do, however, contradict the one previous study on PS/PVME blends,[44] which reported that electric fields induced phase separation. The ultimate reason for this discrepancy is unknown, with several possibilities being considered, although it should be pointed out that this study[44] has long since been considered an outlier in the field.[31] The discovery that electric fields strongly enhance mixing in PS/PVME blends is in agreement with the vast majority of existing experimental data on other blend systems. This study will help bring coherence to the existing experimental data and provide large, unambiguous shifts in $T_s(E)$ with electric field for theoretical predictions to be tested.

Chapter 7
Electric Field Effects on the Time Scale of Remixing Dynamics of Polystyrene / Poly(vinyl methyl ether) Blends

---

In the previous chapter, I presented results demonstrating that electric fields increase the phase separation temperature T_s in PS/PVME blends and as a result enhance the miscibility of this blend. In order to learn more about the electric field effect on polymer blends, I studied how electric fields affect the temperature dependence of remixing time scales. In this chapter the experimental technique developed to measure the remixing time scale in PS/PVME blends is discussed and results showing that electric fields do not affect the time scale of remixing dynamics are presented.

Figure 7.1 illustrates the experimental protocol used in this study to measure the remixing time scale in PS/PVME blends at different temperatures. If a sample is forced through a temperature jump from the one phase region (at an initial temperature T_{remix}) to the two phase region at a temperature T_{unmix}, as shown in Figure 7.1a and b, a thermodynamic driving force will induce an onset of phase separation of the blend

components. As the molecules of PS and PVME start diffusing away from each other, the fluorescence quenching effect by the polar PVME to the dye on PS is reduced and as a result the fluorescence intensity is expected to increase, as shown in Figure 7.1c. Subsequently, when the sample is quenched down from the two phase region at T_{unmix} to the one phase region at T_{remix}, as shown in Figure 7.1a and b, the thermodynamic driving force will cause remixing of the blend molecules and the fluorescence quenching effect by PVME to the dye grows stronger as the PVME molecules move closer to PS molecules. As a result the fluorescence intensity is expected to decay at the temperature T_{remix} with a time scale related to the interdiffusion of the two components (see red curve in Figure 7.1c). As we will find, the fluorescence intensity decays following a single exponential decay, which can be fit to an exponential decay function whose decay constant τ (from here on called the remixing time scale) at the temperature T_{remix} can be found. This remixing time scale τ, is the amount of time that an exponentially decaying quantity, here the fluorescence intensity, takes to decrease by a factor of $1/e$, that is about 36.8% of its original amount.[147] The system can be assumed to be stable after time $5\times\tau$, when the intensity reaches a value less than 1 % of its original. Hence, in this study time $5\times\tau$ can be considered as the time it is needed for the PS/PVME blends components to interdiffuse, to remix.

It can be argued that as the remixing temperature T_{remix} is lowered, the dynamics of the polymer blend grow slower and the corresponding remixing time scale τ grows longer. In Figure 7.1d, the red circles illustrate the expected temperature (T_{remix}) dependence of the remixing time scale τ. As the remixing time scale τ characterizes the interdiffusion of the two components, I anticipate that its temperature dependence should

follow that of the diffusion coefficient or viscosity of the PS/PVME blend, typically described by a Vogel-Fulcher-Tammann (VFT) function.[2,148] In Figure 7.1d, the black solid curve is an illustration of the VFT function

$$\tau = \tau_\infty e^{\frac{B}{T-T_o}}, \tag{7.1}$$

where the temperature dependence of the remixing time scale $\tau(T)$ is described by the parameters B, T_o, and τ_∞. In polymer science, the VFT function (or equivalently a law described by the Williams-Landel-Ferry equation) is well known and is shown to successfully describe the temperature dependence of viscosity, self-diffusion, and many relaxation times of a polymer chain. T_o is called Vogel temperature and is typically found to be about 50 ^oC below the polymer's glass transition temperature T_g. At temperature $T = T_o$ the VFT function goes to infinity, whereas if $T_o = 0$ K, the VFT equation reduces to an Arrhenius equation.[2]

I am interested in determining if this remixing time scale $\tau(T)$ is affected by the presence of electric fields. Figure 7.2 illustrates the experimental protocol to be used in this study to determine the electric field effect on the remixing time scale of PS/PVME blends. Following the same protocol described in Figure 7.1 to briefly unmix the sample at a temperature T_{unmix}, an electric field is now applied across the sample at the same time as the sample is quenched back to the temperature T_{remix} from T_{unmix} (see Figure 7.2a, b and d). As demonstrated in Chapter 6, the presence of the electric field will increase the phase separation temperature of the sample. The electric field effect on the remixing time scale is found by comparing the remixing time scale $\tau(T)$ in the presence of an electric field E (blue circles in Figure 7.2e), found from the fluorescence intensity decay

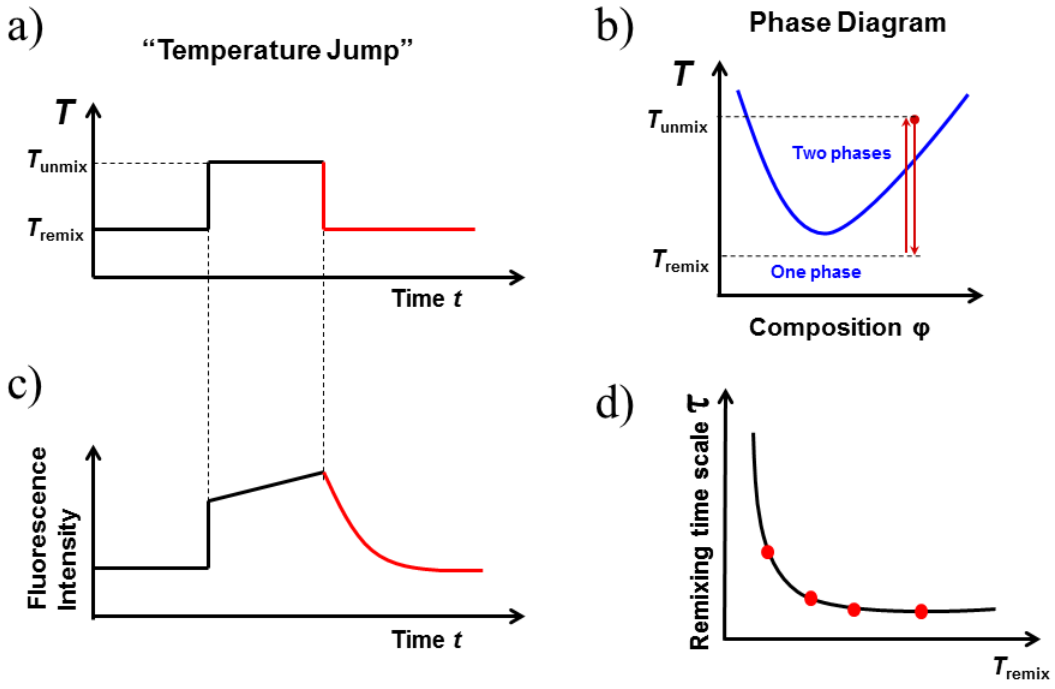

Figure 7.1 Illustration of the fluorescence protocol to measure the time scale of remixing dynamics in PS/PVME blends. (a) Sample is heated from T_{remix} (one phase region) to T_{unmix} (two phase region), kept at T_{unmix} for 5 min and then quenched back to T_{remix}. (b) Red arrows indicate the temperature changes of the sample relative to the phase diagram. (c) Expected change in fluorescence intensity as a result of the temperature jumps. Fluorescence intensity increases when sample is in the two phase region and decreases when sample is forced back to the one phase region. This is because fluorescence quenching effect by PVME to the fluorescent dye attached to PS is reduced when blend components move away from each other during the phase separation and increased when blend components diffuse back together during remixing. Remixing time scale at temperature T_{remix} is found from a single exponential fit to the fluorescent intensity decay. (d) Red circles indicate the remixing time scales found at different T_{remix} temperatures. Expected sample remixing dynamics become slower (remixing time scale increases) as T_{remix} decreases. Black solid line is an illustration of the Vogel-Fulcher-Tammann function, often used in polymer science to describe the temperature dependence of viscosity.

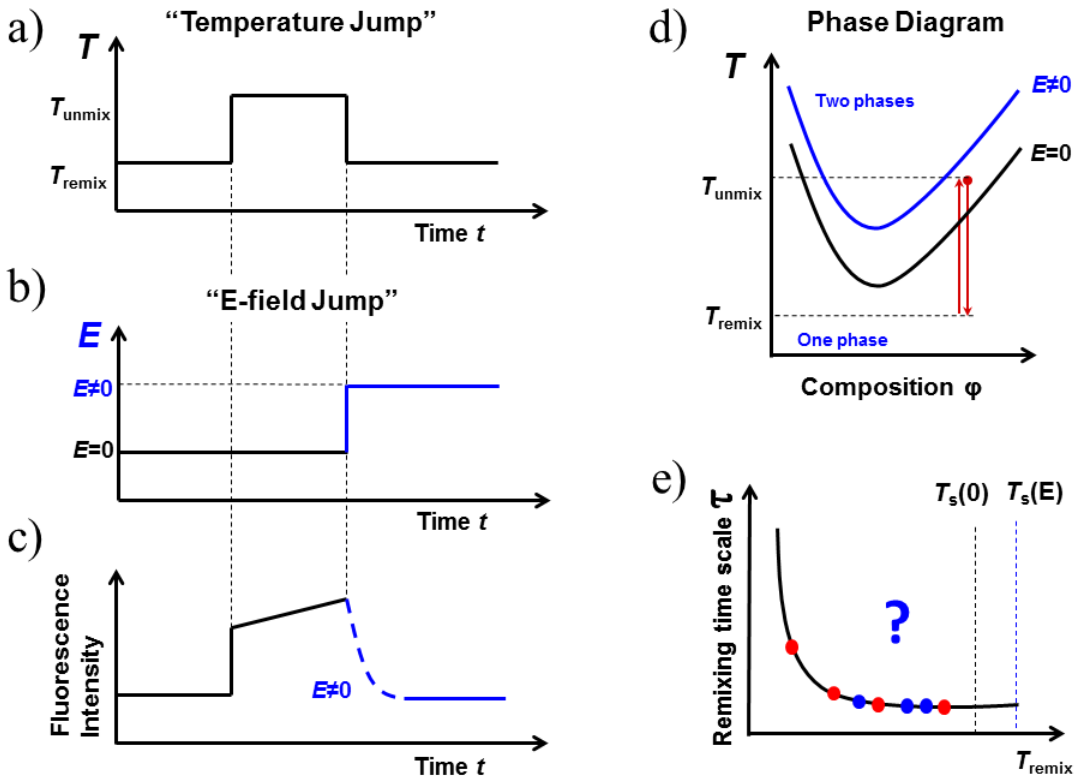

Figure 7.2 Illustration of the fluorescence protocol to find the electric field effect on the remixing time scale in PS/PVME blends. (a) Sample is heated from T_{remix} (one phase region) to T_{unmix} (two phase region), kept at T_{unmix} for 5 min and then quenched to temperature T_{remix}. (b) At the same time as sample is forced back into the one phase region at T_{remix}, an external electric field is applied across the sample. (c) Expected change in fluorescence intensity. (d) Phase diagram: the presence of an electric field increases the phase separation temperature higher. (e) Red and blue circles indicate the remixing time scales found at different temperatures T_{remix} in the presence of zero and non-zero electrical fields, respectively. Here the blue circles are drawn so to fall on the same curve with the red circles. However, before conducting the experiment it is not known whether the electric field would change (or not change) the remixing time scale of the blend. Dashed vertical blue and black lines indicate the positions of the phase separation temperatures of the sample, with and without the presence of electric fields, $T_s(E)$ and $T_s(0)$, respectively, relative to the temperature T_{remix}.

measured in the presence of an electric field (blue curve in Figure 7.2c), to the remixing time scale $\tau(T)$ found from the fluorescence intensity decay measured under zero electric field (red curve in Figure 7.1c) and illustrated as red circles in Figure 7.2e. If the electric field has no effect on the remixing times scales then $\tau(T)$ with and without electric fields measured at different remixing temperatures T_{remix} would fall on the same temperature curve (black solid line in Figure 7.2e). Alternatively, one might anticipate that the remixing time scale $\tau(T)$ might be shorter in the presence of an electric field reflecting an increased driving force for remixing as the blend would be located further from the phase boundary at the same temperature T_{remix}: $T_s(E) - T_{remix} > T_s(0) - T_{remix}$. It is also possible to apply a strong enough electric field so that the blend phase separation temperature under electric fields, $T_s(E)$, is higher than the unmixing temperature, T_{unmix}. Thus, it may be experimentally possible to observe remixing, and measure $\tau(T)$, at the temperature T_{unmix} if $T_s(E)$ becomes greater than $T_{unmix.}$

7.1 Experimental

In this study, a total of 4 different samples were used to determine the electric field effect on the temperature dependence of the remixing times scale in PS/PVME blends. All samples were prepared following the same sample preparation protocol and identical PS/PVME blend composition and components used as for the study of electric field effects on miscibility of PS/PVME blends discussed in Chapter 6. Using the "remixing protocol" discussed in Chapter 5 Figure 5.1, reproducible phase separation

temperatures, T_s were determined for each sample of 101.2 ^oC, 99.4 ^oC, 99.5 ^oC, and 99.2 ^oC, with an average T_s of 99.8 $^oC \pm 0.8$ ^oC across the 4 different samples. The samples were heated up three times from 80 ^oC (in one-phase region) to 104 ^oC (in two-phase region) at a rate of 1 ^oC/min while simultaneously collecting fluorescence intensity as a function of temperature. Between these three ramps, sample was remixed at 94 ^oC for 2 hours. As shown in Chapter 5 Figure 5.1, reproducible phase separation temperatures with an experimental error less than a degree can be measured after the first ramp. The reproducible phase separation temperature, T_s was found as an average of the phase separation temperatures measured during the second and third ramp. The T_s measured during the first ramp was discarded.

After finding the reproducible phase separation temperature, each sample was again remixed for 2 hours in one phase region at initial temperature $T^i_{remix} = 94$ ^oC and then heated quickly at a rate of ~ 30 ^oC/min into the two phase region to temperature $T_{unmix} = 104$ ^oC. Samples were kept at 104 ^oC for 5 minutes and then quenched back into the one phase region to temperature T_{remix}. For this study three different temperatures for T_{remix} were used, $T_{remix1} = 94$ ^oC, $T_{remix2} = 90$ ^oC, $T_{remix3} = 85$ ^oC. Fluorescence intensity was collected simultaneously before, during and after the temperature jump. Samples were left at T_{remix} for up to an hour so that enough fluorescence signal could be collected. If the $T_{remix} = T_{remix1} = 94$ $^oC = T^i_{remix}$ the sample was kept at 94 ^oC for total of 2 hours and the experiment was then continued with the next temperature jump. However if the $T_{remix} = T_{remix2} = 90$ ^oC or $T_{remix} = T_{remix3} = 85$ ^oC, the sample was heated back to T^i_{remix} at 94 ^oC and left for 2 hours before the next temperature jump, to guarantee proper remixing of the blend.

Figure 7.3 shows the data analyses used in this study to determine the remixing time scale of the PS/PVME blend at a temperature T_{remix} = 94 ^{o}C when no electric field is present. Figure 7.1a shows the temperature profile[k] of a sample heated from T^{i}_{remix} = 94 ^{o}C to T_{unmix} = 104 ^{o}C (from A to B), kept at T_{unmix} = 104 ^{o}C for 5 min (from B to C) and quenched from T_{unmix} = 104 ^{o}C to T_{remix} = 94 ^{o}C (from C to D). The black curve in Figure 7.3a corresponds to the temperature profile assigned to the temperature controller while the red curve shows the actual sample temperature during the experiment. Figure 7.3b shows the fluorescence intensity, *I*, as a function of time, *t*, collected during the temperature profile presented in Figure 7.3a.

The fluorescence intensity profile follows the expected trend described in Figure 7.1c: the intensity is essentially stable while the blend is in equilibrium at T^{i}_{remix} = 94 ^{o}C, then the intensity jumps up and begins to increase steadily when the temperature quickly changed to T_{unmix} = 104 ^{o}C in the two phase region, after 5 min the temperature is returned quickly to T_{remix} = 94 ^{o}C and the fluorescence intensity decays back to its previous value. It is clear from the data that there appears to be a small linear background drift of the intensity with time. This slow increase in fluorescence intensity at constant temperature was present in all measurements, although no direct explanation was found. However, we note that the total change in fluorescence intensity during these temperature jumps are rather small. This small linear background (blue line in Figure 7.3b) has been subtracted off to arrive at the fluorescence intensity *I** as a function of time shown in Figure 7.3c. The small linear background was not found to be temperature dependent ,

[k] Temperature profile was recorded with Wintemp software while controlling the sample temperature with the MK1000 High Precision Temperature Controller.

that is, it was found to follow the same linear trend before the jump from T^{i}_{remix}=94 ^{o}C to T_{unmix}=104 ^{o}C and after the jump from T_{unmix} =104 ^{o}C to T_{remix}= 94, 90 or 85 ^{o}C. If the small linear background is indeed weakly temperature dependent, the change in its trend at different temperatures was concealed within the noise of the fluorescence intensity data.

Figure 7.3c shows a sharp downward peak in fluorescence intensity when the temperature is increased from 94 ^{o}C to 104 ^{o}C (from A to B). This abrupt intensity change can be explained by the fact that the sample temperature does not instantaneously reach the unmixing temperature T_{unmix} = 104 ^{o}C (see red curve in Figure 7.3a). As discussed in Chapter 4, due to the nonradiative decay the fluorescence intensity of a mixed blend is always lower at higher temperatures. Thus, in Figure 7.3c, the fluorescence intensity drops sharply between points A and B because though the sample temperature increases fast, initially the sample is still in a mixed state but at higher temperature than the initial 94 ^{o}C. Once the sample reaches T_{unmix} the components in the PS/PVME blend are driven apart by the strong thermodynamic driving force and as expected a sharp increase in the fluorescence intensity is observed signifying phase separation.

While the sample is held at 104 ^{o}C for 5 min (from B to C in Figure 7.3a) the PS/PVME blend components diffuse away from each other and the fluorescence intensity continues to increase (from B to C in Figure 7.3c) as a result of reduced fluorescence quenching by the close proximity of PVME to the fluorescent dye attached to PS. Because the samples do not show any visual signs of phase separation (looked

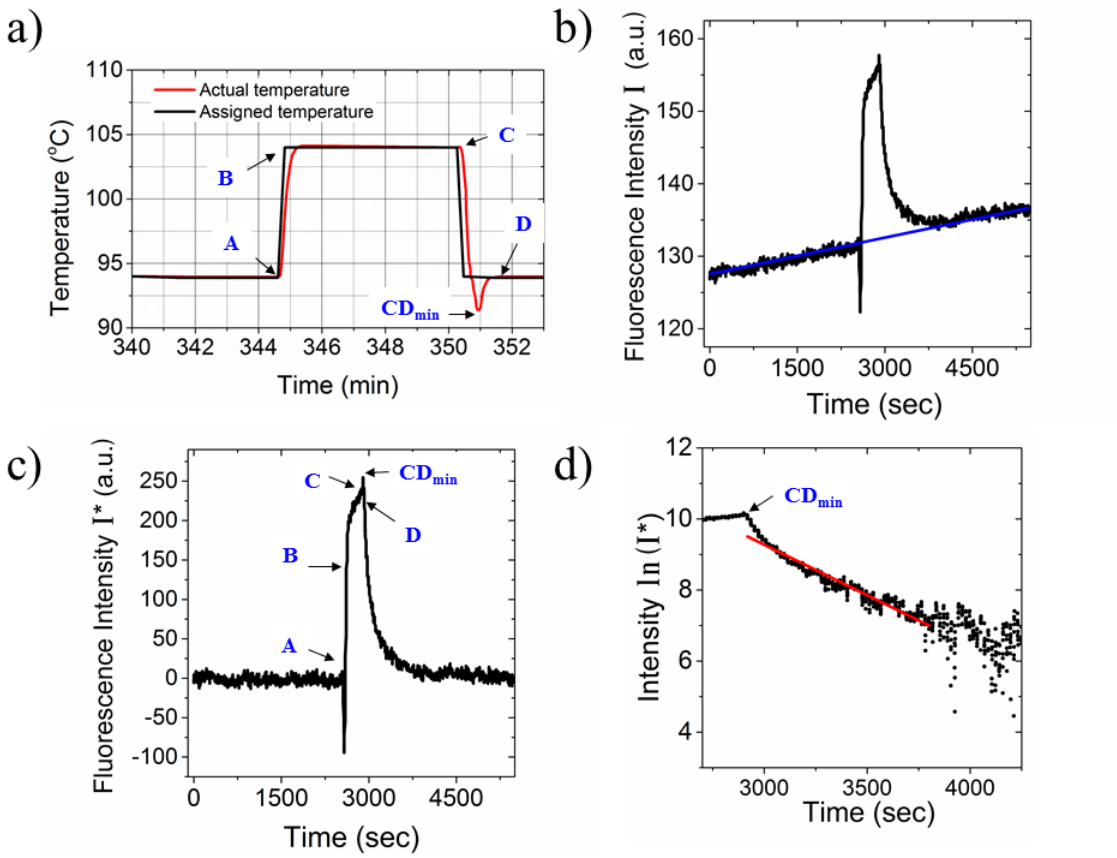

Figure 7.3 The data analyses used to determine the remixing time scale τ for a sample of (40/10)/50 (PS/PS*)/PVME blend from data collected under zero electric field. After determining the reproducible phase separation temperature at T_s = 99.8 °C, the sample was subjected to the temperature jumps (a) while simultaneously measuring the fluorescent intensity, *I*, as a function of time, *t*, (b). The sample temperature was changed from T^i_{remix} = 94 °C to T_{unmix} = 104 °C (from A to B), kept 5 min at T_{unmix} = 104 °C (from B to C) and quenched to T_{remix} = 94 °C (from C to D). (a) The temperature assigned to the temperature controller and the actual sample temperature during the experiment are shown as black and red curves, respectively. During the quench from 104 °C to 94 °C, the temperature before leveling at 94 °C (D), undershoots at 92 °C (point CD_{min}). During that period the fluorescence intensity increases and peaks at $CD_{min.}$ (c) The fluorescent intensity, *I**, as a function of time, *t*, after subtraction of the linear background shown as a blue line in (b). (d) Semi-log plot of fluorescent intensity measured after sample is quenched from T_{unmix} = 104 °C to T_{remix} = 94 °C. Red solid line marks the area expected to be linear.

transparent with no evidence of cloudiness) after being held at 104 ^{o}C for 5 min, that is approximately 4.5 degrees above $T_s(E=0)$, it can be argued that the phase separation is still in the early stages. The phase separated domain dimensions in the samples must be below the wavelength of light, otherwise the samples would appear cloudy. This estimation is confirmed by Larbi et al.,[149] who measured the fluorescence intensity versus phase separation time in PS/PVME blends using a similar fluorescence technique to that applied in this study. They observed that the intensity exhibits a logarithmic increase with time and tends to a limiting value I_∞ at long enough phase separation time (longer than 12 minutes, if the unmixing temperature T_{unmix} is about 4.5 degrees above T_s). They stated that phase separation in the PS/PVME blend reached the late stages when the intensity I_∞ was attained. From Figure 7.3c it is clear that during the 5 min time period the sample spends at 104 ^{o}C (from B to C), the fluorescence intensity does not reach a limiting value.

As seen in Figure 7.3a, the sample does not instantaneously reach the remixing temperature T_{remix} = 94 ^{o}C when quenched back down from T_{unmix} = 104 ^{o}C. During this quench the temperature undershoots to 92 ^{o}C (point CD_{min}) and it takes approximately 30 s for the sample temperature to level off at T_{remix} = 94 ^{o}C (point D). Notice that, when the sample temperature is at its lowest at 92 ^{o}C (point CD_{min} in Figure 7.3 a) the fluorescence intensity reaches its maximum (point CD_{min} in Figure 7.3c). Once the temperature reaches the remixing temperature T_{remix} in the one-phase region, the PS and PVME molecules in the unmixed PS/PVME blend are driven by the thermodynamic driving force to interdiffuse. As a result the fluorescence intensity decays because the fluorescence quenching effect by the PVME to the fluorescent dye on the PS is growing stronger. In Figure 7.3c beyond point D, where the sample temperature is stable at T_{remix}

= 94 ^{o}C, the decline in fluorescence intensity as a function of time resembles a single exponential decay

$$I^*(t) = I_o e^{-\frac{t}{\tau}} \tag{7.1}$$

where $I^*(t)$ is the time-dependent fluorescence intensity, I_o is the initial intensity at time t = 0 (which I redefine as the time at point D when the sample temperature has reached T_{remix} = 94 ^{o}C), and τ is the decay constant. To see whether the fluorescence intensity decay in Figure 7.3c truly follows a single exponential decay, Eq. (7.1), the data is plotted as the logarithmic intensity vs. time in Figure 7.3d. The red solid line in Figure 7.3d marks the area expected to be linear. We notice that in the very beginning of the fluorescence intensity decay, that is about 1 min after point CD_{min}, the data seems to curve slightly upwards. Most likely explanation to this slight upturn is that after point CD_{min} the sample takes about 1 min to reach equilibrium at T_{remix} = 94 ^{o}C. According to Figure 7.3a, measured with Wintemp software, it takes about 30 sec for the temperature at point CD_{min} to reach equilibrium at T_{remix} = 94 ^{o}C at point D. However, it should be noted here, that the Wintemp software measures the temperature at the sample holder and not the temperature of the sample itself. To test the accuracy of the Wintemp software, I measured the sample temperature *in situ* during the quench from T_{unmix}=104 ^{o}C to T_{remix}=94 ^{o}C and the quench from T_{unmix}=104 ^{o}C to T_{remix}=85 ^{o}C using a separate thermocouple and compared the measured temperatures to the values simultaneously recorded by Wintemp software. I found that after the quench to T_{remix} the sample reached equilibrium temperature at T_{remix}=94 ^{o}C about 15 to 30 s and at T_{remix}=85 ^{o}C about 1 min to 1min 15 s later than indicated by Wintemp software. This means that after the sample holder reached the T_{remix} at point D the sample itself needed extra time to catch up with

the temperature of sample holder. As the sample is quenched deeper into one phase region, even more time is needed for the sample to equiliberate at T_{remix}.

Figure 7.4 plots the time dependence of fluorescence intensity measured under zero electric field at remixing temperatures (a) T_{remix} = 94 ^{o}C, (c) T_{remix} = 90 ^{o}C, (e) T_{remix} = 85 ^{o}C and under electric field of 1.28×10^{7} V/m at remixing temperatures (b) T_{remix} = 94 ^{o}C, (d) T_{remix} = 90 ^{o}C, (f) T_{remix} = 85 ^{o}C are plotted in. Data shown in Figure 7.4 is shifted here so that the first point of the data starts at t=0. The starting point for the linear fit was chosen approximately at time when the sample (and not sample holder) reached its remixing temperature T_{remix}. The end point for the linear fit was chosen at around a time when the data visibly started looking more scattered (as can be seen in Figure 7.3d). Although, the criteria for the starting and ending points of the linear fit allowed some randomness, changing the linear fit region a few data points one way or the other did not change the remixing time scale value. From Figure 7.4, it appears that the fluorescence intensity collected at different remixing temperatures, T_{remix}, with and without electric field agrees well with Eq. (7.1), as the logarithmic intensity seems to follow a straight line, at least to first approximation. Remixing time scales (a) τ = 390 s, (b) τ = 280 s, (c) τ = 440 s, (d) τ = 440 s, (e) τ = 760 s, and (f) τ = 1600 s were found from linear fit to $\ln(I^{*}) = -\frac{t}{\tau} + \ln(I_0)$ through data.

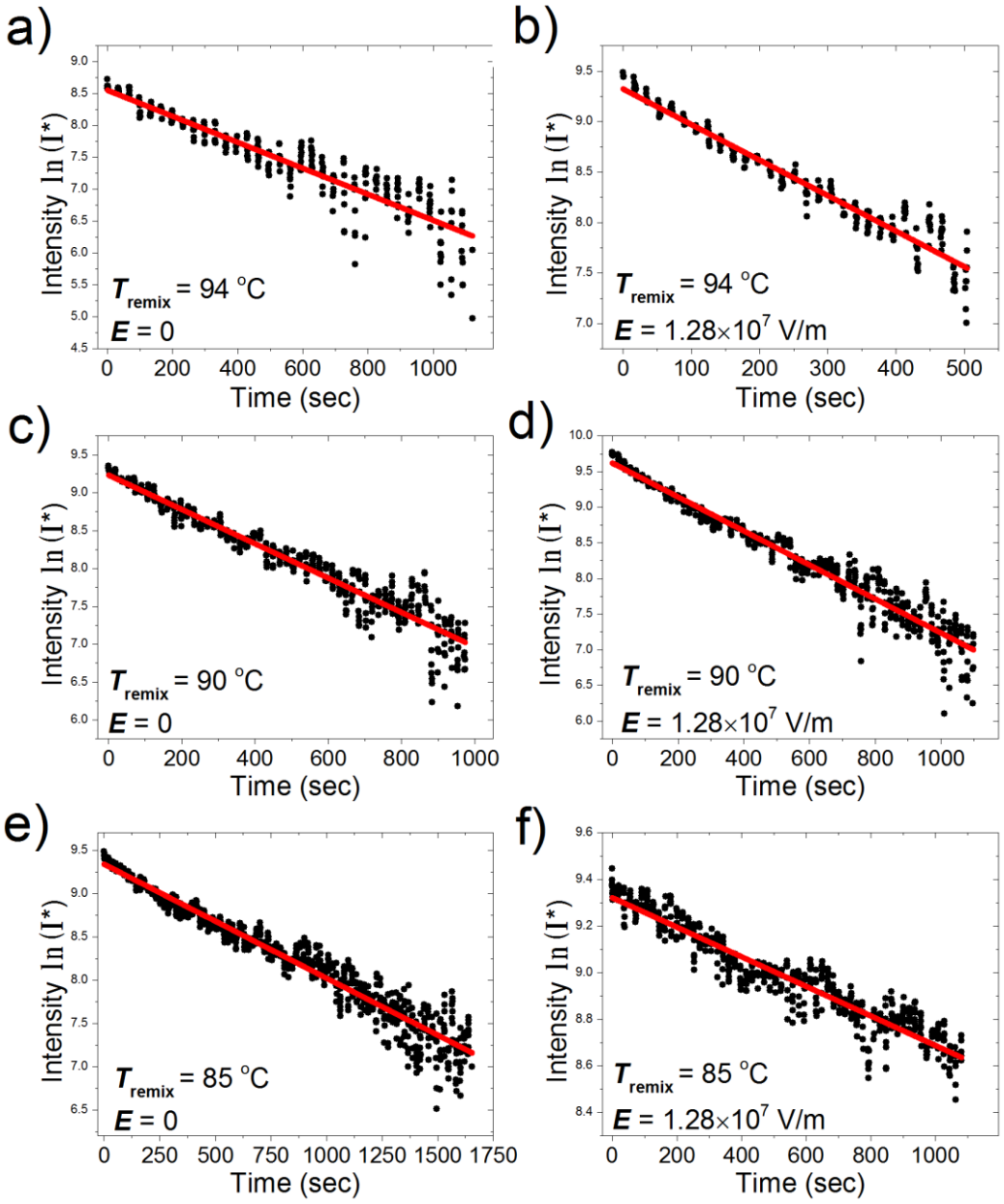

Figure 7.4 Time dependence of fluorescence intensity for samples of (40/10)/50 (PS/PS*)/PVME blends measured under zero electric field at remixing temperatures (a) T_{remix} = 94 °C, (c) T_{remix} = 90 °C, (e) T_{remix} = 85 °C and under electric field of 1.28×10^7 V/m at remixing temperatures (b) T_{remix} = 94 °C, (d) T_{remix} = 90 °C, (f) T_{remix} = 85 °C. Remixing time scales (a) τ = 390 s, (b) τ = 280 s, (c) τ = 440 s, (d) τ = 440 s, (e) τ = 760 s, and (f) τ = 1600 s are found from linear fit to $\ln(I^*) = -\frac{t}{\tau} + \ln(I_0)$ through data. Data shown are shifted here so that the first point of the data starts at t=0.

7.2 Results and discussion

Figure 7.5 shows the logarithmic fluorescence intensity as a function of time for samples of (40/10)/50 (PS/PS*)/PVME blends at one remixing temperature T_{remix} = 94 ^{o}C. Circles represent data collected, while lines represent linear fits to $\ln(I^*) = -\frac{t}{\tau} + \ln(I_0)$ through each set of data. (Note that the data in Figure 7.5 is shifted so that the first point of data and linear fit start at t=0 and, the first point of linear fit corresponds to I=0. However, the remixing times scales are found from data plotted as shown in Figure 7.4). Figure 7.5a shows a total of ten runs on four different samples (black, blue, green, orange) measured when no electric field is present. We notice from Figure 7.5a that the slope (time constant) of the decay in fluorescence intensity is reproducible at a temperature of 94 ^{o}C. The remixing time scale τ for each set of data were found from the slope of the linear fit, giving an average remixing time scale τ = 330 ± 40 sec at T_{remix} = 94 ^{o}C under zero electric field. In Figure 7.5b, all the data collected under zero electric field at 94 ^{o}C (shown in black; same data as plotted in Figure 7.5a) is compared to data collected in the presence of an electric field of E = 1.28 × 10^7 V/m (shown in red). Using the data shown in Chapter 6, Figure 6.4, the electric field of E = 1.28 × 10^7 V/m is expected to increase the phase separation temperature of the PS/PVME blend by at least by ~5 ^{o}C and up to as much as ~12 ^{o}C. This very large variability in the estimated ΔT_s(E) shift corresponds to the lower and upper limit of the error bars of the data collected with electric field strengths of about 1.3 × 10^7 V/m in Figure 6.4. Thus, the average T_s here is estimate to change from $T_s(0)$ = 99.8 ^{o}C to $T_s(E) \approx$ 105– 112 ^{o}C. The average remixing time scale τ = 260 ± 50 s for data measured under an electric field of E = 1.28 × 10^7 V/m

at T_{remix} = 94 ^{o}C matches within experimental error to the average remixing time scale τ = 330 ± 40 s measured under zero electric field at T_{remix} = 94 ^{o}C.

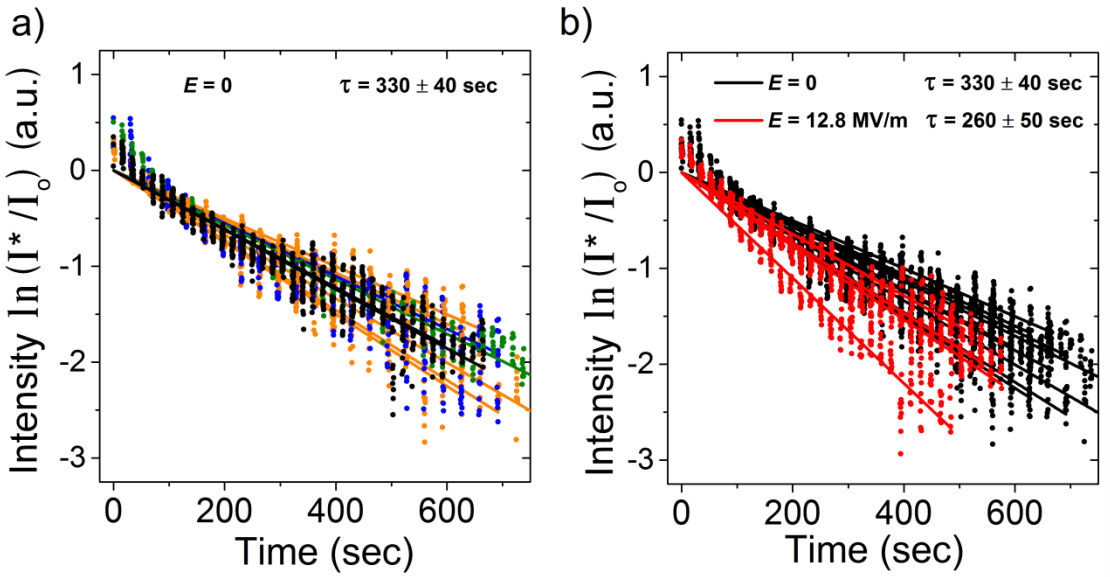

Figure 7.5 Time dependence of fluorescence intensity for samples of (40/10)/50 (PS/PS*)/PVME blends at one remixing temperature T_{remix} = 94 ^{o}C. Circles represent data collected, while lines represent linear fit to $\ln(I^*) = -\frac{t}{\tau} + \ln(I_0)$ through each set of data. Remixing time scale τ is found from the slope of the linear fit. (Here for the purpose of visual aid the data is shifted so that the data and linear fit start at t=0, and the linear fit starts from point where intensity I=0 However, the remixing times scales are found from data graphed as shown in Figure 7.4.) (a) Ten runs on four different samples (black, blue, green, orange) collected under zero electric fields give an average remixing time scale τ = 330 ± 40 s. (b) (red) Four runs measured under an electric field of E = 1.28 × 10^7 V/m giving an average remixing time scale τ = 260 ± 50 sec. (black) ten runs from plot (a) at zero electric field.

As was discussed at the beginning of this chapter, in this study it is assumed that 5×τ gives the time required for the PS/PVME blend components to remix. According to the data shown in Figure 7.5, the time needed for the blend to remix at 94 ^{o}C is approximately t = 25 min, found as an average from 5×τ = 28 min for E = 0 and 5×τ = 22 min for E = 1.28 × 10^7 V/m. Using the equation for three dimensional diffusion time t =

$\frac{<r^2>}{6D} = \frac{<x^2+y^2+z^2>}{6D}$ and the values for the diffusion constants D found in the literature, the average distance $<r^2>$ the polymer chains travel during t = 25 min can be estimated. Jabbari and Peppas[136] reported that $D = 4.2 \times 10^{-14}$ cm^2/s at 85 ^{o}C and $D = 1.1 \times 10^{-12}$ cm^2/s at 105 ^{o}C for PS/PVME blends with molecular weights M_w = 105 kg/mol, M_w/M_n = 1.06, for PS and M_w = 99 kg/mol, M_w/M_n = 2.10, for PVME (comparable to molecular weights in the present study). The diffusion constants by Jabbari and Peppas yield fairly realistic estimations for the average distance $\sqrt{< r^2 >} \approx 0.2$ μm during 25 min at 85 ^{o}C and $\sqrt{< r^2 >} \approx 0.4$ μm during 5 min at 105 ^{o}C. These values agree with the fact mentioned earlier in this chapter, that the samples after staying 5 min at T_{unmix} = 104 ^{o}C in the two phase region, do not show visual signs of phase separation, suggesting the domain sizes are expected to be smaller than the wavelength of light.

Figure 7.6 graphs the remixing time scale τ for samples of (40/10)/50 (PS/PS*)/PVME blends plotted (a) versus temperature T_{remix} for T_{remix} = 85, 90, and 94 ^{o}C and (b) as log of remixing time scale versus inverse temperature T_{remix}. The time scales found under zero electric field (hollow triangles) match well with the time scales found under an electric field of $E = 1.28 \times 10^7$ V/m (red circles). The solid curve in Figure 7.6a and b is calculated from Eq. (7.1), the Vogel-Fulcher-Tammann (VFT) temperature-dependence function, using the parameters B =1731 K and T_o = 271 K by Halary et al.[150] for a 50/50 PS/PVME blend, with M_w = 35 kg/mol and PDI = 1.06 of PS, and M_w = 99 kg/mol PDI = 2.12 of PVME. Halary et al.[150] studied the temperature dependence of molecular mobility in PS/PVME blends in the one phase region using a fluorescence polarization technique developed in their lab. Although the data collected (triangles and

circles) in Figure 7.6 seem to match well to the VFT curve, a wider temperature window would need to be explored to be able to definitely conclude that the remixing time scale follows the temperature-dependent dynamics described by a VFT function.

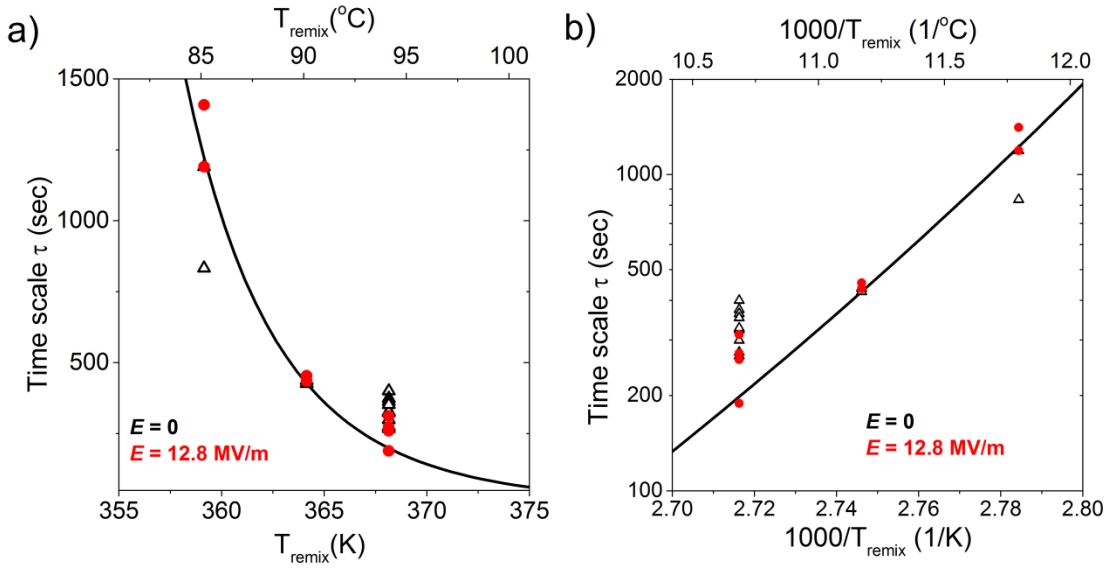

Figure 7.6 Remixing time scale τ for samples of (40/10)/50 (PS/PS*)/PVME blends plotted (a) versus temperature T_{remix} and (b) as log remixing time scale versus inverse temperature T_{remix}: (hollow triangles) data collected under zero electric field and (red circles) data collected under an electric field of $E = 1.28 \times 10^7$ V/m. Black solid curve in (a) and (b) is calculated from a Vogel-Fulcher-Tammann (VFT) temperature-dependence function Eq. (7.1) using parameters $B = 1731$ K and $T_o = 271$ K by Halary et al.[150] previously found to work well for PS/PVME blends.

Overall, the data in Figures 7.5 and 7.6 demonstrate that electric fields do not appear to affect the remixing time scale of PS/PVME blends. On one hand these results are perhaps not surprising. Although in the presence of electric field the phase boundary shifts upwards, the mobility and viscosity of the blend molecules are not expected to change because the mobility and viscosity should only depend on the blend temperature. On the other hand, the driving force for remixing, the force that drives the blend

molecules towards interdiffusion, should increase in the presence of electric fields because the distance from the phase boundary at T_{remix} increases due to electric fields. Using the definition for the thermodynamic driving force ~ $(T-T_s)/T_s$ for spinodal decomposition estimated by Larbi et al.[149], at T_{remix} = 94 ^oC, the driving force under electric fields ($(T-T_s)/T_s$ = (94 – 108.5)/108.5 = - 0.13) is roughly double of the value compared to the thermodynamic driving force under zero field ($(T-T_s)/T_s$ = (94 – 99.8)/99.8 = - 0.06). Larbi et al.[149] investigated the kinetics of phase separation of PS/PVME blends using the fluorescence emission technique developed by Halary et al.[61] (discussed in Chapter 2.2), that is very similar to the fluorescence technique used in this thesis. They were able to determine initial rates of spinodal phase separation (that is at the beginning of phase separation) at different depths of quench ΔT into the two phase region from one phase region. The ΔT values ranged from 0.5 to 5.5 ^oC. They demonstrated that the initial values of phase separation rates vary linearly with the driving forces predicted by $(T-T_s)/T_s$. It could be assumed that the rates of phase separation are same, or very similar to the rates of remixing. Then, from the results by Larbi et al.[149]showing that the initial rate of phase separation increase linearly with driving force, one could expect that also the remixing rates get faster, that is the remixing time scales get smaller as the driving force increases. However, as our data show, the times scales under electric field stay the same. Now, here it should be mentioned that the maximum values for the driving force Larbi et al. calculated for their systems were <0.03, that is half the value of the driving force for the blend in this study under zero electric field. So, even though for driving forces <0.03 the rate increases linearly, it is not known how this rate might change with driving forces higher than 0.03. It is possible that at higher driving forces the

rates plateau out. Then, though electric fields increase the driving force of the blend, the time scale would not change, which agrees with the results shown here.

I conclude this chapter, by suggesting a future study with a measurement protocol illustrated in Figure 7.7. I suggest measuring the fluorescence intensity for a PS/PVME blend while it is forced through a temperature jump from the one phase region at an initial temperature T^{i}_{remix} to the two phase region at a temperature T_{unmix}, as shown in Figure 7.7a. After holding the sample at T_{unmix} for 5 min, an electric field strong enough to increase the phase separation temperature above the T_{unmix} is applied, as shown in Figure 7.7b and d. It would then be expected that after the electric field is turned on, the driving force causing the phase separation of the blend components when no electric field is present, now changes direction and starts forcing the sample to remix. Experimentally this remixing would be observed as a decay of fluorescence intensity, as shown in Figure 7.7c. Based on the measurements presented in this chapter, one might expect the remixing time scale $\tau(T)$ would follow the same time-temperature dependence as the time scales measured under zero field but now extended to 104 ^{o}C, as shown in Figure 7.7e. If indeed the suggested experiments follow the predicted results described above, then it would mean that it is possible use the electric fields to jump in and out of two phase region of the phase diagram. Application of electric fields to PS/PVME blends would then provide a control of both the distance from the phase boundary, dictating the strength of the driving force for phase separation, and the temperature, governing the dynamics or speed of phase separation.

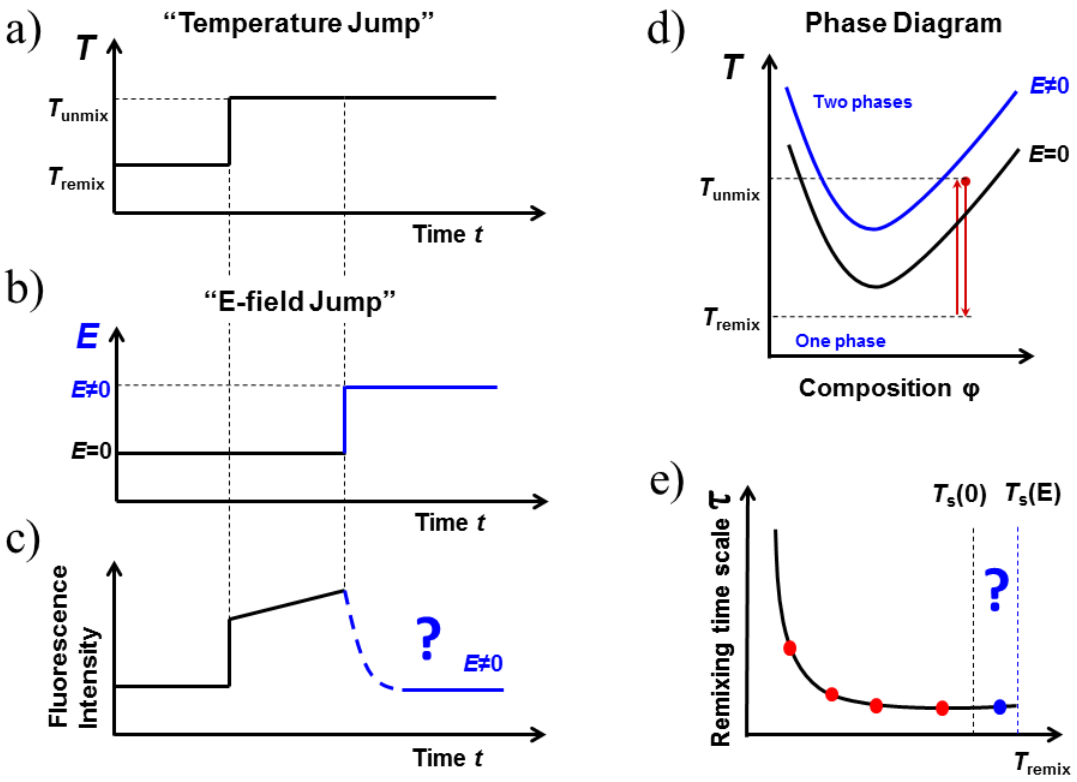

Figure 7.7 Illustration of proposed measurement to test whether electric fields can be used to jump in and out of two phase region of polymer blends. (a) Sample is heated from T_{remix} (one phase region) to T_{unmix} (two phase region). (b) After sample has been at the unmixing temperature T_{unmix} for 5 min, an external electric field is applied across the sample. (c) Expected change in fluorescence intensity (black) known (blue) unknown. (d) Phase diagram: the presence of an electric field increases the phase separation temperature higher. (e) Red and blue circles indicate the remixing time scales found at different temperatures T_{remix} in the presence of zero and non-zero electrical fields, respectively. Before conducting the experiment it is not known whether the blue circle fall on the same curve with the red circles. Dashed vertical blue and black lines indicate the positions of the phase separation temperatures of the sample, with and without the presence of electric fields, $T_s(E)$ and $T_s(0)$, respectively, relative to the temperature T_{remix}.

Chapter 8

Summary

From the very beginning, the main goal of this Ph.D. research was to find out how electric fields affect the miscibility of polymer blends, characterized as a shift in phase separation temperature T_s. As demonstrated in Chapter 6, I was able to reach this goal and find that electric fields strongly enhance the miscibility of PS/PVME blends. All the other results obtained from the separate studies presented in the chapters prior to Chapter 6, were the necessary steps aimed towards achieving that main goal.

In this thesis the investigation of the effect of varying the chemical structure of an extrinsic fluorescent label on the measured phase separation of PS/PVME blends was presented. This study[131] was the first to investigate the changes in fluorescence emission spectra of various aromatic dyes covalently bonded to PS upon phase separation. It was found that the fluorescence intensity increases primarily uniformly upon phase separation for all fluorophores with little change in spectral shape. Also, it was found that the proximity of the dye to the PS backbone in its covalent attachment influences this measure of the early stages of phase separation, with fluorophores covalently attached in closer proximity to the PS backbone identifying phase separation a few degrees earlier. Aromatic dyes pyrene and anthracene behave similarly, exhibiting a uniform increase in

intensity at all wavelengths consistent with static fluorescence quenching occurring in the one phase region. Based on work by Green et al.,[46] it seems likely that the fluorescence quenching in the presence of PVME is a result of a weak hydrogen bond between the ether oxygen in PVME and aromatic hydrogens on the pyrene and anthracene dyes.

In this thesis I have demonstrated reproducible and highly reliable shifts in T_s of PS/PVME blends in the presence of electric fields.[151] It was conclusively demonstrated that the presence of electric fields substantially enhances the miscibility of the blend by measuring large increases in T_s, significantly outside experimental error by over an order of magnitude, and subsequently recovering the same original T_s at zero field after the electric field has been turned off. The measured shifts $\Delta T_s(E)$ of up to 13.5 ± 1.4 K for field strengths of $E = 1.7 \times 10^7$ V/m are some of the largest absolute shifts in T_s ever reported, although the relative magnitude of the shift $\Delta T_s / E^2 = (4.8 \pm 0.4) \times 10^{-14}$ Km^2/V^2 is comparable to values from literature on other blends. These results help bring coherence to the existing experimental data and provide large, unambiguous shifts in $T_s(E)$ with electric field for theoretical predictions to be tested.

My results directly contradict the one previous work by Reich and Gordon[44] who reported a decrease in $\Delta T_s \approx 50$ K under electric fields, indicating reduced miscibility. The ultimate reason for this discrepancy is unknown, although as was explained in Chapter 6.2.3, their results have stood in direct contrast to the majority of other studies on blend miscibility under electric fields, which otherwise consistently indicate enhanced mixing under electric fields.

Future efforts should focus on determining which parameters are important in altering electric field miscibility effects in PS/PVME blends. In this research, only the

effect of electric fields on a 50/50 composition of PS/PVME was studied. I suggest measuring the electric field effect also on other compositions and mapping out the full phase diagram under different electric fields. Then these phase diagrams of PS/PVME blends under electric fields could be fit to the Flory-Huggins Eq. (6.1) in Chapter 6. This way the free energy contribution due to the presence of electric fields could unambiguously be determined. In order to perform the suggested study, first the full diagram of PS/PVME blends without electric fields needs to be measured. The most difficult part of this is finding the T_s for compositions containing mostly one or the other component of the blend (for example the compositions of 20/80 or 80/20 PS/PVME). One possible issue would then be that for a composition like 20/80 PS/PVME the dye content as a ratio of polystyrene chains might need to be adjusted to get enough fluorescent signal from the sample. However, this might mean that very high percentage of the PS part of the PS/PVME blend, would contain fluorescently labeled-PS (PS*). A possible solution to this issue would be to polymerize a fluorescently labeled-PS (PS*) that contains more labels per polystyrene chain.

The importance of the entropic contribution to the electric field effect could be tested by comparing the electric field shift in phase separation between the high and low molecular weight blends. Though this might seem like an easy experiment, several problems may arise when performing the proposed study. Using all my experience that I have gained during the experiments for this dissertation research, I think that probably the biggest issue, that might end up creating unsurpassable problem will be with measuring PS/PVME blends containing low molecular weight PS (for example M_w =25kg/mol), because the phase separation temperature T_s is considerably higher for low molecular

weight blends (for example 140 ^{o}C or higher for PS/PVME blend with M_w =25kg/mol of PS, as shown from Figure 5.3 in Section 5.1). I noticed during this dissertation research, that the higher the temperature the more probable was dielectric breakdown. Thus, it might be more difficult if not impossible to measure fluorescence emission under electric fields when the measurement temperature range gets higher.

The importance of the enthalpic contribution to the electric field effect could be tested by comparing the electric field shift in phase separation between the hPS/PVME and dPS/PVME polymer blends.[1] It has been known for decades now that the T_s of dPS/PVME blends, where the hydrogens in aromatic ring of PS are deuterated, is ~40 ^{o}C higher than the T_s of hPS/PVME blends.[62,63] Green et al.[46] found that weak hydrogen bonds between the aromatic hydrogens of PS and the ether oxygen of PVME account for the miscibility of PS/PVME blend. So, the considerably higher T_s in dPS/PVME blends are most likely due to the stronger weak hydrogen bonds between dPS and PVME than the weak hydrogen bonds holding the blend together in hPS/PVME blends. Thus, if it is found that electric fields shift the T_s in hPS/PVME and dPS/PVME blends by the same amount, then it could be argued that electric fields do not affect the weak hydrogen bond in these blends and do not contribute to the enthalpic free energy of mixing. On the contrary, if it is found that the electric field effect on the T_s in dPS/PVME is not as strong as it is in hPS/PVME blends, then not only could it be argued that electric fields contribute to the enthalpic interaction, but also a quantitative measure of the difference in the interaction strength of the weak hydrogen bond in hPS/PVME and dPS/PVME could

[1] Here hPS and dPS stand for hydrogenated and deuterated polystyrene, respectively.

likely be found. It should be noted here again, that measuring the T_s of dPS/PVME blends under electric fields might not be a possibility. As mentioned in the paragraph above, dielectric breakdown happens more likely at higher temperatures. As was shown in Section 5.1, Figure 5.2, the T_s is close to 130 ^oC for the dPS/PVME blends, which is roughly 30 ^oC higher than the T_s in hPS/PVME blends used in study in Chapter 6.

I also suggest measuring the composition dependent dielectric constant $\varepsilon(\phi)$ of PS/PVME blends as this dependence is not known at this time. The theoretical arguments for the shift in phase separation temperature with electric field predict that the shift depends on the curvature of the dielectric constant with respect to the composition, $\partial^2\varepsilon/\partial\phi^2$, as shown in Eq.(6.2). Additionally the most recent theory by Orzechowski et al,[43] have suggested that the inconsistencies between the theory and the experimental results on the direction and magnitude of the shift in phase separation temperature with electric field could be resolved by adding an additional term to the equation predicting shifts in T_s under electric fields. This additional term accounting for the dielectric contrast between the components, contains both $\varepsilon(\phi)$ and $\partial\varepsilon/\partial\phi$. Thus, knowing the exact value of $\varepsilon(\phi)$ for PS/PVME blends would provide an exact quantitative measure of the difference (or the lack of) between the theoretical predictions and the experimental results presented here. Main problem with measuring $\varepsilon(\phi)$ for PS/PVME blends, is that we do not have equipment to perform this measurement and collaboration with another scientist with sufficient equipment from another university is needed.

Experimental results presented in Chapter 7, showing that electric fields do not seem to have an effect on the temperature dependence of the remixing time scale, should be considered as a starting point with more advanced experiments needed to fully

understand the electric field effect on the kinetics of PS/PVME blends. In Chapter 7, a future experiment was suggested, with the goal of testing whether phase separation and remixing could be turned on and off simply by applying electric fields, obtaining unprecedented control of the phase separation dynamics. The purpose of these experiments would be to determine if electric fields could be used to decouple the distance from phase boundary, dictating the strength of the driving force for phase separation, and the temperature, governing the dynamics or speed of phase separation. However, it should be noted here that the few attempts to run this proposed experiment have failed, because the sample had dielectric breakdown shortly after applying electric fields at a temperature of 104 ^{o}C. Thus, unless the problem with dielectric breakdown is solved, it might not be possible to perform this experiment at all.

Appendix 1

For polymers the classic Flory-Huggins equation gives the free energy of mixing

$$\Delta G_m(0) = k_B T \left\{ \frac{\varphi_A ln\varphi_A}{v_A N_A} + \frac{\varphi_B ln\varphi_B}{v_B N_B} + \frac{\varphi_A \varphi_B \chi}{v_{ref}} \right\}$$

The free energy of mixing with additional term for electrostatic energy

$$\Delta G_m(E) = k_B T \left\{ \frac{\varphi_A ln\varphi_A}{v_A N_A} + \frac{\varphi_B ln\varphi_B}{v_B N_B} + \frac{\varphi_A \varphi_B \chi}{v_{ref}} \right\} - \frac{1}{2} \varepsilon_0 E^2 \{ \varepsilon(\phi) - \phi_A \varepsilon_A - \phi_B \varepsilon_B \}$$

Taking $\varphi_A = \varphi$ and $\varphi_B = 1 - \varphi$

$$\frac{\partial \Delta G_m(0)}{\partial \varphi} = k_B T \left\{ \frac{1 + ln\varphi}{v_A N_A} - \frac{1 + \ln(1-\varphi)}{v_B N_B} + \frac{\chi(1-2\varphi)}{v_{ref}} \right\}$$

$$\frac{\partial \Delta G_m(E)}{\partial \varphi} = k_B T \left\{ \frac{1 + ln\varphi}{v_A N_A} - \frac{1 + \ln(1-\varphi)}{v_B N_B} + \frac{\chi(1-2\varphi)}{v_{ref}} \right\} - \frac{1}{2} \varepsilon_0 E^2 \left\{ \frac{\partial \varepsilon(\varphi)}{\partial \varphi} - \varepsilon_A + \varepsilon_B \right\}$$

$$\frac{\partial^2 \Delta G_m(0)}{\partial \varphi^2} = k_B T \left\{ \frac{1}{v_A N_A \varphi} + \frac{1}{v_B N_B (1-\varphi)} + \frac{2\chi}{v_{ref}} \right\}$$

$$\frac{\partial^2 \Delta G_m(E)}{\partial \varphi^2} = k_B T \left\{ \frac{1}{v_A N_A \varphi} + \frac{1}{v_B N_B (1-\varphi)} + \frac{2\chi}{v_{ref}} \right\} - \frac{1}{2} \varepsilon_0 E^2 \frac{\partial^2 \varepsilon(\varphi)}{\partial \varphi^2}$$

From stability $\frac{\partial^2 \Delta G_m}{\partial \varphi^2} = 0$, the critical interaction parameter with and without electric fields, $\chi_c(0)$ and $\chi_c(E)$, respectively are

$$\chi_C(0) = \frac{v_{ref}}{2} \left(- \frac{1}{v_A N_A \varphi} - \frac{1}{v_B N_B (1-\varphi)} \right)$$

$$\chi_C(E) = \frac{v_{ref}}{2}\left(-\frac{1}{v_A N_A \varphi} - \frac{1}{v_B N_B (1-\varphi)} + \frac{\varepsilon_0 E^2}{2k_B T}\frac{\partial^2 \varepsilon(\varphi)}{\partial \varphi^2}\right)$$

Change in interaction parameter due to electric fields

$$\chi_C(E) - \chi_C(0) = \frac{v_{ref}\varepsilon_0 E^2}{4k_B T}\frac{\partial^2 \varepsilon(\varphi)}{\partial \varphi^2}$$

If interaction parameter χ is defined so that $\chi = A + B/T$, where empirical parameters have been found $A>0$ and $B<0$ for LCST-type phase diagram (or $A<0$ and $B>0$ for LCST-type phase diagram), then $1/T_s = (\chi_c - A)/B$ and

$$\frac{1}{T_s(E)} - \frac{1}{T_s(0)} = \frac{\chi_C(E) - \chi_C(0)}{B} = \frac{v_{ref}\varepsilon_0 E^2}{B4k_B T_s(E)}\frac{\partial^2 \varepsilon(\varphi)}{\partial \varphi^2}$$

$$\frac{1}{T_s(E)} - \frac{1}{T_s(0)} = \frac{T_s(0) - T_s(E)}{T_s(E)T_s(0)}$$

$$\frac{T_s(0) - T_s(E)}{T_s(0)} = \frac{v_{ref}\varepsilon_0 E^2}{B4k_B}\frac{\partial^2 \varepsilon(\varphi)}{\partial \varphi^2}$$

The direction of the phase separation temperature due to electric field cannot be estimated unless the sign of $\frac{\partial^2 \varepsilon(\varphi)}{\partial \varphi^2}$ is known. However, often it has been found that relation $\varepsilon = n^2$, where n is refractive index, holds for different materials, then $\frac{\partial n}{\partial \varphi} = n_A - n_B$ and $\frac{\partial^2 \varepsilon(\varphi)}{\partial \varphi^2} = 2\left(\frac{\partial n}{\partial \varphi}\right)^2 > 0$. So, if $\frac{\partial^2 \varepsilon(\varphi)}{\partial \varphi^2} > 0$ the shift of T_s under electric fields will shift into lower temperature for LCST-type phase behavior (as $B<0$) and higher temperature for UCST-type behavior ($B>0$). Thus according to the thermodynamic argument shown above the electric fields are expected to reduce the miscibility, which is in conflict with the majority of experimental results, as discussed in Chapter 6.

Appendix 2

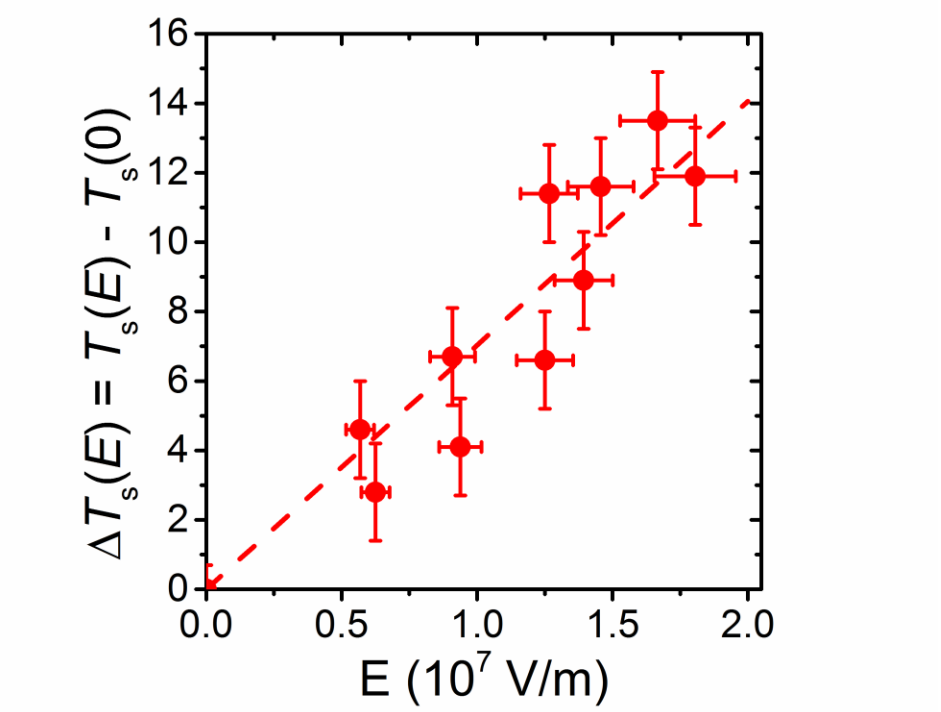

Shift in phase separation temperature $\Delta T_s(E) = T_s(E) - T_s(0)$ as a function of the electric field strength. The dashed line is a linear fit through the experimental data points with slope $\Delta T_s/E = (7.0 \pm 0.4) \times 10^{-7}$ Km/V. Compare to Figure 6.4.

References

1. Grosberg, A. Y. & Khokhlov, A. R. *Giant Molecules Here, There, and Everywhere ...* (Academic Press, San Diego, CA, 1997).

2. Hiemenz, P. C. & T.P. Lodge. *Polymer Chemistry, 2nd Ed.* (CRS Press, Taylor & Francis Group, Boca Raton, FL 2007).

3. Schaffer, E., Thurn-Albrecht, T., Russell, T. P. & Steiner, U. Electrically induced structure formation and pattern transfer. *Nature* **403,** 874–877 (2000).

4. Schaffer, E., Thurn-Albrecht, T., Russell, T. P. & Steiner, U. Electrohydrodynamic instabilities in polymer films. *Europhys. Lett.* **53,** 518–524 (2001).

5. Thomas, K. R., Chenneviere, A., Reiter, G. & Steiner, U. Nonequilibrium behavior of thin polymer films. *Phys. Rev. E* **83,** 021804 (2011).

6. Closa, F., Ziebert, F. & Raphael, E. Interplay of internal stresses, electric stresses, and surface diffusion in polymer films. *Phys. Rev. E* **83,** 051603 (2011).

7. Xi, K. & Krause, S. Droplet deformation and structure formation in two-phase polymer/polymer/toluene mixtures in an electric field. *Macromolecules* **31,** 3974–3984 (1998).

8. Moriya, S., Adachi, K. & Kotaka, T. Effect of electric field on the morphology of a poly(ethylene oxide)/ polystyrene blend. *Polym. Commun.* **26,** 235–237 (1985).

9. Venugopal, G., Krause, S. & Wnek, G. E. Modification of polymer blend morphology using electric fields. *J. Polym. Sci. Part C-Polymer Lett.* **27,** 497–501 (1989).

10. Serpico, J. M., Wnek, G. E., Krause, S., Smith, T. W., Luca, D. J. & Vanlaeken, A. Effect of block copolymer on the electric field induced morphology of polymer blends. *Macromolecules* **24,** 6879–6881 (1991).

11. Hori, H., Urakawa, O., Yano, O. & Tran-Cong-Miyata, Q. Phase separation of binary polymer mixtures under an electric field. *Macromolecules* **40,** 389–394 (2007).

12. Wang, C. H., Chen, P. L. & Lu, C. Y. D. Phase separation of thin-film polymer mixtures under in-plane electric fields. *Phys. Rev. E* **81,** 06150 (2010).

13. Amundson, K., Helfand, E., Davis, D. D., Quan, X., Patel, S. S. & Smith, S. D. Effect of an electric field on block copolymer microstructure. *Macromolecules* **24,** 6546–6548 (1991).

14. Amundson, K., Helfand, E., Quan, X. & Smith, S. D. Alignment of lamellar block copolymer microstructure in an electric field. 1. Alignment kinetics. *Macromolecules* **26,** 2698–2703 (1993).

15. Amundson, K., Helfand, E., Quan, X. N., Hudson, S. D. & Smith, S. D. Alignment of lamellar block copolymer microstructure in an electric field. 2. Mechanisms of alignment. *Macromolecules* **27,** 6559–6570 (1994).

16. Morkved, T. L., Lu, M., Urbas, A. M., Ehrichs, E. E., Jaeger, H. M., Mansky, P. & Russell, T. P. Local control of microdomain orientation in diblock copolymer thin films with electric fields. *Science* **273,** 931–933 (1996).

17. Thurn-Albrecht, T., Schotter, J., Kastle, C. A., Emley, N., Shibauchi, T., Krusin-Elbaum, L., Guarini, K., Black, C. T., Tuominen, M. T. & Russell, T. P. Ultrahigh-density nanowire arrays grown in self-assembled diblock copolymer templates. *Science* **290,** 2126–2129 (2000).

18. Thurn-Albrecht, T., DeRouchey, J., Russell, T. P. & Kolb, R. Pathways toward electric field induced alignment of block copolymers. *Macromolecules* **35,** 8106–8110 (2002).

19. Gurovich, E. Why does an electric field align structures in copolymers? *Phys. Rev. Lett.* **74,** 482–485 (1995).

20. Tsori, Y. & Andelman, D. Thin film diblock copolymers in electric field: Transition from perpendicular to parallel lamellae. *Macromolecules* **35,** 5161–5170 (2002).

21. Lin, C. Y., Schick, M. & Andelman, D. Structural changes of diblock copolymer melts due to an external electric field: A self-consistent-field theory study. *Macromolecules* **38,** 5766–5773 (2005).

22. Tsori, Y., Andelman, D., Lin, C. Y. & Schick, M. Block copolymers in electric fields: A comparison of single-mode and self-consistent-field approximations. *Macromolecules* **39,** 289–293 (2006).

23. Matsen, M. W. Stability of a block-copolymer lamella in a strong electric field. *Phys. Rev. Lett.* **95,** 258302 (2005).

24. Matsen, M. W. Electric field alignment in thin films of cylinder-forming diblock copolymer. *Macromolecules* **39,** 5512–5520 (2006).

25. Boker, A., Knoll, A., Elbs, H., Abetz, V., Muller, A. H. E. & Krausch, G. Large scale domain alignment of a block copolymer from solution using electric fields. *Macromolecules* **35,** 1319–1325 (2002).

26. Boker, A., Elbs, H., Hansel, H., Knoll, A., Ludwigs, S., Zettl, H., Urban, V., Abetz, V., Muller, A. H. E. & Krausch, G. Microscopic mechanisms of electric-field-induced alignment of block copolymer microdomains. *Phys. Rev. Lett.* **89,** 1355020 (2002).

27. Schmidt, K., Schoberth, H. G., Ruppel, M., Zettl, H., Hansel, H., Weiss, T. M., Urban, V., Krausch, G. & Boker, A. Reversible tuning of a block copolymer nanostructure via electric fields. *Nat. Mater.* **7,** 142–145 (2008).

28. Olszowka, V., Hund, M., Kuntermann, V., Scherdel, S., Tsarkova, L., Boker, A. & Krausch, G. Large scale alignment of a lamellar block copolymer thin film via electric fields: a time-resolved SFM study. *Soft Matter* **2,** 1089–1094 (2006).

29. Schoberth, H. G., Olszowka, V., Schmidt, K. & Boker, A. Effects of electric fields on block copolymer nanostructures. *Adv. Polym. Sci.* **227,** 1–31 (2010).

30. Eitouni, H. B. & Balsara, N. P. Electrochemically controlled self-assembly of an organometallic block copolymer. *J. Am. Chem. Soc.* **128,** 16248–16252 (2006).

31. Tsori, Y. Colloquium: Phase transitions in polymers and liquids in electric fields. *Reviews of Modern Physics* **81,** 1471–1494 (2009).

32. Tsori, Y., Mark, J. E. & Steiner, U. *Polymers, liquids and colloids in electric fields : interfacial instabilities, orientation and phase transitions. Series in soft condensed matter*. (World Scientific Publishing, NJ, 2009).

33. Landau, L. D., Pitaevskii, L. P. & Lifshitz, E. M. *Electrodynamics of Continuous Media, 2nd Ed. American Journal of Physics* **29,** (Elsevier Butterworth-Heinemann, Oxford, 1984).

34. Debye, P. & Kleboth, K. Electrical field effect on the critical opalescence. *The Journal of Chemical Physics* **42,** 3155–3162 (1965).

35. Orzechowski, K. in. *Polymers, Liquids and Colloids in Electric Fields: Interfacial Instabilities, Orientation and Phase Transitions*. (edited by Y. Tsori, J.E. Mark, and U. Steiner, World Scientific Publishing, NJ, 2009, pp. 87–112).

36. Wirtz, D. & Fuller, G. G. Phase transitions induced by electric fields in near-critical polymer solutions. *Physical review letters* **71,** 2236–2239 (1993).

37. Lee, J. S., Prabu, A. A., Kim, K. J. & Park, C. Phase separation and crystallization behavior of poly (vinylidene fluoride)/poly (1, 4-butylene adipate) blends under an electric field. *Macromolecules* **41,** 3598–3604 (2008).

38. Lee, J. S., Prabu, A. A. & Kim, K. J. UCST-type phase separation and crystallization behavior in poly(vinylidene fluoride)/poly(methyl methacrylate) blends under an external electric field. *Macromolecules* **42,** 5660–5669 (2009).

39. Onuki, A. Electric field effects in fluids near the critical point. *Europhysics Letters* **29,** 611 (1995).

40. Beaglehole, D. A critical binary liquid in an electric field. *The Journal of Chemical Physics* **74,** 5251–5255 (1981).

41. Early, M. D. Dielectric constant measurements near the critical point of cyclohexane-aniline. *The Journal of Chemical Physics* **96,** 641 (1992).

42. Orzechowski, K. Electric field effect on the upper critical solution temperature. *Chemical Physics* **240,** 275–281 (1999).

43. Orzechowski, K., Adamczyk, M., Wolny, A. & Tsori, Y. Shift of the critical mixing temperature in strong electric fields. Theory and experiment. *J. Phys. Chem. B* **118,** 7187 (2014).

44. Reich, S. & Gordon, J. M. Electric field dependence of lower critical phase separation behavior in polymer–polymer mixtures. *Journal of Polymer Science Part B-Polymer Physics* **17,** 371–378 (1979).

45. Schoberth, H. G., Schmidt, K., Schindler, K. A. & Böker, A. Shifting the order-disorder transition temperature of block copolymer systems with electric fields. *Macromolecules* **42,** 3433–3436 (2009).

46. Green, M. M., White, J. L., Mirau, P. & Scheinfeld, M. H. C-H to O hydrogen bonding: The attractive interaction in the blend between polystyrene and poly(vinyl methyl ether). *Macromolecules* **39,** 5971 (2006).

47. Bank, M., Leffingwell, J. & Thies, C. Thermally induced phase separation of polystyrene-poly(vinyl methyl ether) mixtures. *J. Polym. Sci. Part A-2* **10,** 1097 (1972).

48. Nishi, T., Wang, T. T. & Kwei, T. K. Thermally induced phase separation behavior of compatible polymer mixtures. *Macromolecules* **8,** 227–234 (1975).

49. Nishi, T. & Kwei, T. K. Cloud point curves for poly(vinyl methyl ether) and monodisperse polystyrene mixtures. *Polymer* **16,** 285–290 (1975).

50. Ubrich, J. M., Larbi, F. B., Halary, J. L., Monnerie, L., Bauer, B. J. & Han, C. C. Molecular weight effects on the phase diagram of polystyrene-poly(vinyl methyl ether) blends. *Macromolecules* **19,** 810–815 (1986).

51. Pavawongsak, S., Higgins, J. S., Clarke, N., McLeish, T. C. B. & Peiffer, D. G. Phase separation in entangled polystyrene/poly(vinyl methyl ether) blends. *Polymer* **41,** 757–763 (2000).

52. Sharma, J. & Clarke, N. Miscibility determination of a lower critical solution temperature polymer blend by rheology. *J. Phys. Chem. B* **108,** 13220–13230 (2004).

53. Cheon, K.-S. & Green, M. M. Structural deuterium isotope effects reveal the cooperativity of polymers. *J. Labelled Comp. Radiopharm.* **50,** 961–966 (2007).

54. Desiraju, G. R. & Steiner, T. *The Weak Hydrogen Bond in Structural Chemistry and Biology*. (Oxford University Press, NY, 1999).

55. Desiraju, G. R. Hydrogen bridges in crystal engineering: Interactions without borders. *Acc. Chem. Res.* **35,** 565–573 (2002).

56. Bank, M., Leffingwell, J. & Thies, C. The influence of solvent upon the compatibility of polystyrene and poly(vinyl methyl ether). *Macromolecules* **4,** 43–46 (1971).

57. Lu, F. J., Benedetti, E. & Hsu, S. L. Spectroscopy of polystyrene and poly(vinyl methyl ether) blends. *Macromolecules* **16,** 1525–1529 (1983).

58. Garcia, D. Fourier-transform infrared study of polystyrene/poly(vinyl methyl ether) blends. *J. Polym. Sci. Part B-Polymer Phys.* **22,** 107–115 (1984).

59. Garcia, D. High-temperature fourier transform infrared study of polystyrene/poly(vinyl methyl ether) blends. *J. Polym. Sci. Part B-Polymer Phys.* **22,** 1773–1779 (1984).

60. Yang, H., Hadziioanou, G. & Stein, R. S. The effect of deuteration on the phase equilibrium of the polystyrene / poly (vinyl methyl ether) blend system. *J. Polym. Sci. Part B - Polym. Phys.* **21,** 159–162 (1983).

61. Halary, J. L., Ubrich, J. M., Nunzi, J. M., Monnerie, L. & Stein, R. S. Phase separation in polystyrene-poly(vinylmethylether) blends: a fluorescence emission analysis. *Polymer* **25,** 956–962 (1984).

62. Larbi, F. B. C., Leloup, S., Halary, J. L. & Monnerie, L. Phase diagrams of poly(vinyl methyl ether) selectively deuterated polystyrene - an original route to the precise nature of polymer-polymer interactions. *Polym. Commun.* **27,** 23–25 (1986).

63. Yang, H., Shibayama, M., Stein, R. S., Shimizu, N. & Hashimoto, T. Deuteration effects on the miscibility and phase separation kinetics of polymer blends. *Macromolecules* **19,** 1667–1674 (1986).

64. Halary, J. L., Ubrich, J. M., Monnerie, L., Yang, H. & Stein, R. S. Isotope effects on the phase-separation in polystyrene poly(vinyl methyl ether) blends. *Polym. Commun.* **26,** 73–76 (1985).

65. Valeur, B. *Molecular Fluorescence: Principles and Applications*. (Wiley-VCH, Weinheim, 2001).

66. Robeson, L. M. *Polymer Blends: A Comprehensive Review*. (Hanser Gardner Publications, Cincinnati, OH, 2007).

67. Rubinstein, M. & Colby, R. H. *Polymer Physics*. (Oxford University Press, NY, 2003).

68. Brazel, C. S. & Rosen, S. L. *Fundamental Principles of Polymeric Materials, 3rd Ed.* (John Wiley & Sons, Hoboken, NJ, 2012).

69. Han, C. C., Bauer, B. J., Clark, J. C., Muroga, Y., Matsushita, Y., Okada, M., Tran-cong, Q. & Chang, T. Temperature, composition and molecular-weight dependence of the binary interaction paramter of polystyrene/ poly(vinyl methyl ether) blends. *Polymer* **29,** 2002–2014 (1988).

70. Qian, C., Mumby, S. J. & Eichinger, B. E. Phase diagrams of binary polymer solutions and blends. *Macromolecules* **24,** 1655–1661 (1991).

71. Thomas, K. R., Clarke, N., Poetes, R., Morariu, M. & Steiner, U. Wetting induced instabilities in miscible polymer blends. *Soft Matter* **6,** 3517–3523 (2010).

72. Lipson, J. E. G. A Born-Green-Yvon integral-equation treatment of incompressible lattice mixtures. *J. Chem. Phys.* **96,** 1418–1425 (1992).

73. Lipson, J. E. G. & Andrews, S. S. A Born-Green-Yvon integral-equation treatment of a compressible fluid. *J. Chem. Phys.* **96,** 1426–1434 (1992).

74. White, R. P. & Lipson, J. E. G. Chain fluids: Contrasts of theoretical and simulation approaches, and comparison with experimental alkane properties. *J. Chem. Phys.* **131,** 074109 (2009).

75. White, R. P. & Lipson, J. E. G. Fluid mixtures: Contrasts of theoretical and simulation approaches, and comparison with experimental alkane properties. *J. Chem. Phys.* **131,** 074110 (2009).

76. Luettmer-Strathmann, J. & Lipson, J. E. G. Phase separation in polymer solutions from a Born-Green-Yvon lattice theory. *Fluid Phase Equilib.* **150,** 649–656 (1998).

77. White, R. P. & Lipson, J. E. G. Origins of unusual phase behavior in polymer/ionic liquid solutions. *Macromolecules* **46,** 5714–5723 (2013).

78. White, R. P. & Lipson, J. E. G. How pure components control polymer blend miscibility. *Macromolecules* **45,** 8861–8871 (2012).

79. White, R. P. & Lipson, J. E. G. New correleations in polymer blend miscibility. *Macromolecules* **45,** 1076–1084 (2012).

80. White, R. P. & Lipson, J. E. G. Free volume, cohesive energy density, and internal pressure as predictors of polymer miscibility. *Macromolecules* **47,** 3959–3968 (2014).

81. Strobl, G. *The Physics of Polymers. Concepts for Understanding Their Structures and Behavior*. (Springer-Verlag, Berlin, Heidelberg, 2007).

82. Jones, R. A. L. *Soft Condensed Matter*. (Oxford University Press, NY, 2002).

83. Cahn, J. W. Phase separation by spinodal decomposition in isotropic systems. *J. Chem. Phys.* **42,** 93–99 (1965).

84. Larson, R. G. *The Structure and Rheology of Complex Fluids*. (Oxford University Press, NY, 1999).

85. Segalman, R. A. Patterning with block copolymer thin films. *Mater. Sci. Eng. R-Reports* **48,** 191–226 (2005).

86. Tao, Y., Zohar, H., Olsen, B. D. & Segalman, R. A. Hierarchical nanostructure control in rod-coil block copolymers with magnetic fields. *Nano Lett.* **7,** 2742–2746 (2007).

87. Segalman, R. A., McCulloch, B., Kirmayer, S. & Urban, J. J. Block copolymers for organic optoelectronics. *Macromolecules* **42,** 9205–9216 (2009).

88. Shah, M., Pryamitsyn, V. & Ganesan, V. Effect of anisotropic charge transport on device characteristics of polymer solar cells. *Appl. Phys. Lett.* **95,** 194101 (2009).

89. Shah, M. & Ganesan, V. Correlations between morphologies and photovoltaic properties of rod-coil block copolymers. *Macromolecules* **43,** 543–552 (2010).

90. Park, M. J. & Balsara, N. P. Anisotropic proton conduction in aligned block copolymer electrolyte membranes at equilibrium with humid air. *Macromolecules* **43,** 292–298 (2010).

91. Xu, T., Zvelindovsky, A. V, Sevink, G. J. A., Gang, O., Ocko, B., Zhu, Y. Q., Gido, S. P. & Russell, T. P. Electric field induced sphere-to-cylinder transition in diblock copolymer thin films. *Macromolecules* **37,** 6980–6984 (2004).

92. Lyakhova, K. S., Zvelindovsky, A. V & Sevink, G. J. A. Kinetic pathways of order-to-order phase transitions in block copolymer films under an electric field. *Macromolecules* **39,** 3024–3037 (2006).

93. Ly, D. Q., Honda, T., Kawakatsu, T. & Zvelindovsky, A. V. Kinetic pathway of gyroid-to-cylinder transition in diblock copolymer melt under an electric field. *Macromolecules* **40,** 2928–2935 (2007).

94. Pinna, M. & Zvelindovsky, A. V. Kinetic pathways of gyroid-to-cylinder transitions in diblock copolymers under external fields: cell dynamics simulation. *Soft Matter* **4,** 316–327 (2008).

95. Ly, D. Q., Honda, T., Kawakatsu, T. & Zvelindovsky, A. V. Hexagonally perforated lamella-to-cylinder transition in a diblock copolymer thin film under an electric field. *Macromolecules* **41,** 4501–4505 (2008).

96. Ly, D. Q., Honda, T., Kawakatsu, T. & Zvelindovsky, A. V. Electric field-induced transitions in perforated lamella of ABA triblock copolymer thin film. *Soft Matter* **5,** 4814–4822 (2009).

97. Schmidt, K., Pester, C. W., Schoberth, H. G., Zettl, H., Schindler, K. A. & Boeker, A. Electric field induced gyroid-to-cylinder transitions in concentrated diblock copolymer solutions. *Macromolecules* **43,** 4268–4274 (2010).

98. Gurovich, E. On Microphase Separation of Block-Copolymers in an Electric-Field - 4 Universal Classes. *Macromolecules* **27,** 7339–7362 (1994).

99. Gunkel, I., Stepanow, S., Thurn-Albrecht, T. & Trimper, S. Fluctuation effects in the theory of microphase separation of diblock copolymers in the presence of an electric field. *Macromolecules* **40,** 2186–2191 (2007).

100. Kawai, H. The piezoelectricity of poly (vinylidene fluoride). *Japanese Journal of Applied Physics* **8,** 975–976 (1969).

101. Lovinger, A. J. Ferroelectric polymers. *Science* **220,** 1115–1121 (1983).

102. Sanchez, I. C. & Stone, M. T. in. *Polymer Blends: Formulation & Performance, Vol. 1*. (edited by D.R. Paul and C.B. Bucknall; Wiley, NY, 2000, pp.15-53).

103. Eitouni, H. B. & Balsara, N. P. *Physical Properties of Polymer Handbook, 2nd Ed*. (edited by J.E. Mark, Springer, NY, 2007, pp. 339-356).

104. Jackson, J. D. *Classical Electrodynamics, 3rd Ed. American Journal of Physics* **67,** 841 (John Wiley & Sons, New York, 1999).

105. Onuki, A. Interface instability induced by an electric field in fluids. *Physica A: Statistical Mechanics and its Applications* **217,** 38–52 (1995).

106. Wirtz, D., Berend, K. & Fuller, G. G. Electric-field-induced structure in polymer solutions near the critical point. *Macromolecules* **25,** 7234–7246 (1992).

107. Lakowicz, J. R. *Principles of Fluorescence Spectroscopy, 2nd Ed.* (Kluwer Academic/Plenum Publishers, NY, 1999).

108. Seymour, I. & Carraher, C. E. *Polymer Chemistry, 7th Ed.* (CRC Press, Taylor & Francis Group, Boca Raton, FL, 2008).

109. Sperling, L. H. *Introduction to Physical Polymer Science, 4th Ed.* (John Wiley & Sons, Hoboken, NJ, 2006).

110. Nucleophilic addition / elimination in the reaction between acyl chlorides and alcohols. Retrieved from: *http://www.chemguide.co.uk/mechanisms/addelim/alcohol.html (Date Accessed: 2/09/2015)*

111. Bruice, P. Y. *Organic Chemistry, 4th Ed.* (Prentice Hall, Upper Saddle River, NJ, 2004).

112. Coleman, M. M., Graf, J. F. & Painter, P. C. *Specific Interactions and the Miscibility of Polymer Blends*. (Technomic Publishing, Lancaster, PA, 1991).

113. Coleman, M. M. & Painter, P. C. Hydrogen-bonded polymer blends. *Prog. Polym. Sci.* **20,** 1–59 (1995).

114. Dudowicz, J. & Freed, K. F. Effect of monomer structure and compressibility on the properties of multicomponent polymer blends and solutions: 1. Lattice cluster theory of compressible systems. *Macromolecules* **24,** 5076–5095 (1991).

115. Dudowicz, J. & Freed, K. F. Effect of monomer structure and compressibility on the properties of multicomponent polymer blends and solutions: 3. Application to deuterated polystyrene [PS(D)]poly(vinyl methyl ether) (PVME) blends. *Macromolecules* **24,** 5112–5123 (1991).

116. White, R. P., Lipson, J. E. G. & Higgins, J. S. Effect of deuterium substitution on the physical properties of polymer melts and blends. *Macromolecules* **43,** 4287–4293 (2010).

117. Taylor, R. & Kennard, O. Crystallographic evidence for the existence of C-H...O, C-H...N, and C-H...C1 hydrogen bonds. *J. Am. Chem. Soc.* **104,** 5063–5070 (1982).

118. Gaikwad, A. N., Choperena, A., Painter, P. C. & Lodge, T. P. Restoring thermorheological simplicity in miscible polymer blends: How many hydrogen bonds are required? *Macromolecules* **43,** 4814–4821 (2010).

119. Vala, M. T., Haebig, J. & Rice, S. A. Experimental study of luminescence and excitation trapping in vinyl polymers, paracyclophanes, and related compounds. *J. Chem. Phys.* **43,** 886–897 (1965).

120. Torkelson, J. M., Lipsky, S. & Tirrell, M. Polystyrene fluorescence: effects of molecular weight in various solvents. *Macromolecules* **14,** 1601–1603 (1981).

121. Gelles, R. & Frank, C. W. Phase separation in polystyrene/poly(vinyl methyl ether) blends as studied by excimer fluorescence. *Macromolecules* **15,** 1486–1491 (1982).

122. Gelles, R. & Frank, C. W. Effect of molecular weight on polymer blend phase separation kinetics. *Macromolecules* **16,** 1448–1456 (1983).

123. Qian, R. Y. & Gu, X. H. A study of polystyrene / poly(vinyl methyl ether) blends by excimer fluorescence. *Angew. Makromol. Chemie* **141,** 1–9 (1986).

124. Kalyanasundaram, K. & Thomas, J. K. Environmental effects on vibronic band intensities in pyrene monomer fluorescence and their application in studies of micellar systems. *J. Am. Chem. Soc.* **99,** 2039–2044 (1977).

125. Roth, C. B. & Torkelson, J. M. Selectively probing the glass transition temperature in multilayer polymer films: Equivalence of block copolymers and multilayer films of different homopolymers. *Macromolecules* **40,** 3328–3336 (2007).

126. Kim, S., Roth, C. B. & Torkelson, J. M. Effect of nanoscale confinement on the glass transition temperature of free-standing polymer films: Novel, self-referencing fluorescence method. *J. Polym. Sci. Part B - Polym. Phys.* **46,** 2754–2764 (2008).

127. Ellison, C. J. & Torkelson, J. M. The distribution of glass-transition temperatures in nanoscopically confined glass formers. *Nat. Mater.* **2,** 695–700 (2003).

128. Bauer, B. J., Hanley, B. & Muroga, Y. Synthesis and characterization of poly(vinylmethyl ether). *Polymer Communications* **30,** 19–21 (1989).

129. Reich, S. & Cohen, Y. Phase separation of polymer blends in thin films. *J. Polym. Sci. Polym. Phys. Ed.* **19,** 1255–1267 (1981).

130. Ellison, C. J. & Torkelson, J. M. Sensing the glass transition in thin and ultrathin polymer films via fluorescence probes and labels. *J. Polym. Sci. Part B - Polym. Phys.* **40,** 2745–2758 (2002).

131. Kriisa, A., Park, S. S. & Roth, C. B. Characterization of phase separation of polystyrene/poly(vinyl methyl ether) blends using fluorescence. *Journal of Polymer Science Part B-Polymer Physics* **50,** 250–256 (2012).

132. Kwei, T. K., Nishi, T. & Roberts, R. F. Study of compatible polymer mixtures. *Macromolecules* **7,** 667 (1974).

133. Chu, C. W., Dickinson, L. C. & Chien, J. C. W. Study of critical phenomena of polystyrene poly(vinyl methyl ether) blends by solid-state NMR. *J. Appl. Polym. Sci.* **41,** 2311 (1990).

134. Wagler, T., Rinaldi, P. L., Han, C. D. & Chun, H. Phase behavior and segmental mobility in binary blends of polystyrene and poly(vinyl methyl ether). *Macromolecules* **33,** 1778 (2000).

135. Davis, D. D. & Kwei, T. K. Phase transformation in mixtures of polystyrene and poly(vinyl methyl ether). *J. Polym. Sci. Part B-Polymer Phys.* **18,** 2337 (1980).

136. Jabbari, E. & Peppas, N. A. Use of ATR-FTIR to study interdiffusion in polystyrene and poly(vinyl methyl ether). *Macromolecules* **26,** 2175 (1993).

137. Valeur, B., Rempp, P. & Monnerie, L. Insertion of anthracene fluorophore in polystyrene chain - study of local movements via inhibition and fluorescence polarization. *C. R. Acad. Sci.* **279 C,** 1009 (1974).

138. Brandrup, J., Immergut, E. H. & Grulke, E. A. *Polymer Handbook, 4h Ed*. (John Wiley & Sons, New York, 1999).

139. P. A. Tipler, G. M. *Physics for Scientists and Engineers, Volume 2: Electricity, Magnetism, Light, and Elementary Modern Physics*. (W. H. Freeman, 2003).

140. DuPont™ Kapton® polyimide film. Retrieved from: *http://www.dupont.com/content/dam/assets/products-and-services/membranes-films/assets/DEC-Kapton-general-specs.pdf (Date Accessed: 10/28/2014)*

141. Umeuchi, S., Nishimura, Y., Yamazaki, I., Murakami, H., Yamashita, M. & Ohta, N. Electric field effects on absorption and fluorescence spectra of pyrene doped in a PMMA polymer film. *Thin Solid Films* **311,** 239–245 (1997).

142. Liedel, C., Pester, C. W., Ruppel, M., Urban, V. S. & Boeker, A. Beyond orientation: The impact of electric fields on block copolymers. *Macromol. Chem. Phys.* **213,** 259–269 (2012).

143. Lodge, T. P., Wood, E. R. & Haley, J. C. Two calorimetric glass transitions do not necessarily indicate immiscibility: The case of PEO/PMMA. *J. Polym. Sci. Part B - Polym. Phys.* **44,** 756–763 (2006).

144. Schmidt-Rohr, K., Clauss, J. & Spiess, H. W. Correlation of structure, mobility, and morphological information in heterogeneous polymer materials by two-dimensional wideline-separation NMR spectroscopy. *Macromolecules* **25,** 3273–3277 (1992).

145. Shimizu, H., Horiuchi, S. & Kitano, T. An appearance of heterogeneous structure in a single-phase state of the miscible PVME/PS blends. *Macromolecules* **32,** 537–540 (1999).

146. Wang, D. & Ishida, H. Surface micro-scale semi-heterogeneous structures in compatible polystyrene and poly(vinyl methyl ether) blend thin films investigated by lateral-force Microscopy. *Macromol. Chem. Phys.* **208,** 2222–2228 (2007).

147. Blanchard, P. & Devaney, R. L. *Differential Equations, 4th Ed*. (Brooks/Cole, Boston, MA, 2012).

148. Jones, R. A. L. & Richards, R. W. *Polymers at Surfaces and Interfaces*. (Cambridge University Press, NY, 1999).

149. Larbi, F. B. C., Halary, J.-L. & Monnerie, L. Kinetic of phase separation in binary mixtures of polystyrene and poly(vinyl methyl ether) as studied by fluorescence emission of labeled polystyrene. *Macromolecules* **24,** 867–871 (1991).

150. Halary, J.-L., Larbi, F. B. C., Oudin, P. & Monnerie, L. Molecular mobility in polystyrene - poly (methyl vinyl ether) blends as studied by fluorescence polarization. *Makromol. Chem.* **189,** 2117–2124 (1988).

151. Kriisa, A. & Roth, C. B. Electric fields enhance miscibility of polystyrene/poly(vinyl methyl ether) blends. *J. Chem. Phys.* **141,** 134908 (2014).

152. Hess, D. B. & Muller, S. J. Secondary effects of antioxidant on PS/PVME blends. *Polymer* **43,** 1567–1570 (2002).

153. Goldman, S. & Joslin, C. Why hydrogen-bonded liquids tend to have high static dielectric constants. *J. Phys. Chem.* **97,** 12349–12355 (1993).